Alma Mater Studiorum - Università di Bologna

DOTTORATO DI RICERCA
in
Ingegneria Biomedica, Elettrica e dei Sistemi

Ciclo XXXV

Settore Concorsuale: 09/E2 - Ingegneria dell'Energia Elettrica
Settore Scientifico Disciplinare: ING-IND/33 - Sistemi Elettrici per l'Energia

Enhancing the Reliability of Electric Transportation Motors through Insulation Coordination and Improved Qualification

Presentata da:
Alberto Rumi

Coordinatore Dottorato:
Prof. **Michele Monaci**

Supervisore:
Prof. **Andrea Cavallini**
Co-Supervisore:
Prof. **Davide Fabiani**

Esame Finale Anno 2023

Abstract

The ambitious goals of increasing the efficiency, performance and power densities of transportation drives cannot be met with compromises in the motor reliability. For the insulation specialists the challenge will be critical as the use of wide-bandgap converters (WBG, based on SiC and GaN switches) and the higher operating voltages expected for the next generation drives will enhance the electrical stresses to unprecedented levels. It is expected for the DC bus in aircrafts to reach 800 V (split ±400 V) and beyond, driven by the urban air mobility sector and the need for electrification of electro-mechanical/electro-hydraulic actuators (an essential part of the "More Electric Aircraft" concept). Simultaneously the DC bus in electric vehicles (EV) traction motors is anticipated to increase up to 1200 V very soon.

The electrical insulation system is one of the most delicate part of the machine in terms of failure probability. In particular, the appearance of partial discharges (PD) is disruptive on the reliability of the drive, especially under fast repetitive transients. Extensive experimental activity has been performed to extend the body of knowledge on PD inception, endurance under PD activity, and explore and identify new phenomena undermining the reliability. The focus has been concentrated on the impact of the WGB-converter produced waveforms and the environmental conditions typical of the aeronautical sector on insulation models. Particular effort was put in the analysis at the reduced pressures typical of aircraft cruise altitude operation.

The results obtained, after a critical discussion, have been used to suggest a coordination between the insulation PD inception voltage with the converter stresses and to propose an improved qualification procedure based on the existing IEC 60034-18-41 standard.

Abstract - Italian Version

Gli obiettivi ambiziosi di aumentare l'efficienza, le prestazioni e le densità di potenza degli azionamenti per il trasporto non possono essere raggiunti con compromessi sulla affidabilità dei motori. Per gli specialisti dell'isolamento la sfida sarà cruciale, poiché sia l'uso di convertitori a wide-bandgap (WBG) basati su semiconduttori SiC e GaN, sia le tensioni operative più elevate previste per i prossimi azionamenti, aumenteranno gli stress elettrici a livelli senza precedenti. Si prevede che il bus DC negli aeromobili raggiunga gli 800 V (split ±400 V) e oltre, spinto dal settore della mobilità aerea urbana e dalla necessità di elettrificare gli attuatori elettromeccanici/elettroidraulici (parte essenziale del concetto di "More Electric Aircraft"). Contemporaneamente, si stima che presto nei motori per trazione di veicoli elettrici il DC bus aumenterà fino a 1200 V.

Il sistema di isolamento elettrico è una delle parti più delicate di una macchina elettrica in termini di probabilità di guasto. In particolare, la comparsa di scariche parziali (PD) è deleteria per l'affidabilità dell'azionamento, soprattutto in presenza di transitori veloci e ripetitivi. In questa tesi è stata condotta un'ampia attività sperimentale per ampliare le conoscenze sull'innesco di PD, sulla resistenza dei materiali in loro presenza e per identificare nuovi fenomeni che compromettono l'affidabilità dell'isolante. L'attenzione si è concentrata sull'impatto che hanno le forme d'onda prodotte da convertitori WGB e le condizioni ambientali tipiche del settore trasporti su modelli di isolamento. Particolare impegno è stato profuso nell'analisi alle pressioni ridotte tipiche del funzionamento alle quote di crociera degli aerei di linea.

I risultati ottenuti, dopo una discussione critica, sono stati utilizzati per suggerire un coordinamento tra le tensione di innesco di scarica e gli stress del convertitore, al fine di proporre una procedura di qualificazione migliorata basata sulla già esistente norma IEC 60034-18-41.

Contents

1 Introduction **6**
1.1 Electric Vehicles and More Electric Aircraft 8

2 State of the Art of Insulation for Transportation Drives **13**
2.1 Insulation System 15
2.2 Routes to Insulation Failure 18
2.2.1 Converter Over-Stresses 19
2.3 PD in MEA and EV systems 23

3 Experimental Methods **30**
3.1 Samples 30
3.2 PDIV and Endurance Tests 31
3.2.1 Generic PDIV and Endurance Test Setup 31
3.2.2 PDIV Test Procedure 32
3.2.3 Endurance Test Procedure 33
3.2.4 PDIV Tests and Setup under UV-irradiation 33
3.2.5 T-T PDIV Tests with Surge Generator 34
3.2.6 Voltage Sources 35
3.2.7 Partial Discharge Detection 36
3.2.8 Test cells 38
3.3 Supplementary Tests 40
3.3.1 Surface Temperature Detection 40
3.3.2 Dielectric Spectroscopy 41
3.3.3 FTIR 42
3.3.4 SEM 42
3.3.5 VNA 42
3.4 PDIV Prediction with Schumann Criterion based Models . . . 42
3.4.1 Prediction of impregnated T-T 43
3.4.2 P-P and P-G 44

4 Electrical Endurance under Partial Discharge Activity **46**
4.1 Combined Impact of Low-Pressure and Next-Gen Voltages Level on PD Endurance 47
4.1.1 Pressure Reduction Impact 48

4.1.2 Air-Moisture Content Impact 50
4.1.3 Aging Impact 51
4.1.4 Converter Voltages Impact 53
4.1.5 Summary 59
4.2 Partial Discharge Endurance on High Performance Multistrand Wires 61
4.2.1 Temperature Effect 61
4.2.2 3-level Waveform Impact 63
4.2.3 Summary 65

5 Partial Discharge Inception Voltage 66
5.1 Turn-Turn Insulation Models 66
5.1.1 Real Turn-Turn Stresses Impact 67
5.1.2 PDIV in Presence of Artificially Generated Seed Electron 73
5.1.3 Temperature Impact on Impregnated Samples 76
5.1.4 PDIV and Dielectric Parameters Correlation 79
5.1.5 Converter Stresses on Thermally Aged Samples 86
5.1.6 Summary 93
5.2 Complete Insulation Models 94
5.2.1 Converter Waveforms Impact 95
5.2.2 Phase-Phase and Phase-Ground Inception Prediction . 97
5.2.3 Thermal Aging Cycles for MEA Application 102
5.2.4 Summary 110

6 Insulation Coordination and Qualification 111
6.1 Lifetime in Case of PD Inception 112
6.2 Major Contributors to PDIV 117
6.2.1 PDIV under Realistic Converter Stresses 117
6.2.2 Critical Role of the Impregnation Resin 122
6.2.3 Systems Operating in Aeronautical Conditions 125
6.3 PDIV-Based Design Approach 129
6.3.1 Proposed Insulation Coordination Route 131
6.3.2 Machine-Level Solutions 134
6.3.3 Converter-Level Solutions 136
6.4 Qualification 137
6.4.1 WBG-Converter and Transportation Drives in IEC 60034-18-41 138
6.4.2 Working Case 144
6.4.3 Combined Electro-Thermal Stress 145

7 Conclusions 154

Objectives, Approach and Organization

The objective of this PhD Thesis was to improve the reliability of transportation drives electrical insulation that operate in the peculiar automotive and aeronautic environmental conditions under fast transient voltage waveforms. The task is accomplished in a twofold approach: by extending the body of knowledge on insulation materials (with a focus on partial discharge phenomena) and by deriving prescription for insulation coordination and qualification in sight of the recent knowledge advancement.

The document is organized in chapters as follow:

- [**1 - Introduction**] Presentation of the sector of transport electrification.
- [**2 - State of Art**] Introduction to insulation systems and failure routes, converter stresses analysis.
- [**3 - Experimental Methods**] Description of the experimental setups, procedures, and equipment.
- [**4 - Electrical Endurance**] Detail of the results for electrical endurance test under partial discharge activity.
- [**5 - Partial Discharge Inception Voltage**] Detail of the results for partial discharge inception voltage trends under various conditions and aging.
- [**6 - Insulation Coordination and Qualification**] Discussion from a broader perspective the experimental results obtained. The insights gathered are utilized to improve reliability through insulation coordination and qualification.
- [**7 - Conclusions**] Summary of the achievement obtained.

Chapter 1

Introduction

The urge for a transition to more sustainable transportation systems is contextualized and the electric vehicle and more electric aircraft concepts are introduced.

The impact of human activity on the planet is so significant that the geological era in which we live is defined as Anthropocene, from the Greek word *ánthrōpos*, human. The transportation sector accounts between one sixth and one quarter of the 50 Gt of greenhouse gases yearly human produced emissions, dependently on the estimation methodology [1][2][3]. This happens despite many regions of the world with enormous or booming population having less than 0.1 vehicle per capita and with air travel remaining available only to 10% of the population. Air travel alone amounts for 11% of the total amount of CO2 emitted by transport. The world population is expected to increase from the present 8 billion to around 11 billion according to the United Nations, primarily from the growth in Africa [4], and hopefully the standard of living will improve across all the globe. As a consequence, the number of domestic vehicles will likely increase from 900 million to 2.5 billion, especially from the growth in the Asian market. The air passenger traffic, that has grown of more than a 10% yearly in the last 60 years (excluding the parenthesis of COVID-19), will become accessible to more and more people [5].

In this increasingly populous, connected, and globalized world, worries about energy conservation and environmental preservation are growing. Important measures are needed to avoid the spiraling of the global warming to irreparable consequences [6]. For that the stabilization of atmospheric greenhouse gases concentration to levels lower than two times the pre-industrial ones is required.

For tackling the climate change, revolutionary technologies are not strictly required, but revolutionary policies and immediate action are, employing technologies already developed or in pilot stage, without waiting for dream solutions [7]. The goal is not achievable with the effort of a single country/sector/technology. Extensive system-level analysis, effective policy im-

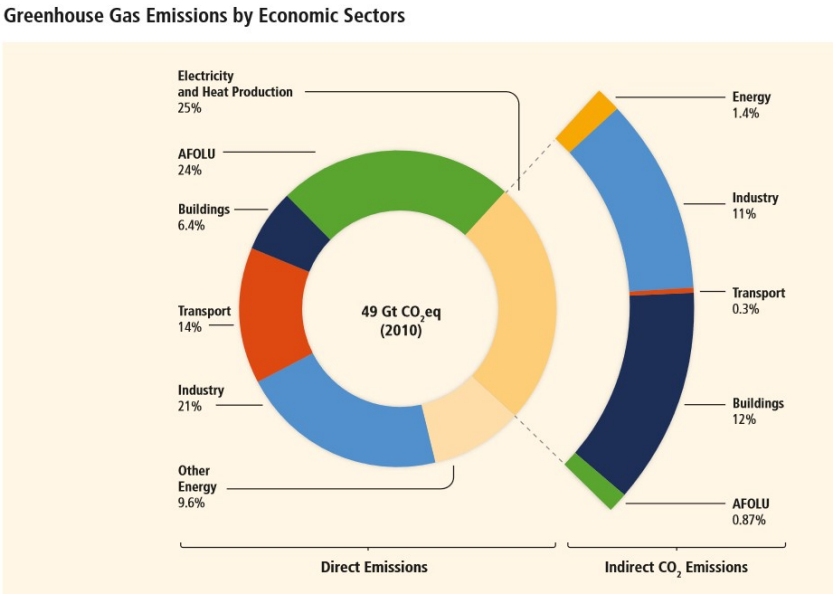

Figure 1.1: Overview of greenhouse gasses emissions by sector, from [1].

plementation and thorough planning are needed to coordinate investments, develop technology, and deploy infrastructure [8].

The electrification of transportation is a crucial element in this path [9]. Electrification definition is: the employment of more electrical energy to drive both propulsion and non-propulsion loads in vehicles.

Electrification of light-duty vehicles will not help in reaching the mitigation targets alone, requiring extreme electricity demands for the power system and excessive amounts of critical materials while dropping to zero only the tailpipe emissions and not the overall emissions [10][11]. It has been demonstrated through life cycle assessments that during their lifetime EVs will generate lower amounts greenhouse gasses, but to obtain that result is crucial that the energy is produced through renewable and sustainable sources [12][13]. Despite the limitations electrification remains one of the most powerful paths available, especially coupled with a globally reduction of vehicles in favor of public transportation, and possible innovative routes like implementation of ride-hailing autonomous fleets. However, this possibly will clash with people's needs, since in the present-being vehicle ownership is a form of freedom, independence and enabler of opportunities. The social costs that new the scenarios may bring in should be confronted [14].

For the aviation sector there is the need to produce a radical transformation as well. By 2050, new technologies are expected to reduce CO_2 emissions by 75% per passenger kilometer, nitrogen oxide emissions by 90%, and noise emissions by 65%. Since there is no unique solution, the combination of ultra-efficient aircraft, alternative fuels and alternative propulsion appear as candidates to reach these objectives [15].

1.1 Electric Vehicles and More Electric Aircraft

The advancements in semiconductor technologies, with the production of switching devices based on wide-bandgap (WBG) semiconductors opened a new chapter for power electronics. WBG materials like Silicon Carbide (SiC) and Gallium Nitride (GaN) have an higher band gap compared to silicon (>3 eV vs 1.1 eV), meaning that the energy required to promote a valence electron to become a conduction electron to make the semiconductor start conducing is higher. This permits to operate the switch at higher temperature and electric fields, to increase the doping level and reduce the semiconductor thickness hence improving the on-resistance and heat extraction enabling higher operation frequencies [16]. While GaN and SiC devices have similar switching capabilities, GaN outperforms SiC as the frequency increases. Unfortunately, it is more difficult to manufacture due to the lack of a native oxide, which is essential for MOS device fabrication.

Converter realized using WBG devices results in smaller footprints and cooling systems. Motors can be reduced in size and weight thanks to the higher voltages and frequencies [17]. System level benefits are achieved with the production of drives with increased efficiency and reduced volumes and weights (obtained for both the converter and the machine). These characteristics are powerful enablers for the transportation electrification (TE) sector [18][19][20].

Electrification of road vehicles follows a straightforward concept, with the substitution of the internal combustion engine (ICE) powertrains with electrical counterparts (electric vehicle, EV), or alternatively uses both the ICE and the electrical engine with various configurations and degrees of hybridization (hybrid electric vehicle, HEV)[9][21]. For a long time, 400 VDC has been the standard system voltage for EVs, some manufacturers seeking better performance lately have begun to adopt 800 VDC (the fist has been the Porsche Taycan).

Heavy goods and passenger vehicles would especially benefit from voltage increase above 800 VDC, combining the benefits of electrification with the ones of a denser transportation, to achieve lower emission per passenger.

Electrification of aircraft is multifaceted, ranging between the concepts of the all-electric aircraft (AEA) and the more electric aircraft (MEA). The AEA is a fully electric aircraft comprehensive of an electric propulsion. For the time being AEA is a dream for the long range airliner but hybrid or full electric propulsion regional or short-medium haul aircrafts are already envisioned before the end of this decade [22]. Alongside, urban air mobility solutions are trending, proposing an innovative mobility system that makes use of the airspace above cities. Interesting electric aircraft prototypes are showcased by companies like Lilium, Joby and Vertical Aerospace. Due to the extreme innovation in this sub-sector it is likely to see disruptive solutions introduced in this marketplace before significant changes appear in the short-

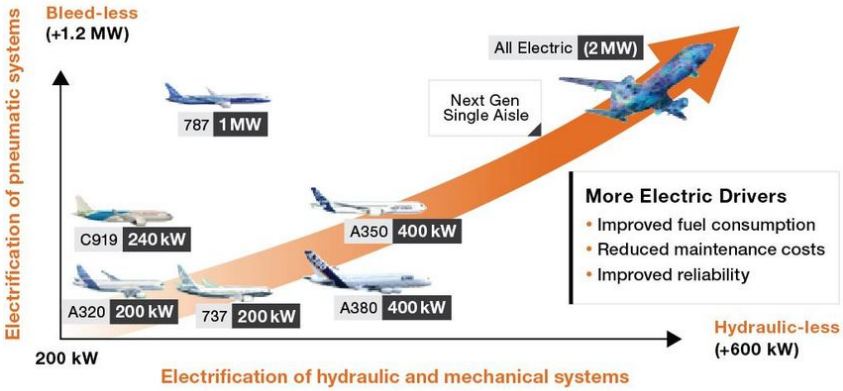

Figure 1.2: Electrical power and airliners models to achieve the more-electric aircraft. In the picture "all-electric" refers to the non propulsive loads. From: [23]

haul aircrafts. For this reason, these vertical take-off aircraft may be the first to operate at 800 VDC level or above.

For the more classical airliner a cornerstone in fuel consumption reduction can be reached also with the electrification of a larger number of (non-propulsive) aircraft subsystem. That is the MEA concept, which ultimate goal is to substitute all the non-propulsive non-electric aircraft systems with electrical counterparts, that are classically pneumatic, hydraulic and to a lesser extent mechanic. For doing so, the electric generators keyed to the engine should be designed to withdraw the required power.

Eliminating the pneumatic systems will avoid the extraction of air from the compressor stage of the gas turbines (namely, tapping the bleed air). The penalties in extracting bleed air are not proportionate to the power extracted and the problem aggravates as the engine technology improves (especially as the bypass ratio of the engine increases, namely as the ratio between the mass flow rate around the engine core with the one through it increases). Avoiding pneumatic systems will enable the so called bleedless turbine, greatly improving the fuel efficiency of the aircraft. Eliminating the hydraulic system will also contribute to energy savings. Hydraulic systems have good characteristics like robustness and high power densities but the benefits are countered by the big disadvantages of an inflexible, prone to leaks and very weighty infrastructure. Electrification will help reducing the aircraft weight by eliminating the infrastructure (e.g. pipeworks, centralized pumps, valves) and improving functionality and maintainability thanks to the de-centralization, modularity and improved fault detection.

Examples of system to be electrified in the MEA context are [24][25]:

- The main engine starter. It is classically a pneumatic system needed to spin the engine up to the critical speed needed for start combustion. Compressed air is obtained using energy from the auxiliary power unit

(a) Electro-Hydraulic Actuator. (b) Electromechanical Actuator.

Figure 1.3: More Electric Actuators, from [24].

(APU) and ducted to the ATS (air turbine starter), placed in the nacelle of the engine. Alternatively ground carts are used for the task. The engine electrical generators could be used as motors to electrify the system.

- The environmental control systems and on-board inert gas generation system. The first is required to provide air supply, thermal control and cabin pressurization. The second is required to fill the tank of the aircraft with the nitrogen (inert gas, to reduce the fire hazard) and uses a membrane to separate it from the air. Classically both use bleed air from the engine, electrification is achievable using electric fed compressors.

- The wings anti-icing system. Classically uses hot air bleed from the engine, can be substituted with heating mats embedded in the wings.

- The engine fuel pumps. Classically have two stages, with the low-pressure already electrically driven and the high-pressure mechanically and hydraulically driven. Electrification will help in decoupling the fuel flow control from the speed of the engine other than improving the maintainability and efficiency.

- The actuators. Actuators in the current aircrafts are hydraulically driven. They may be responsible for moving parts with very different roles and are nowadays the most difficult part to electrify. Electrification may be achieved using an electrical drive through two main paths:

  – electro-hydraulic actuators (EHA): the electric motor drives a reversible pump in a small de-centralized hydraulic circuit

  – electro-mechanical actuators (EMA): the electric motor rotational motion is converted into linear motion by a mechanical mechanism

  For now EHA are preferred, permitting a smoother transition by repurposing existing components with proven experience and using them in parallel with regular hydraulic actuator. The limited knowledge in the jamming probability of EMA concurs to the choice.

Examples of classic hydraulic actuators are the ones in the landing gear (for the extension/retraction, steering and braking) and for ones that control the flight surfaces. Flight control surfaces are divided in primary and secondary. The primary ones (usually elevator, ailerons, and rudder) control the pitch, roll and yaw and are safety critical in every stage of the flight. The secondary ones assist in controlling the flight attitude (examples are flaps, slats and airbrakes).

Other than systems, operations could be electrified as well. One example is taxiing. When the aircraft needs to move in the ground, typically tug vehicles transport it from the terminal gate to the airport apron, while propulsion from its engines is used to navigate the airport's runways. This taxiing procedure does not provide an optimal operating condition for the engines (that alternates between idle and maximum thrust), resulting in significant fuel consumption. E-taxing or green-taxing is the alternative, where introduction of electric motors integrated in the nose wheel and fed by the auxiliary power unit permits the autonomous and efficient movement of the aircraft. The energy savings during taxiing are estimated to be about 97% [26]. Such scenario will also simplify the airport logistic, possibly eliminating the fleet of tug vehicles, and reduce the acoustic pollution.

The MEA implementation is continuously advancing, as the electrical power demand in the aircraft keeps increasing. Both the electrical system and the power generation require innovations in their architectures to sustain the progress [27]. Regardless, as the power increases, the voltage levels will have to increase, to reduce the current in the system. Higher currents are undesirable because they inevitably cause larger joule losses and require conductors with increased size and weight. The aim to reach higher voltage levels has to be coupled with the target of producing an equally safe system [28].

Important steps have already be taken. The Boeing 787 "Dreamliner" features electrified environmental control, wing anti-icing, main engine starters, breaking and some of the fuel pumps, requiring 1 MVA of electric power produced by 4 generators. The B787 has limited air bleed tapping to solely cowl anti-icing; all other functions previously provided by bleed air has been replaced with electric technology. In comparison to the B767, the bleedless architecture reduces fuel consumption at cruising by 2% [25]. To achieve the goals, the DC-bus of the aircraft was increased to $\pm$ 270 VDC, substituting the conventional 115 VAC [29]. On the hydraulic side, Airbus A380 introduced back-up EHA for some of the flight surface actuators starting the pivotal transition [25][30]. Currently they operate at voltages below 300 VDC.

Many important targets lie ahead for the EV and MEA sectors, both looking to increase the power densities of the machines while reducing their size and weight, without compromising on the lifetimes and reliability.

As an example the use of WBG converters might help reducing the weight of the EV traction motors. The same is applicable in the MEA, where the machines needed for the e-taxiing should be able to move an aircraft weighting

hundreds of tons. A peculiar problem of the e-taxiing relies on the need to keep the converter in the body of the aircraft to avoid the excessive mechanical stress, interfacing the motor with very long cables, enhancing the voltage stresses.

Even more ambitious is the complete electrification of the flight surface actuators, requiring fault tolerant electrical machines with extreme reliability to operate in the harsh high-altitude environment.

The ultimate challenge is the production of propulsion motors for aircrafts, where to all the previous requirements are added to the need to deliver the extreme power (in the megawatt range) needed for the take-off. For that the aircraft bus voltage has to increase to limit the losses and the weight of the conductors, likely to values above 1000 V.

Chapter 2

State of the Art of Insulation for Transportation Drives

This chapter provides a very general overview of the machines to be used in transportation electrification. The insulation system is introduced and its impact on machine reliability highlighted. The reader is referred to the extensive literature available if not comfortable with: material/processing of low-voltage machines, classical insulation failure routes and partial discharge phenomenon. Converter-produced stresses are discussed and state of the art regarding partial discharge for the sector is given.

Drives to be used in the transportation sector have to comply to stringent requirements (governed by standards, regulations and codes). This is especially true for the aeronautic field, where some of the them may be part of safety critical systems. For those machines fault tolerant operation is a necessary requirement [31], that if not satisfied intrinsically has to be developed (e.g. with a multi-phase approach).

These drives are expected to be fed with WBG-converters, to deliver the benefits of an increased power density to the entire system. Furthermore, it is clear that the need for a system level weight, volume and loss reduction will push the request of higher voltages. Current transportation voltages are 800 VDC for automotive and 540 VDC for aeronautic sectors. MEA actuators capable of operating at 540 VDC have yet to be deployed. Next generation voltages are thought to be around 1000-1200 V for automotive and 800 V for aeronautic. The operation might include running the system at different DC bus voltage levels, because multiple voltage levels are enabled by design or because DC bus transients (abnormal or not) appear in the drive. Transients in the systems (e.g. due to important load disconnections in an aircraft) cause additional over-voltages for short amounts of time.

The design of the electrical drives is drawn starting from the operation cycles that the machine has to withstand. Operation cycles are a series of data points expressing the torque and speed required versus time for various scenarios. For EV the driving cycles are used, a common example is the

WLTP (Worldwide Harmonized Light-Duty Vehicles Test Procedure) cycle. Several converter topologies and different control strategies can be employed dependently on the requirements. Of special interest is the use of integrated motor drives, where the converter is directly mounted on the motor, option that is more compact and power dense [32].

In general, the rotating machines design for TE should focus on delivering:

- High reliability
- High power density (usually through high torque/weight and torque/ampere ratios)
- Reduced size and weight
- High efficiency for a broad speed range

Electrical motors for EV traction have to deliver power in the range of 30-700 kW (250 kW is an usual value), while actuators for flight surfaces have to deliver lower power (nominal output power is usually lower than 5 kW). Several machine designs may be envisaged for the scopes and in general the technologies do not vary excessively between the EV and MEA sectors. The main three design type evaluated for the TE are [9][21][33]:

- Permanent magnet synchronous machines (usually the one featuring internal permanent magnets), probably the most mature and employed technology. They are capable of obtaining the best torque density in a good speed range, with optimal efficiency. Unfortunately the presence of the rare-earth magnets pose limits in temperature and increases costs and the possibility of supplying issues.
- Induction machines, employed successfully in the EV sector. Performances are reduced compared to PMSM, especially at low speeds because of the lack of independent rotor excitation, and at high torques operation because of rotor losses.
- Reluctance machines, today employed marginally in the TE sector, but with a good potential in the long run thanks to their rugged and cheap rotor construction. They feature lower power factors and torque densities than IM and PMSM. Important disadvantages are the torque ripple and increased vibration and noise.

A detailed comparison and analysis can be found in to the specialized literature about transport electrification machine design.

Electrical rotating machines used in industrial applications are designed to have an operative life of at least 20-30 years (20,000 operation hours), while in road transportation applications the expectancy is relaxed to around 10 years (10,000 operation hours). The value might be similar for non-propulsive

aerospace application with rigorous maintenance and replacement cycles and significantly higher in aerospace applications related to propulsion probably sitting around 100,000 hours. When the machines are manufactured to the highest standards, are operated and maintained properly, as the transportation sector requires, the failure of the machine is eventually caused by fatigue and degradation. Failures modes of a rotating machine are generally grouped in: stator, rotor bearing or other faults. While for larger machines almost half of the failures are in the bearings, some evidence show that for motors with nominal power lower than 10 kW the most common faults are in the stator [34]. Data for transportation drives are not easily and publicly available, but the use of WBG-converters and the push for higher operating voltages might skew the failure distribution towards stator failures [35]. This document will focus on electrical faults of the stator only.

Regardless of the typology of the machine, the stator always comprise three main components that are: the copper conductors, the iron core and the electrical insulation system (EIS). While the metallic conductors and core have an active role in the power conversion, either by that generating or guiding the rotating magnetic field, the insulation has a passive role. That is to avoid short circuits between parts at different voltage levels and doing so in the reduced volumes needed. The EIS has also secondary purposes that cannot be overlooked, like providing mechanical support, aiding the machine cooling and avoid the ingress of contaminants. The insulation materials (being polymeric, mineral and ceramics materials) have reduced capability of enduring common stresses compared to the metals of the conductors and core. This makes the insulation system the bottleneck of the reliability of the stator.

2.1 Insulation System

The EIS of low-voltage machines is usually simpler than the one of medium and high voltage machines. Low voltage machines, from an insulation point of view can be divided mainly dependently on the types of stator winding structures: random-wound or form-wound. In the former the conductor usually consist of round wires that are wound in the stator slot randomly, so that in principle each turn (loop) could be placed in contact with any other turn of the coil. In the latter, pre-formed coils are inserted inside the slot, so to control the coil distribution.

An overview of the materials in the EIS is in Fig.2.1. The functional materials, namely the ones that have to withstand the full electric stress are:

- **Turn Insulation** that for transportation motors consist of enamel deposited on the conductors (tapes are not used). The insulation is classified depending on the layers deposited during manufacturing and indicated as "grade". The enamel is usually composed of a base-coat (typically polyester-imide, PEI) and an over-coat (typically polyamide-imide,

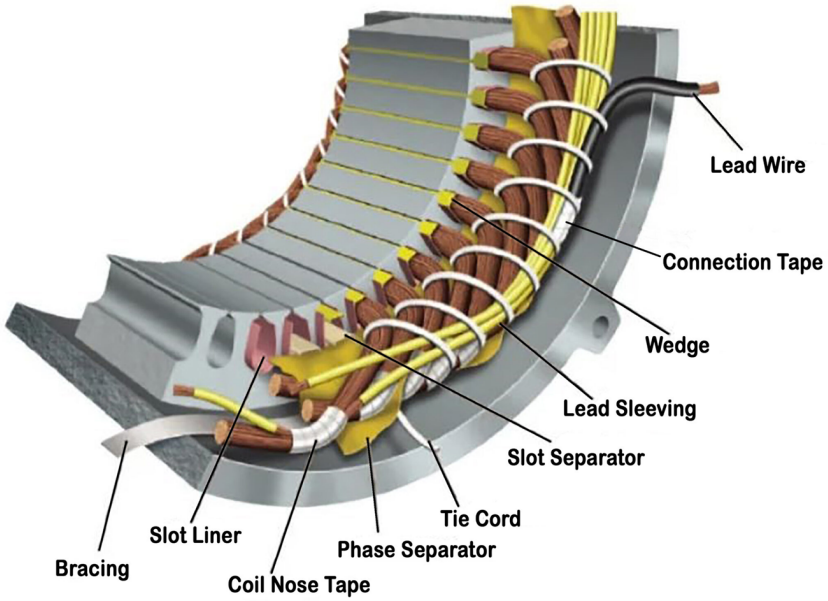

Figure 2.1: Overview of the electrical insulation system components for a low-voltage rotating machine. From: [36]

PAI). The different kind of wires that can be employed are:

  - **Rounded Wires**, used in random-wound configurations. They are single rounded enameled wires (also called magnet wires), available in plenty diameter sizes with three insulation grades [37]. They permit to optimize the slot filling factor at the cost of the random structure.
  - **Rectangular and Hairpin Wires**, used in form-wound configurations. They are rectangular shaped, with only two grades standardized, independent from the conductor thickness [38]. Manufacturers are starting to provide enamel thicknesses outside of the standardized grades, to expand the otherwise limited options.
  - **Litz Wires** Consist of many strands wires, with different twisting configuration (single or bundled twisted round strands, rectangular transposed wire strands). They represent an interesting approach for reducing skin effect losses in electrical machine wires, particularly during high frequency operation. In addition, they feature an excellent mechanical flexibility comparatively to other winding types. They are typically used in form-wound configurations but the application in random ones is not excluded.

- **Liners and Separators**, both slot and phase ones. They usually consists of papers, films, or flexible laminates with different thicknesses. The most relevant for the transportation sector where higher performance

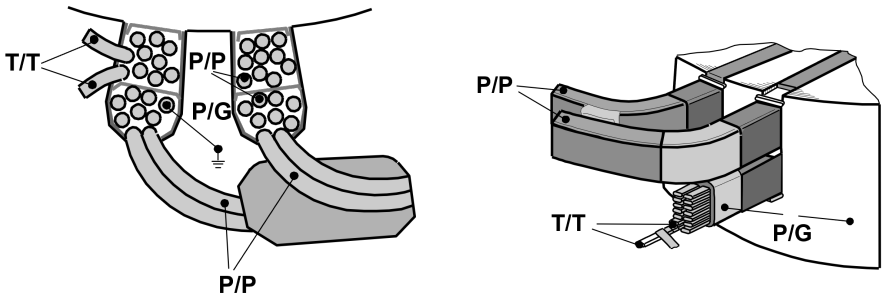

(a) Random-wound. (b) Form-wound.

Figure 2.2: Schemes of insulation subsystems for random and form wound machines. From [39]

are required are: aramid paper (commercially DuPont Nomex™), polyimide films (commercial DuPont Kapton™), polyester films (commercially DuPont Mylar™), polyester fleece (commercially DuPont Dacron™) and laminates of their combination.

- **Impregnation varnish/resin**, based either on polyester, epoxy, and polyester-imide chemistry. Crucial for the performance of the impregnation is the processing. It can be dividend in two main typologies: impregnation and casting. In impregnation, either the stator is immersed in the liquid resin (dipping) or the resin dripped inside the stator (trickle). In casting, the stator is inserted into a mold. The best performances are usually achieved with impregnation processes performed in vacuum so that the impregnation materials infiltrates better in the slot. An example is the VPI (Vacuum Pressure Impregnation) that is the most expensive process, delivering the best performance. For VPI after the low pressure phase an high pressure phase is performed in order to eliminate the remaining cavities.

The other materials not required to withstand the voltage include slot wedge, adhesive tapes, lead sleevings and bandaging cords.

The insulation system is usually divided in three subsystem, correspondent to the three voltage level of stresses appearing in the machine:

- T-T subsystem, that has to withstand the voltage appearing between the turns inside the slot. It comprises the conductor insulation (typically the enamel) and the impregnation varnish/resin.

- P-G subsystem, that has to withstand the voltage appearing between one phase and the grounded parts of the machine (e.g. frame). It comprises all the components of the T-T subsystem plus the slot liners and separators.

- P-P subsystem, that has to withstand the voltage appearing between the phases. It comprises the T-T subsystem plus the phase liners and separators.

A schematic of the subsystems is in Fig.2.2.

The reader is referred to more detailed and comprehensive literature for the manufacturing and composition of the EIS in: [40][41][42][36].

2.2 Routes to Insulation Failure

Failure of a machine can arise from improper actions like operating errors, incorrect installation and maintenance or defective manufacturing. Such faults, originating from human errors or environmental accidents can only be avoided with increased care, like standardized and supervised procedures.

Most failures occur due to the progressive deterioration of the insulation over time, due to the continuous action of the so called TEAM stresses (thermal, electrical, ambient, mechanical) [43]. The unavoidable presence of contaminants and imperfections in the EIS may provide the starting point from where the fail develops. The impact of the aging mechanism in the EIS is detailed in [44], showing the most important and known routes to insulation failure.

A critical phenomenon that may appear, is the inception of Partial Discharges (PD). A partial discharge is a localized electrical discharge that only partially bridges the insulation, hence not determining a sudden failure but eventually bringing the insulation to failure due to sustained erosion.

In low voltage rotating machines the partial discharges develop in the void or cavities present inside the slot or on the surfaces of the dielectrics. They usually appear in the air pockets left by an incomplete impregnation and at the boundaries between different insulation materials.

The physical discharge mechanisms typical of dielectric bounded systems involving small air gaps in non-uniform electric fields are not totally clarified [45]. Nonetheless, the basic principle of any discharge is the generation of an electron avalanche that transfer the charges from one electrode to the other [46][47]. Indeed, a minimum electric field capable of causing air ionization is required to incept it.

The minimum voltage at which PD presents is called partial discharge inception voltage (PDIV).

The insulation components of low voltage machines are materials of organic nature, vulnerable to the electronic bombardment, hence eroded after some time under PD activity. Especially when the machine is fed by power electronics, the onset of PD activity has a profound impact on its lifetime (hence on its reliability)[48][49][50][51]. For such reason qualification of a machine operating under converter-produced voltages can be accomplished through two very distinct paths: designing and qualifying the machine to work in presence

of partial discharge activity or in absence of such, situation regulated by standards IEC60034-18-41 [39] and IEC60034-18-42 [52] respectively. Two kind of insulation types are consequently identified:

- **Type I** not expected to experience partial discharge activity within specified conditions in their service lives
- **Type II** expected to withstand partial discharge activity in any part of the insulation system throughout their service lives

A particular focus will be put on the T-T, that is often the weakest subsystem for inverter-fed motors, featuring thinner insulation and being subjected to stress comparable to the other more robust insulation subsystems (it will be shown in the next section). Two major failure routes can be envisaged for it: crack formations and PD inception. Crack formations lead to excessive leakage current, that eventually melts the insulation and generate a breakdown. Cracks may be formed by different thermal expansion coefficients of the wire enamel and the impregnating resin, after the insulation has been embrittled by thermal degradation. The mechanism is the typical T-T failure for motors working under AC sinusoidal voltages, with thermal and mechanical stresses that are the two most important factors. On the other hand the overshoots, uneven voltage distribution and high repetition rates make the T-T the single most critical point of the insulation subsystem and the relative PD inception the most dangerous phenomena in inverter-fed machines.

2.2.1 Converter Over-Stresses

It is well known and reported [53][54][55][56][57][58][59] that operation under converter waveforms poses an extra electric stress to the insulation subsystems, over-stress emerging from two phenomena not present under sinusoidal grid frequency voltages:

1. voltage reflection at the machine terminal, causing overshoots
2. uneven voltage distribution among the coils and turns, increasing the potential between the first turn and the surrounding ones

To them it is added a further hazard: the increased speed of voltage transitions. The inverter, employing a PWM technique to obtain the desired fundamental frequency voltage, alternates the voltage with a frequency up to the maximum switching frequency of the switches. In case of PD inception, their repetition rate is greatly increased compared to sinusoidal AC operation.

1 - Overshoots The motor and its feeding cable have different characteristic (surge) impedance, with the former usually being in the order of thousands of ohm and the latter of tens of ohm. The characteristic frequencies varies along

the frequency spectrum and the numbers reported refer to the impedance seen by pulses typically produced by the inverter stage of a converter. As the voltage wave produced by the inverter travels along the conductors, meets the important mismatch of impedance at the machine terminals. Thereby reflection happens and overshoots are generated.

The overshoot could be theoretically estimated knowing the characteristic impedance of the cable and motor, resorting to transmission line theory [60]. The reflection coefficient (the parameter represent the complex ratio of the voltage of the reflected wave to that of the incident wave) at the point of impedance discontinuity is:

$$\Gamma = \frac{Z_m - Z_c}{Z_m + Z_c} \tag{2.1}$$

to be calculated for any of the spectral component of the incident wave (and is in theory a value between -1 and 1, and since $Z_m > Z_c$ is between 0 and 1 in this framework).

When the voltage rise time t_r at the inverter output is less than half the time required for voltage pulse to propagate to the motor t_p, the voltage at the terminals can be expressed as:

$$V_{mot} = (1 + \Gamma) * V_{inv} \tag{2.2}$$

often resulting in an overstress factor approaching two, due to the order of magnitude of difference between Z_m and Z_c. The overvoltage is decreased if $t_r > t_p$, resulting in a stress that can be approximated to:

$$V_{mot} = (1 + \frac{\Gamma * t_p}{t_r}) * V_{inv} \tag{2.3}$$

The overvoltage can be reported using the overshoot factor OF, namely the ratio between the voltage at the motor and at the converter. Hence $OF = (1 + \Gamma)$.

The rise time impacts both the calculation of the reflection coefficient of Eq. 2.1 (changing the spectrum of the incident voltage waveform) and the propagation phenomena of Eq. 2.3. It is important to stress here that is the rise time and not the slew rate the parameter that determines the spectrum of the wave and hence the reflection properties. Overall, the overshoot increases for shorter rise times and longer connecting cables. The standard [39] provides the Fig. 2.3 as reference for estimating the voltage overshoot.

Generation of transient over-voltages exceeding double the DC-bus is possible, with the so-called double pulses phenomenon [61]. It emerges from the interaction of between the modulation technique and carrier frequency with cable parameters (natural oscillation frequency, high-frequency damping losses) and the inverter output rise time. It is duty of the controller designer to avoid the condition.

The overvoltage generated from voltage reflection causes increased stresses in all the insulation subsystems.

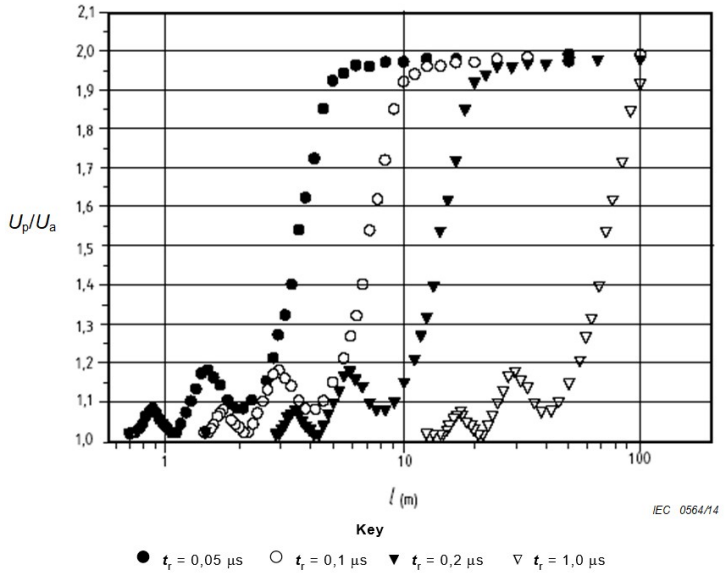

Figure 2.3: Voltage enhancement at the terminals of a motor due to reflection as a function of cable length for various impulse rise times. From: [39]

2- Uneven Distribution In converter-fed machines, the propagation of the voltage inside the windings cannot be though neither as an instantaneous or ideal process.

The machine presents a characteristic impedance that is dominated by the stray capacitances at high frequencies, where the converter-produced voltage waveform can have significant spectral energy. The turns of a slot can be modeled as a series of inductances each with a stray capacitance to ground and to the other turns. When the voltage waveshape featuring an high dV/dt meets the circuit, a portion of the current (according to $I = C * dV/dt$) will flow through those capacitances, generating a voltage drop for the turn under analysis with respect to ground or the other turns.

Furthermore, as the rise time of the voltage wave becomes comparable to the time needed for the pulse to propagate in the windings, the voltage appearing in the first turn might reach its peak while the ones in the subsequent turns/coils are still rising or worse still to zero.

For both reasons, the voltage drop across the winding distributes unevenly throughout the turns and coils, with the voltage drop across the first turns, coils or coil groups being the highest. The phenomenon is accentuated as the rise time shortens. This generates an overstress in the turn-turn insulation subsystem, causing the potential between the first turn and the others to be as high as the jump voltage of the phase to star point voltage. The jump voltage is the voltage step occurring for each impulse.

The standard [39] provides the Fig. 2.4 as reference for estimating the portion of jump voltage going to stress the T-T. Very likely the use of WBG-converters makes the figure outdated.

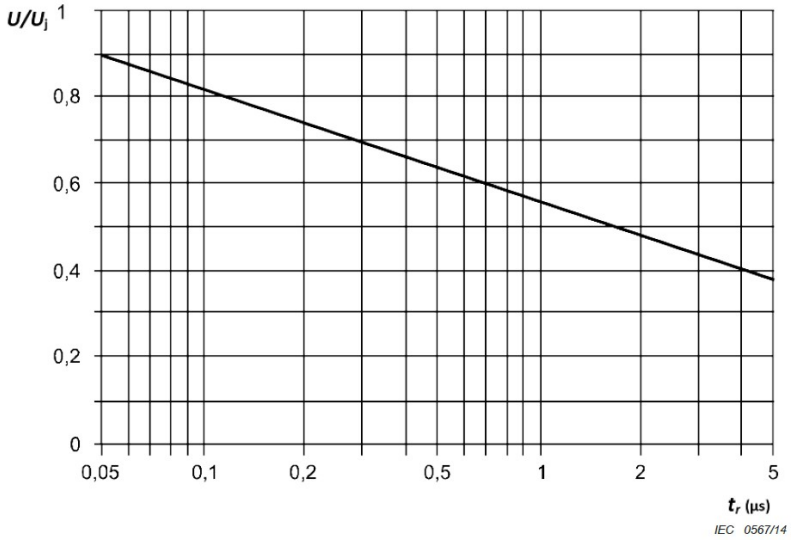

Figure 2.4: Fraction of jump voltage to stress the T-T in a variety of random wound stators as a function of the rise time of the impulse. From: [39]

Considerations for Insulation Stresses In a random-wound machine fed by sinusoidal three-phase symmetrical and balanced voltages, defined V the line-to-line voltage in peak the instantaneous maximum worst-case stressing voltages in each of the subsystems in peak are:

- $U_{P-P(peak)} = V$
- $U_{P-G(peak)} = V/\sqrt{3}$
- $U_{T-T(peak)} = V/\sqrt{3}$, as the star point voltage is zero and the phase-ground voltage is present between the first and last turn of the winding that can potentially be in contact

As comparative, consider a n-level converter with the same line-to-line fundamental frequency voltage V (value in peak) and a reflection factor at the terminals Γ. The instantaneous maximum worst-case stressing voltages in each of the subsystems in peak are:

- $U_{P-P(peak)} = V(1 + \frac{\Gamma}{n-1})$, as the overshoot (applied to a single converter stage step) enhance the stress
- $U_{P-G(peak)}$ can be potentially as high as the U_{P-P} depending on the common mode voltage of the star point (that is linked to the topology and the grounding system). In most cases, due to symmetry in the operation, it is half of that value.
- $U_{T-T(peak)} = \frac{2}{3}(\Gamma + 1)\frac{V}{n-1}$, in case the first and last turn of the winding are adjacent or in case all the voltage drops on the first turn or in case

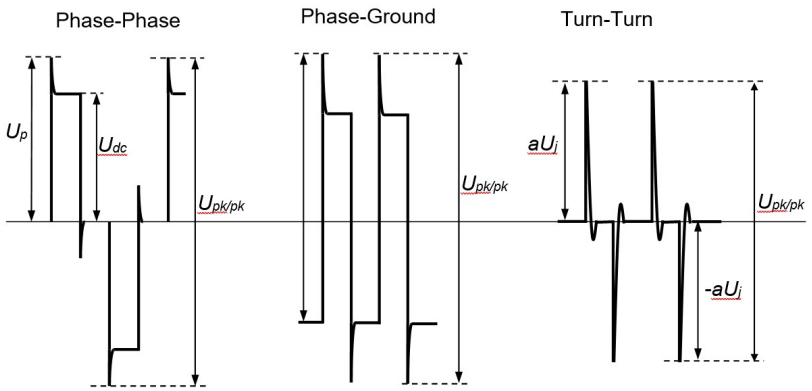

Figure 2.5: Schematic representation (not scaled) for phase-phase, phase-ground and turn-turn voltages for a 2-level converter waveform. From: [39]

of a combination of distant turn placement and short rise time appear. More generally, depending on the which turns are in contact and the rise time of the wave, the value is a fraction a of the jump voltage: $U_{T-T(peak)} = a * U_j$, with $U_j = \frac{2}{3}(1+\Gamma)\frac{V}{n-1}$.

The detailed calculation of the stressing voltages, accounting for the various topologies and grounding configurations, hence properly evaluating the common mode voltage can be found in [60]. The standard [39] prefer to express the stresses in peak-peak in the fundamental frequency cycle for P-P and P-G and in the impulse cycle for the T-T. Figure 2.5 has their schematic representation.

For form-wound machines, the contact between the first and last turns/coils can easily be avoided in the design stage. Nonetheless, as already mentioned, very short rise times causing strongly inhomogeneous voltage distribution may generate relevant T-T overstresses also in this context.

The advancement required in the transportation sector, with the increment of the DC-bus voltages up to 1000 V and the employment of WBG-converters with rise time as low as 10 ns, aggravate the issues, worsening all the phenomena explained. An example of such increase is reported in Fig. 2.6, from [62]. That makes the onset of PD more difficult to avoid. Coupled to the destructive power of the PDs in the context, for the estimation of the entire drive lifetime are crucial both: (a) the study of the EIS endurance times under their presence and (b) the study of parameters impacting PDIV and its trend.

2.3 PD in MEA and EV systems

Transportation drives have to operate in rough environmental conditions under the enhanced stress produced by WBG-converters. Here, the service conditions for an EV traction motor (expected to reach operating DC bus of 1200 V) and for a MEA EHA actuator are considered (to operate at DC buses of

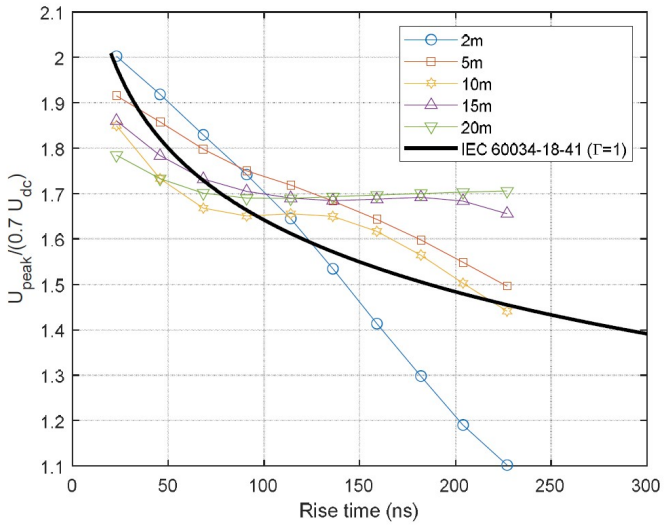

Figure 2.6: Turn-turn worst case voltage as a function of rise time and for different cable lengths, simulated for a WBG-driven actuator compared to the maximum curve recommended by IEC 60034-18-41.

540 V nowadays and possibly 800 V in the future). A brief review of the knowledge on PD (endurance and inception) for the cases is given.

The existence of dedicated standards evaluating the PD inception and endurance in machine fed by converters demonstrate the importance of the phenomenon for obtaining reliable motors. For the sake of clarity, the effect of high voltage gradients shall be separated in macroscopic level and microscopic level. The macroscopic level effects are the changes in overshoot factor and turn voltage distribution and have been already discussed in the previous section. For them the theory is established and prediction tools are limited only by the access to the modeling parameters. The microscopic level effects refer to the impact of the voltage waveform on the PDIV and PD endurance, on which the knowledge is more fragmented and often contradictory. The characteristics of pulse waveform produced by the converters that may impact the PDIV are: the rise time, the pulses repetition frequency (switching frequency), the polarity and the pulses duration times. The model of the waveform shapes appearing at the insulation subsystems are in Fig. 2.5. It should be noted that in the T-T stress the voltage has not the shape of a train of square pulses but rather the one of surge pulses. That is determined mainly by derivative behavior of the system, as the intern-turn stress is generated form the drift of the capacitive current, as previously explained. The employment of WBG-converters reduces the time scale of all the parameter illustrated, making the pulses shorter, more frequent and rising faster. Unfortunately, the high slew rate makes the electromagnetic PD detection very difficult, as the PD signal typically lays in the same frequency spectrum range of commutation noise usually with lower amplitudes. This poses strong limits

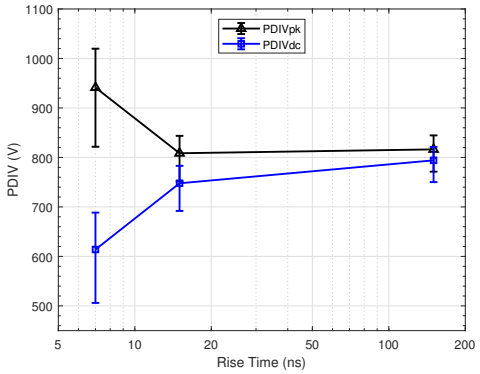

(a) Trend as function of rise time (increasing OF for shorter rise times), frequency 10 kHz.

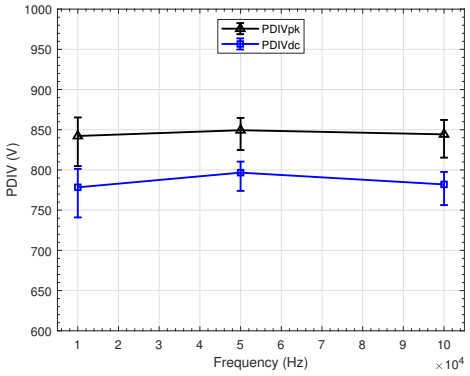

(b) Trend as function of frequency, rise time around 15 ns.

Figure 2.7: PDIV trend, under bipolar waveform from a SiC converter. Data reported as 10th percentile with confidence intervals of 95%.

to the conventional detection methods and complicates the PDIV measure [63]. For the same reason, PD on-line monitoring is a troublesome challenge to solve.

With increasingly short times rise times (typically associated with oscillations) and fast switching voltages some authors found increasing PDIV [64][65][66][67], while others found decreasing PDIV [68][69][70]. Separation between the overshoots caused by the oscillations and the rise time is difficult to obtain especially for very short rise times. Previous studies carried out in our research group showed an increase of PDIV when rise time was reduced below 20 ns for non-impregnated magnet wires under bipolar square waveform if the voltage magnitude was measured relying on the peak of the wave. Relying on DC bus, instead showed reduced PDIV values, as the waveform with shorter rise times presented higher overshoots. Differently, for switching frequency up to 100 kHz no statistical variation of PDIV was observed. The results are shown in Fig. 2.7 [71]. A detailed discussion on the phenomena is postponed to 6. An equivalent comparative analysis for P-P and P-G has yet to be completed.

The impact of voltage waveform polarity on the PDIV is more subtle to evaluate. In principle, the instantaneous voltage difference applied to the EIS determines the PDIV, but not the RPDIV, namely the voltage at which at least one PD is present in 50% of the voltage wave cycles. Indeed, after the first PD event the space charge from the avalanche is deposited on the surface of the insulation materials. There, the charge contributes to the reduction of the effective local field through the charge-produced field opposing the external one (this is called memory effect in classical PD theory). A polarity reversal or of the external voltage (or a voltage increase in the same polarity)

can cause the residual local field to exceed the inception one and cause another discharge. Continuous (symmetrical) polarity reversals are needed for producing continuous PD activity at PDIV. In practice, if testing waveforms are unipolar, PDIV could be reached with a single PD event that could be missed. If the voltage is then further increased other discharges may start appearing and that value mistakenly reported as PDIV. For this reason, bipolar waveforms ease the estimation of the PDIV, being capable of producing continuous discharge activity that is easier to be detected. To avoid dealing with the problem the standards [39][52] prefer to evaluate the stressing voltage as peak-peak of the voltage (in the time frame of the fundamental frequency for P-P and P-G, in the one of two commutations for the T-T, obtaining there bipolar stressing voltages) rather than on the instantaneous peak. Nonetheless the latter remains the preferred in this document for its link with the underlying discharge physics.

The endurance of the samples under PD activity is easier to test, as the difficulties of PD detection may be avoided and in principle only the simpler short circuits detection is needed. A richer literature about the accelerated degradation of motor windings under inverter-produced waveforms is available for the topic. A review article mainly focusing on the issue is [72]. The results generally show reduced lifetimes under inverter operation, mainly from the increased voltage pulse repetition frequency producing more discharges [73]. Some evidence demonstrate that short rise times cause higher magnitude PDs (more than five times higher), while higher switching frequency generate a lower number of discharges per cycle (reducing from multiple events per cycle to a single event per cycle) [74][75]. Overall, the short lifetimes achieved in presence of PD pose even more importance on the analysis of the PDIV and its trend under aging. So called corona-resistant solution appear to be effective in the conditions typical of the industrial drives [76], but the one of transportation drives need scrutiny.

The non-electrical stresses present in transportation drives strongly depend on the operation environment. EVs have to operate in a wide range of environmental conditions with: external temperatures ranging from -40°C to +60°C, the full relative humidity spectrum and altitudes as high as 5000 m above the sea level. These conditions are never met simultaneously and rather uncommon for most vehicles, being sustained in few places on the planet and consequently not met in a single operation cycle (low pressure in high plateau regions, high temperatures in the deserts, low temperature in sub-arctic regions etc.). Due to the continuous operation at full torque the EV motors have internal hot spots up to 200–220°C.

Much harsher are the conditions in the aeronautic sector. The current requirements in EHA/EMA flight control actuators for MEA include the full torque operation at –40°C and the capability to start up at –55°C . Drives have to operate in unpressurized areas [30], possibly the most problematic requirements regarding PD inception. Electronic controllers are required to be

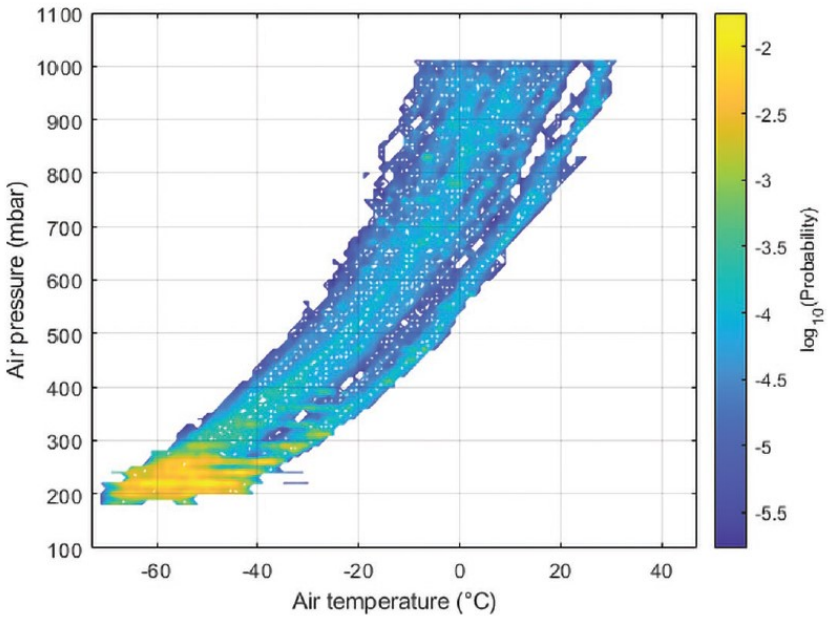

Figure 2.8: Histogram showing the density of air pressure and temperature outside a commercial aircraft. From: [77]

integrated to the actuators or to be installed nearby. A map illustrating the probability of the combination of pressure and temperature conditions sustained by a commercial aircraft is in Fig. 2.8 after [77]. Often operating only for brief times at full torque the typical hot spot temperatures of MEA drives are lower (150°C), aided by the lower outside temperature. However, they face rapid temperature changes that might increase the mechanical stress due to the different expansion and contraction coefficient of the materials. Besides reduced pressure and temperature, high humidity levels and UV radiation should also be expected. In all transportation drives the mechanical stresses are important, as the vibration profile of vehicles is clearly more important than industrial drives.

The body of knowledge on the impact of ambient conditions is more consolidated, despite the limited number of studies carried specifically for each insulation subsystem of low voltage rotating machines and the condition typical of transportation. Generally, phenomenological studies that single out the influence of the ambient conditions on the materials and discharge properties that drive the PDIV reduction have yet to be performed.

Studies that attempt to determine the impact of environmental factor on the PDIV are many: [78][79][80][81]. It is well reported that when the temperature increases the PDIV decreases, with the standard [39] suggesting a maximum decrease around 17%. Temperature impacts the air density (where the discharge develops) and the materials electrical and geometrical properties. The impact of temperature on PDIV by air density and insulation

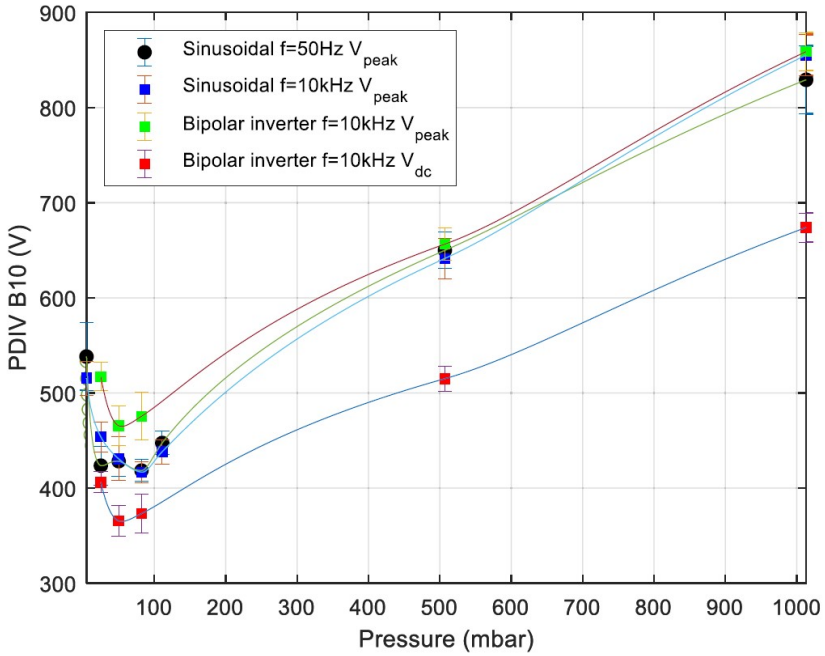

Figure 2.9: PDIV values obtained using different supply voltage waveforms as a function of pressure at room temperature. From: [86]

permittivity variation has been modeled together with the impact of the geometric characteristic on the magnet wires in [82]. The paper constructs and makes use of a predictive tool using insulation FEM models. Different predictive tools with similar characteristics have been realized by other researchers [83][84][85]. The presence of impregnating resin changes the scenario, featuring materials less stable in temperature than enamels.

More ambiguous is the impact of humidity, that varies the PDIV in non-monotonous fashion. Indeed, the humidity impacts the discharge kinetics of the air mixture, might vary the permittivity after moisture absorption and alter significantly the surface conductivity.

The impact of reduced pressures has been investigated by various research groups, e.g. in [87][88]. Identically to temperature increase, pressure reduction diminishes the air density, increasing the mean free path of the electron accelerated by the field. Hence, lower voltages are required to reach the onset of PDs. The Fig. 2.9 illustrated the PDIV as function of the pressure reduction [86]. According to [89] PD appearing at lower pressures feature lower magnitudes, as the PD pulse flattens, while the electronic temperature increases (kinetic energy of the avalanche electrons). This is concordant with other results as [90] with the PD amplitude at high frequency reducing significantly. These changes contributes to making the PD detection even more difficult.

So far, the study of EIS behavior under converter waveforms in transport sector environments remains a research niche, despite its centrality to the

successful development of electrification motors. A clear and complete phenomenology is certainly lacking, with fragmented knowledge caused by the complexity of the topic.

Chapter 3

Experimental Methods

This chapter illustrates the experimental setups, procedures, and equipment.

3.1 Samples

The samples mainly employed in the experimental activities are the models of machine insulation like twisted pairs (TP) and motorettes, other than their constituent materials. The models were produced according to the standards, for twisted pairs according to [91], for motorettes according to [92].

Twisted Pairs are model of the turn-turn insulation and are simple enameled wires twisted together. They can be impregnated, to account for the resin influence. Standard [39] states that they should not be used for qualification. To guarantee the homogeneity of the manufacturing process a custom-made machine was used for the production of all the TP tested.

Motorettes are complete insulation models that replicate the complete winding design features using the same materials and geometries, including the impregnation, creepage distances and clearances.

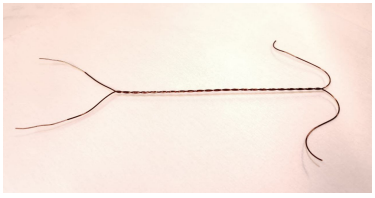

(a) Twisted pair, model of turn-turn insulation.

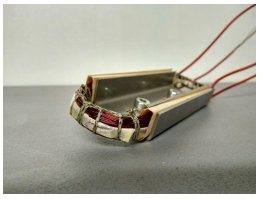

(b) Motorette, model of whole insulation systems.

Figure 3.1: Pictures of the typical samples.

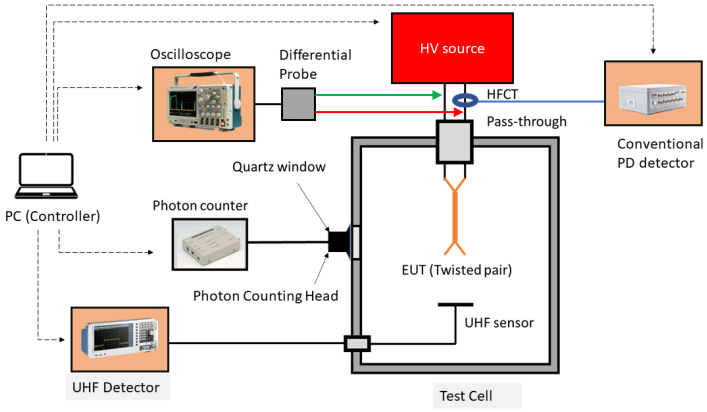

Figure 3.2: Generic setup for PDIV and endurance tests.

3.2 PDIV and Endurance Tests

3.2.1 Generic PDIV and Endurance Test Setup

The generic setup of Fig. 3.2 allows PD inception and endurance tests to be performed on twisted pairs and other insulation models like motorettes. Every test is carried out in a specific test cell where the specimen under test is located. Voltage is provided by one of the sources later described. Typically more than one PD detection instrument is connected, to be used in parallel with others to determine the inception or presence of PD activity.

The voltage was monitored with a Tektronix MDO3054D oscilloscope (four channel, 500 MHz bandwidth, 2.5 GSa/s of sampling rate) using an Agilent 10076A probe (250 MHz bandwidth, passive probe) for the non differential sources and a Tektronix THDP0200 differential probe (200 MHz bandwidth, active probe) for the differential sources. Alternatively, a Tektronix MSO54B (four channel, 1 GHz bandwidth, 6.25 GSa/s of sampling rate) was employed when larger bandwidth or sampling frequency were needed in the experiment.

Specimen Connection

The connection schemes of the samples are here explained.

Twisted Pairs The connection of the specimen to the voltage for the tests is quite straightforward in case of twisted pairs. Therein, in one extremity of the sample, where the enameled wire is not twisted, the two wires have been stripped of the insulation materials and connected one to the two poles of the voltage source.

Connection name	HV (surge)	GND	FLOAT	FLOAT
1-2	1	2	3	4
2-1	2	1	3	4
3-4	3	4	1	2
4-3	4	3	1	2

Table 3.1: Connection naming for T-T tests in motorettes.

Pressure (mbar)	Time Step (s)
100	500
150	200
1000	30

Table 3.2: Time waited for each voltage step, as function of pressure.

Motorettes For motorettes, the possible connection schemes are varied, especially for specimens with two coils in the slot. In this regard, testing of the P-G was achieved connecting both coils to the high voltage with the frame grounded. Testing of the P-P was achieved connecting to the high voltage to the top coil and the ground to the bottom one, while the frame was insulated from the ground. For specimens featuring only one coil clearly only P-G testing was possible (e.g. model of pole wounded machines).

For testing the T-T a surge generator is needed. For two coil motorettes the top coil terminals were termed 1 and 2, the bottom coil 3 and 4, enabling 4 possible T-T tests for each motorette, as illustrated in Tab. 3.1. Single coil motorettes presented only the 1 and 2 terminals. During the tests, the motorette frame was grounded, the top coil connected to the surge generator connectors 1 and 2, the bottom coil to connectors 3 and 4. The coil not connected to the source was left floating (to limit surge waveform distortions).

3.2.2 PDIV Test Procedure

Each measurement was performed by increasing the peak voltage in steps of 5–15 V every 30 seconds and the PDIV recorded as the first voltage level where PD activity occurred.

When measured, the PDEV was recorded as the first voltage in which during the decreasing voltage steps no PD activity was ever incepted along the whole step.

At reduced pressures the step time was extended inversely proportional to the air density, as reported in Tab. 3.2. Thus, if a constant ratio of seed electron generation in the air volume is hypothesized, the probability of having

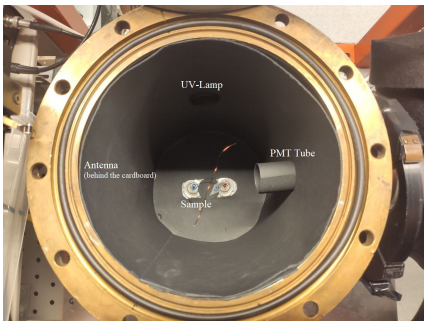

(a) Photo of the setup.

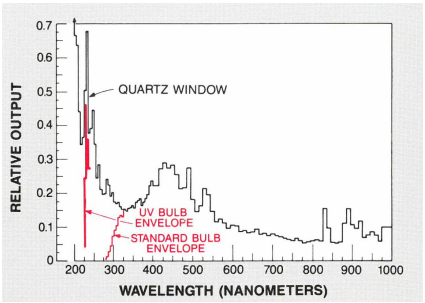

(b) Spectral output of the UV lamp employed.

Figure 3.3: UV-irradiated PDIV test setup.

a starting electron is constant for all the pressures.

The experimental results obtained for the many samples for each condition were usually fitted to a 2-parameter Weibull distribution, and the tenth percentile of the distribution (B10) was used to summarize the PDIV results.

3.2.3 Endurance Test Procedure

Endurance tests were performed monitoring the voltage applied to the sample and recording the time endured under voltage, in the chosen test cell and with the selected source. A constant voltage was applied and when a short-circuit was detected the time elapsed from the switching-on of the voltage was saved. The sensitivity for the measure of the endurance time is 1 second.

The experimental results obtained for the many samples for each condition were usually fitted to a 2-parameter Weibull distribution, and the tenth percentile of the distribution (B10) was used to summarize the endurance results.

3.2.4 PDIV Tests and Setup under UV-irradiation

Tests with ultraviolet irradiation of the samples were performed in a dedicated test cell where a UV-lamp was mounted, shown in Fig. 3.3a. The UV-lamp used is a EG&G Xenonflash nano-pulsed lamp (model FX-247) with UV bulb envelope, fed by a EG&G PS350 power supply. The flash duration lasts for around 1 μs has an energy of around 5 J and a spectral output that is reported in Fig. 3.3b. Photons energy is calculated from equation:

$$E = \frac{hc}{\lambda} \tag{3.1}$$

where h is the Planck constant and c the speed of light in the vacuum and λ the wavelength of the photon. That means that for the UV-lamp under consideration (wavelength down to 220 nm) the photon energy tops to around 5.6 eV.

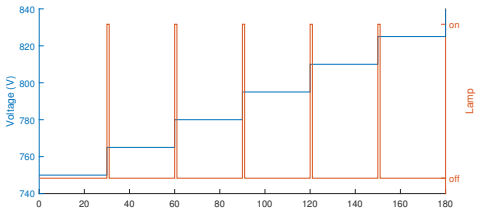

(a) Test procedure, the voltage is raised and only during the first second of the step the lamp flashes.

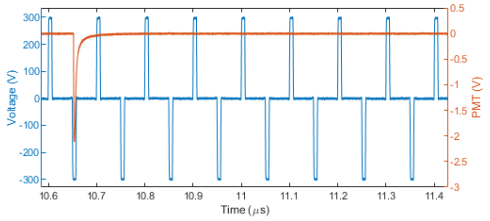

(b) Snapshoot of the UV-lamp flash (500 Hz), captured by a PMT tube, synchronized to the voltage waveform (50 kHz).

Figure 3.4: UV-irradiated PDIV test procedure.

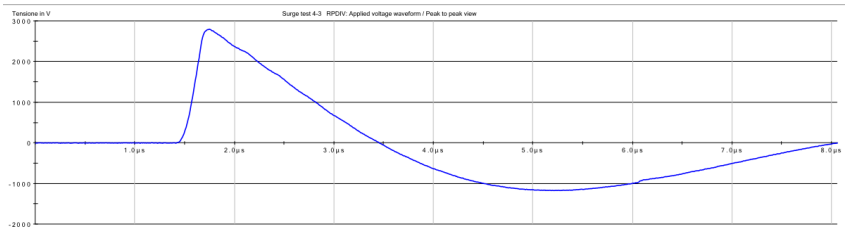

Figure 3.5: Surge waveform generated by a Schleich MTC2.

Test were conducted raising the voltage in steps as in Sec. 3.2.2, but for the first second of the step the sample was flashed, having the lamp flashing 500 times per second. The procedure is illustrated in Fig. 3.4a. The flash was synchronized with the voltage source though a digital delayer (Stanford Research System DG535), taking into account the cables and probes delays (shown in Fig. 3.4b). This ensures that the flashing occurs while the voltage is present and makes the irradiation time per step around 500 μs.

PD activity was detected in the time domain with a PMT tube in direct line of sight with the sample. The photo-multiplier tube is a Philips 56UVP, featuring a quartz window and suitable for UV detection, with 1.2 ns of rise time and 0.4 μA of dark count current. PD were simultaneously detected electromagnetically with an UHF antenna (an 8 cm monopole) connected to a Tektronix MSO64 2.5 GHz of bandwidth and 25 GS/s of sampling frequency.

3.2.5 T-T PDIV Tests with Surge Generator

Tests requiring a surge generator were carried out using a Schleich MTC2 surge generator. PD detection is achieved through the UHF detection system of the system (antenna provided with the Schleich MTC2) according to IEC 61934 [93], measuring both the PDIV and RPDIV. Background noise was below 10 mV (typically around 5 mV). The typical surge waveform is reported in Fig. 3.5. The rise time of the surge was 150 ns. Pre-conditioning was employed to

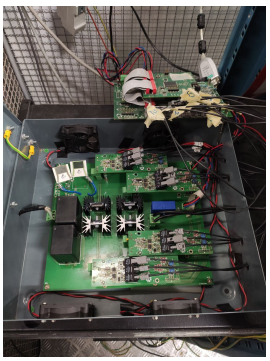

(a) Picture.

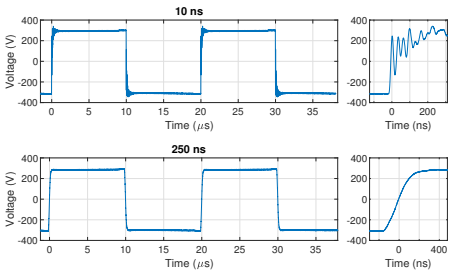

(b) Waveforms produced (different rise times).

Figure 3.6: Custom SiC-converter.

facilitate the inception of the discharges [94].

3.2.6 Voltage Sources

Subjecting the insulation systems to different voltage waveforms is crucial for understanding the impact of the various features of the stressing voltage on the insulation materials properties. Various voltage sources have been used in the experiment carried out. In the spotlight are the ones producing voltages similar to the stresses that new-generation and next-generation rotating machines can expect in operation, namely the one producing waveforms with switching frequencies in the order on tens of kilohertz, risetimes faster than 100 ns and pulse width shorter than 1 μs.

SiC converter

Wide-bandgap levels of switching frequency and rise times were obtained through a full-bridge SiC inverter designed and assembled by the University of Modena, shown in Fig. 3.6. The inverter is based on Wolfspeed C2M1000170D SiC MOSFETs (having a blocking voltage of 1700 V) and operable with compatible MOSFETS like ROHM SCT3160KLGC11 (with a lower blocking voltage of 1200 V), sometimes used as backup due to the semiconductor shortage [95].

The converter can operate with different switching frequencies in the range of 10 to 100 kHz. The rise time of the output waveform can be modified and is controlled by the gate driver resistances. The lowest rise time employed was 7 ns with a gate resistance of 27 ohm, the highest around 240 ns with 500 ohm. Combining the voltages and rise times obtainable the source can generate exceptionally high slew rates (more than 200 kV/µs). The waveforms generated present overshoots. Different rise time settings produce different overshoot factors, as can be observed in Fig. 3.6b. In the low slew rate

configuration, the overshoot is below 2% while in the high slew rate is around 20%. Due to the presence of overshoots, each result can be expressed by resorting to either the peak value or the steady part of the wave (often referred to as "DC" in the following). In this document usually the peak value is used, unless otherwise specified.

The converter can produce both 2-level and 3-level square waveforms, achieving the latter short circuiting the sample to ground.The duty cycle of the waveform can be controlled, with a lower limit for the voltage pulse width of 1.1 μs.

Due to the limitations of the switches maximum peak current, only capacitive load smaller than 1 nF could be fed by the converter.

Standard AC Voltage

For producing the 50Hz sinusoidal AC voltage a step up 220/3000 V transformer controlled on the primary side by a variable autotransformer was used. The autotransformer was manually controlled and fed by the grid.

High Frequency AC Voltage

A sinusoidal resonant power supply was used to feed the samples with AC sinusoidal waveforms with frequencies ranging from 15 kHz to 50 kHz. The source is a custom-made generator, composed of two parts. The low-voltage portion generates a square waveform of the selected frequency with a manually adjustable amplitude. Its output is then filtered and elevated by means of a high frequency transformer that also provides the inductance for the resonance with the capacitive samples.

BELKE-Based Full-Bridge

A generator based on a Belke Full-Bridge switch capable of generating square waveforms with a 100 ns rise time and a frequency up to 300 Hz was employed for tests on motorettes. The generator can produce up to 10 kV peak voltages.

Industrial SiC inverter

A three-phase inverter was used for feeding stator dummies It features silicon-carbide (SiC) MOSFET-type switches, working with up to 860V of DC-bus and implements SVPWM modulation to realize a field-oriented control. The voltage waveform produced has risetimes of about 60 ns and the switching frequency is variable up to 22.5 kHz.

3.2.7 Partial Discharge Detection

When fed with AC sinusoidal sources, classical detection of PD is usually performed, using the prescription of standard IEC 60270 [96].

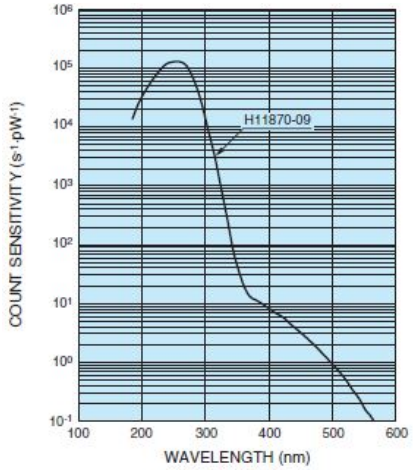

Figure 3.7: Sensitivity of the photo-multiplier head.

Under squarewave sources, the voltage pulses of the converter may interfere with the detection of the PD, as both the noise produced by the commutation and the PD signals present high frequency content. In this condition the optimal system should perform a strong suppression of the residual voltage impulse and no suppression at all of the PD pulses. Under waveforms produced by SiC-converter the frequency spectra of supply impulse and PD pulse overlaps, and detection becomes more and more difficult as rise time decreases.

In such context, the classical detection methods have been substituted with optical detection [97]. Electromagnetic detection in the high frequency domain is still attempted in parallel with the optical methods.

Conventional PD detection

As a conventional PD detection system, a PDBaseII manufactured by Techimp HQ Srl was employed. The instrument has a bandwidth of 40 MHz and a sampling rate of 200 MSa/s. The detector provides the PRPD pattern, PD pulse waveform and a T/F map, features particularly useful to distinguish discharges from noise [98][99].

A conventional ferrite-core high-frequency current transformer (HFCT) was used to sense PD signals. An external capacitor (1 nF) was connected in parallel to the twisted pairs to improve the detection sensitivity, down to 3pC.

Optical Detection

Optical partial discharge detection is achieved using a photon-counting system. The system consists of two pieces manufactured by Hamamatsu Photonics: (a) a H11870-09 photon counting head, and (b) a C8855-1 photon

counting unit. The H11870-09 photon counting head provides a binary signal (0-5V) per each photon detected. Hence, it is well suited to operate in an environment with elevated EM noise. Its count sensitivity characteristic is shown in Fig. 3.7. One of the main reasons for selecting this unit was the extremely low dark count rate (typically less than 3 pulses/s), to avoid false positives. The systems requires a complete dark environment and a direct line of sight between the discharge site and the detector to operate satisfyingly. The systems provides an information whether PD activity is incepted or not, thanks to the great signal to noise ratio.

In its basic configuration the system counts the photons in a selected gating time, therefore is capable of measuring the number of photons released every selected unit of time but does not provide the pulses time in relation with the voltage waveform. For such reason, PD amplitude and patterns can not be evaluated directly with the instrument.

UHF Detection

Emission of electromagnetic signal from PD can be found mainly in VHF and UHF bands [93][100].

In the setups built usually an antenna was placed in the test cell at around 20 cm from the sample. Given the proximity of the antenna to the test object, the system often works in the near field region and can be treated as a capacitive sensor. The signal from the antenna was probed to an acquisition instrument, like an oscilloscope or spectrum analyzer.

Typically the acquisition instrument was an Rohde& Schwarz FPC1500 spectrum analyzer. The spectrum analyzer was typically set to acquire data in the frequency range from 0.2 to 3 GHz, with a resolution bandwidth of 3 MHz and a reference level set to -20dBm. The instrument has a typical sensitivity of -165dBm and an input impedance 50 ohm. The signals were recorded with a max peak detector and traces were hold to the maximum value (“max hold” mode).

Various antennas were used, most commonly were used:

- A monopole of various length, usually 8 cm.
- A log-periodic antenna featuring an array of 17 log-spaced dipoles of increasing length and has been designed to operate in the 0.25 - 3 GHz frequency range.

3.2.8 Test cells

Different test cells were used for the experiments as tests needed to be carried out under controlled environment conditions. Each of the cells was able to withstand the test voltages and has been tested in no-load conditions to guarantee the PD absence above the testing levels, generally with sensitivity lower

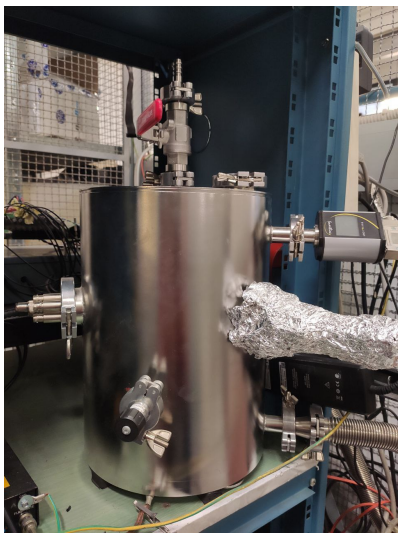

Figure 3.8: Low-pressure tank.

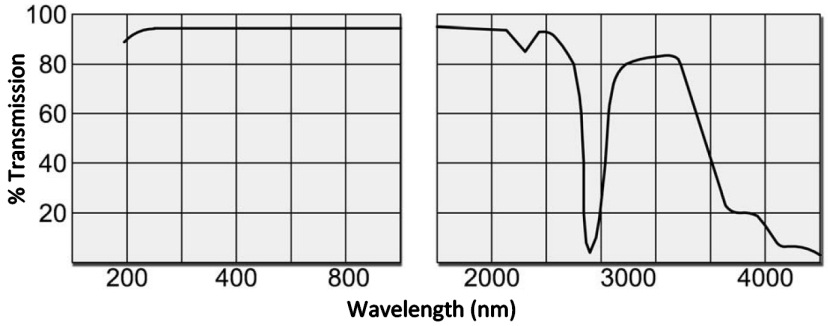

Figure 3.9: Silica windows transmission curve.

than 5 pC. The dimensions of each cell were enough to contain the samples with the appropriate clearances to avoid spurious discharges from the samples to the cell walls.

Low-Pressure Tank

To perform tests at reduced pressure a custom-made tank was employed. The cell consists of a sealed cylindrical tank (internal diameter 220 mm, height 310 mm), and is equipped with 20 kV high voltage bipolar pass-throughs on the side, three fused silica windows (two on the side and one on the bottom), other than four BNC pass-throughs. The three fused silica-glass windows are positioned around the EUT to establish optical paths from the discharge site to the photon measurement system used for PD detection. The windows have the transmission curve reported in Fig. 3.9. The selection of the transmission curve is based on evidence that partial discharges phenomena in the air emit in the UV range, particularly 300 nm to 400 nm [96]. During the test campaign,

the cell was upgraded with a purging system able to extract the unconditioned air with the humidity-controlled one drawn from a climatic chamber.

Climatic Chamber

As tests were performed also at controlled levels of temperature and humidity, a 206L climatic chamber manufactured by Angelantoni (model 200C) was employed. The climatic chamber has a temperature range -70°C to 180°C and a relative humidity range 10–95% (in the 0°C to 100°C range, with some limitation for very low values of absolute humidity). A reasonable amount of time was waited to let the sample reach steady state conditions before testing.

Oven

When only a temperature-controlled environment was needed, tests were performed inside forced-convection ovens. Many models are available in the lab, as the Galli G-Term and Thermo Scientific Heratherm Ovens, typically able to reach up to 250°C. A reasonable amount of time was waited to let the sample reach steady state conditions before testing.

Others

Experiments on larger samples (e.g. full stators) were typically carried out outside of a test cell in the laboratory room environment, that has a fairly constant temperature around the year (around 20°C) and a variable humidity depending on the season and the outside weather. Other simple test cells used consisted of an uncontrolled environment with various degrees of electromagnetic shielding or enclosed environments where the complete darkness enables the optical detection of the discharges.

3.3 Supplementary Tests

3.3.1 Surface Temperature Detection

Thermal imaging of the surface of the specimens was possible through a FLIR System P25 infrared thermo-camera. With the camera the temperature profile of the sample surface can be recorded.

The thermographic measurement depends other form the temperature also on ambient factors (distance from the sample, humidity) and the emissivity of the material under analysis. Calibration has been performed, but to avoid doubts acquisitions have been performed prior to subjecting the sample with the test conditions as comparative. Often a sample not subjected to test condition has been placed near the one under test as comparative. So, while the absolute values of the temperatures measured could be questioned (e.g.

different emissivity for the different materials), the generation of heat should not.

The camera operates in the spectral range between 7.5 and 13 μm and hence is incompatible with the use at reduced pressure with the windows of the tank of Sec. 3.2.8.

3.3.2 Dielectric Spectroscopy

The dielectric properties of materials can be investigated in the frequency range between 1×10^{-3} and 1×10^{6} Hz with a NovoControl Alpha Dielectric Analyzer, using a voltage up to 3 V rms. To reduce the noise, the instrument collects an average of three measurements. The instrument can be connected to a chamber for testing flat specimens or be used for the test of non-planar specimens.

Flat Specimens

On flat specimens testing is possible at higher voltages and different temperatures. Through the HVB4000 High Voltage Test Interface data can be collected in the range between 1×10^{-3} and 3×10^{4} Hz with a voltage up to 1 kV rms. Temperature could be set in a range from -50°C to 300°C on the sample within a nitrogen-filled chamber taking advantage of the Novocool Cryosystem heater. Typically the dielectric permittivity (both real and imaginary parts) are collected as a function of the frequency and temperature.

The instrument automatically raise the temperature and sweeps in frequency.

Full-Size Samples

On full-size specimens the measurement of dielectric properties is achieved without a fixture, connecting the sample directly to the instrument, or through connecting cables. In the latter scenario, calibration is carried out.

Capacitance and dissipation factor are typically measured instead of permittivity values, as the non-controlled geometry of the specimens forbids the instrument calculation of dielectric permittivity values. Specimens can be placed in a test cell like an oven to increase the testing temperature range or a climatic chamber to limit the impact of unforeseen ambient factors.

High Frequency

Alternatively, a Keysight 16451B Dielectric Test Fixture connected to an Agilent 4294a impedance analyzer enabled capacitance tests up to 30 MHz on films. The fixture employs the parallel plate method, which sandwiches the material between two electrodes to form a capacitor.

3.3.3 FTIR

FTIR (Fourier Transform Infrared) spectroscopy is a non-destructive technique based on infrared spectrum absorption or emission employed to evaluate chemical composition of the materials.

A Bruker Alpha was used for the tests.

3.3.4 SEM

The surface of some sample was observed using a Phenom Pro X scanning electron microscope (SEM). Samples were sputter-coated with gold prior to the examination.

3.3.5 VNA

A network analyzer was employed to measure s–parameters, transmission and reflection coefficients, characteristic impedance and propagation constant of machine models and stators.

The model employed is the Agilent E5061B, working in the frequency range 5 Hz to 3 GHz.

3.4 PDIV Prediction with Schumann Criterion based Models

The tool described in [64][82] for the prediction of the PDIV in twisted pairs model has been expanded to evaluate the inception of impregnated TP models, P-P and P-G models. The specimens have been modeled in 2-D, as their cross sections. Detailed description and theoretical foundation can be found there.

The tool is based on the Schumann criterion for partial discharge inception [101], that the electronic population $n(x)$ present at a certain distance x from x_0 after the avalanche ionization processes described by the Townsend effective ionization coefficient α_{eff} (that accounts also for attachments beside ionization) is described by [46][102]:

$$n(x) = n(x_0) \exp\left[\int_{x_0}^{x} \alpha_{eff}(x)\, dx\right] \tag{3.2}$$

Considering the existence of a critical electronic population beyond which discharge incepts n_c, that is produced in a length x_c, whose value is at maximum the distance in the gap, one obtains the more popular expression:

$$\int_{0}^{x_c} \alpha_{eff}\, dx = K \tag{3.3}$$

Many problems exist on attributing a physical meaning to the Schumann constant values K, for the micro-scale gaps here considered. Examples of this

problems are the non-exponential growth of the discharge in the early stages or the possible distortion of the electric field where the discharge develops due to space charge [45][103][104]. The constant is here simply treated as a fitting parameter, and its physical justification is not addressed.

Starting from the basic theoretical model described the tool predicts the PDIV in steps that can be divided in two main parts. Prior to the estimation of the PDIV:

1. The geometry under analysis is selected. The electrostatic problem is solved for a reference voltage, in the preferred electrostatic solver.

2. The curves for the ionization coefficient (α_{eff}) as function of the reduced electric field E/p are calculated in BOLSIG+ [105] (a Boltzmann's equation solver) using the LXCat Database [106], considering the environmental conditions. The electronic growth equation typical of Townsend avalanche growth, at the base of Eq. 3.3 is a particular case of the Boltzmann's equation [107].

These data are then imported into MATLAB. Thus, inside MATLAB an iterative calculation is performed:

1. The reference field is scaled to a new value (a tentative value for the first iteration and increasing values for the following iterations), assuming linearity.

2. The left term of Eq. 3.3 is computed using the values of $\alpha_{eff}(x)$ and $E(x)$ previously calculated for any of the electric field lines.

3. It is verified if the Eq. 3.3 is satisfied for at least one field line. If this happens, the PDIV is found, otherwise the steps are repeated with an higher voltage (typically increased of 1 V).

This general algorithm has been implemented for modeling impregnated TP, P-P insulation and P-G insulation.

3.4.1 Prediction of impregnated T-T

The tool for prediction of PDIV of impregnated TP has been realized porting the FEM from COMSOL Multiphysics to FEMM [108], for solving the electrostatic problem. FEMM is a software free from licensing.

The geometry employed is in Fig. 3.10, is representative of the insulation of a TP with an extra insulation layer given by the impregnation resin. From the figure is also evident the limitation of the design of the region where the wires contact, here modeled with a cusp. Some experiments have been carried out rounding the cusp, but ultimately this does not impact the field distribution where typically the critical discharge line appears. The model has been kept in this version to simplify the geometry import in MATLAB.

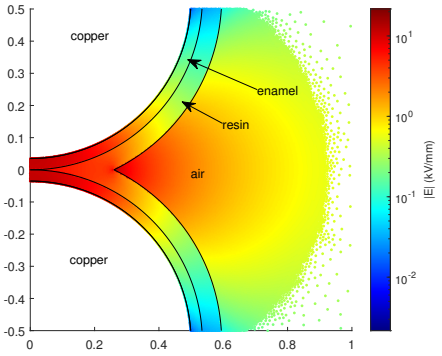

Figure 3.10: Geometry and electric field distribution at 800 V_{pk} for the impregnated twisted pair model.

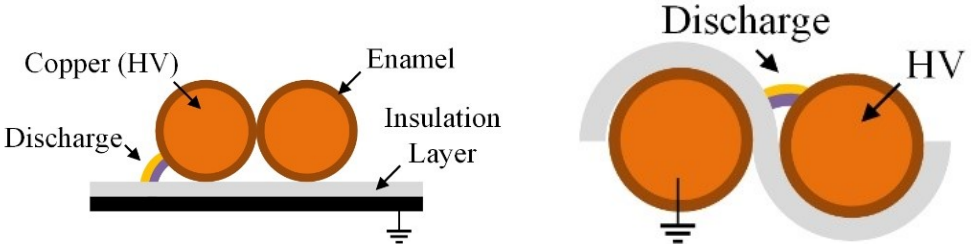

(a) P-G (b) P-P

Figure 3.11: Modeled geometries.

Relevant changes start to appear when the curvature radio is increased to the point where the resin region increases the thickness where the critical line would appear.

For the PDIV prediction the value $K = 6$ found in [64][82] has been used.

3.4.2 P-P and P-G

The selection of the geometry is a critical portion of the modeling. While the selection of the P-G one is quite straightforward, the one for the P-P is more complicated. After some iteration the geometries of Fig. 3.11 has been selected, representing the worst case where conductors are tightly packed. Other arrangements for the P-P considered the wires tangent to a flat paper surface, and predicted higher PDIV.

The tool has been used in first place to calculate the Schumann constant K, starting from PDIV values. In this scenario the second part of the algorithm is substituted with the following:

1. The reference field is scaled to the PDIV.

2. The left term of Eq. 3.3 is computed for any of the electric field lines

using the proper values of $\alpha_{eff}(x)$ and the values of $E(x)$ calculated from the PDIV. A set of K values is found, one for each field line.

3. The maximum K is the one that produces the highest number of critical carriers, hence the candidate for the PD inception. This is justified by the idea that if a lower K had triggered the discharge, that would have happened at lower voltages.

In second instance the tool has been used as prediction tool, with the same procedure described in the previous paragraph.

Chapter 4

Electrical Endurance under Partial Discharge Activity

This chapter illustrates the investigation on the endurance under partial discharge activity of turn-turn insulation models in the typical operating conditions of machines for current and next-gen electrical transportation vehicles as more electric aircraft and high-performance electric vehicle.

As noted earlier in Chap. 2, the qualification of a machine to operate under converter-produced voltages can be accomplished through two paths: designing the machine to work in the presence of partial discharge activity or in the absence of such, situation regulated by standards IEC60034-18-41 [39] and IEC60034-18-42 [52] respectively.

With the increase of the stresses in the T-T subsystem stresses due to the new WBG converters and the push for ambitious DC bus voltage levels the insulation thickness might not be sufficient to operate the machine above the PDIV and ensure the desired reliability. It is unclear if the qualification through the IEC60034-18-42 is a practical or even feasible approach. A detailed study of the endurance times under partial discharge activity for various materials, both corona-resistant and organic only types is crucial for doing so. Important is the contribution of thermal aging and environmental factors like pressure and humidity. Furthermore, the study is helpful in providing the margins of the insulation life if sporadic PD activity appears (e.g. failure driven transients) even when the qualification is carried out according to IEC60034-18-41.

The particularly challenging operation conditions of in MEA and EV sector will be thoroughly explored.

The results will be detailed in the chapter, but their discussion in a broader perspective will be performed in Chap. 6.

4.1 Combined Impact of Low-Pressure and Next-Gen Voltages Level on PD Endurance

The need to operate electrical systems in a reduced-pressure environment is critical. At low pressure, the dielectric strength of the air is reduced, and preventing PD inception becomes challenging. At the same time, the waveforms of the converters increase the electrical stresses. As PD activity strongly affects the life of an insulation system, especially if the system is composed of purely organic dielectrics, it is critical to estimate the performance increase achievable from these materials.

This section will focus on the feasibility of employing corona-resistant insulation in MEA applications at reduced pressures, exploring the validity of different materials at various voltage levels. To unravel the withstand capability of CR insulation systems in the MEA, electrical endurance tests were carried out above the PDIV and at voltages typical of MEA drive systems, simulating the atmospheric conditions of a machine operated at sea level, but also at higher terrestrial elevation and in flight. In addition, PDIV tests were performed to find any improvement in the inception voltages given by such materials.

Samples

Tests were performed on freshly manufactured twisted pairs, produced in accordance with [91]. For the wires dimensions selected the standard prescribes twisting the winding wires with 12 rotations while applying a load of 7 N. The wires used in the following experiment are:

- **NCRW** Non-Corona-Resistant winding wire with enamel composed of a basecoat in THEIC-modified polyester or polyesterimide and overcoat of polyamide-imide. It features a diameter of 0.56 mm and grade 2 insulation, with thermal index of 200°C.
- **CRW** Corona-resistant version of NCR, containing inorganic nanoparticles. It features a diameter of 0.56 mm and grade 2 insulation, with thermal index of 200°C.
- **CRW2** Corona-resistant modified polyesterimide plus polyamide imide enamel. It features a diameter of 0.56 mm and grade 2 insulation, with thermal index of 200°C.
- **CRW3** Corona-resistant wire featuring a diameter of 0.63 mm and grade 2 insulation, with thermal index of 200°C.

The CRW and NCRW wires are from the same manufacturer. The CRW2 and CRW3 from two other different manufacturers.

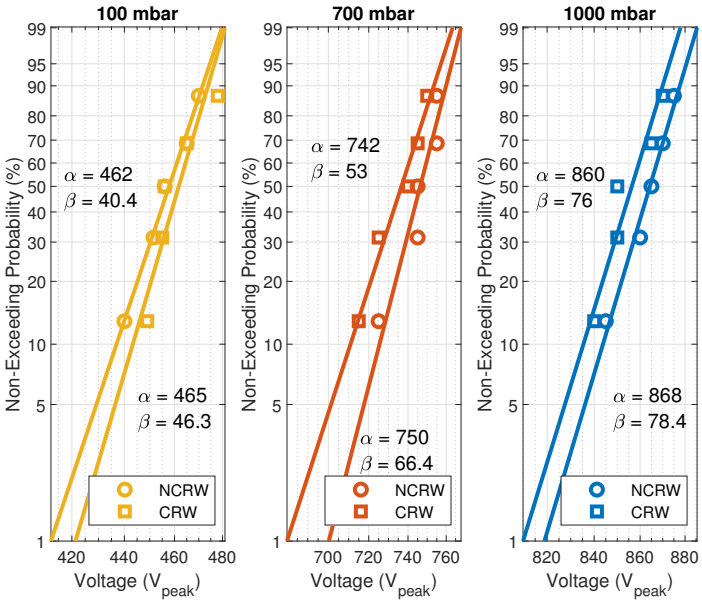

Figure 4.1: Weibull plots of the measured values of PDIV various pressures for neat (NCR) and Corona Resistant (CR) wires, under AC 50 Hz sinusoidal voltage.

4.1.1 Pressure Reduction Impact

To investigate the endurance of inter-turn insulation under wide-bandgap converters waveforms as ambient pressure decreases, twisted pairs model were tested in a vacuum chamber with pressures of 1000 mbar, 700 mbar and 100 mbar. They respectively correspond to sea level, 3000 meters and 15000 meters altitude. Those values are representative of different operating conditions: the standard ground level, the high terrestrial altitudes that also electric vehicles could access (plateaus and mountains), and the maximum altitude for component qualification of an airliner [109]. Five samples for each test condition were subjected to the voltage produced by the SiC converter described in section 3.2.6, with a bipolar 2-level waveform. The switching frequency was set to 100 kHz and the rise time to 12 ns, causing an overshoot varying from 20% to 30% depending on the voltage level. A stressing voltage of 1080 V_{pk} was derived considering the standard DC bus voltage used in the MEA (540 V) and a reflection factor at the motor terminals of 2. Although this approach is highly simplified (the actual propagation of the voltage wave with the winding and the common-mode potential of the star point were not considered), the same number can be achieved considering future generation DC bus voltages (800 or 1000 V), a milder reflection factor and proper propagation calculation.

A preliminary measurement of the PDIV under sinusoidal voltage at grid frequency was carried out to investigate differences in the inception among the CR and NCR wires (as described in section 3.2.2).

Material	Pressure	Life		
		α	β	B10
	(mbar)	(s)	(-)	(s)
CRW	100	6	3.4	3
NCRW	100	1	∞	1
CRW	700	765	4.6	471
NCRW	700	414	22.8	375
CRW	1000	9640	2.6	4081
NCRW	1000	545	28.9	494

Table 4.1: Endurance times Weibull distribution fitting parameters for various pressures.

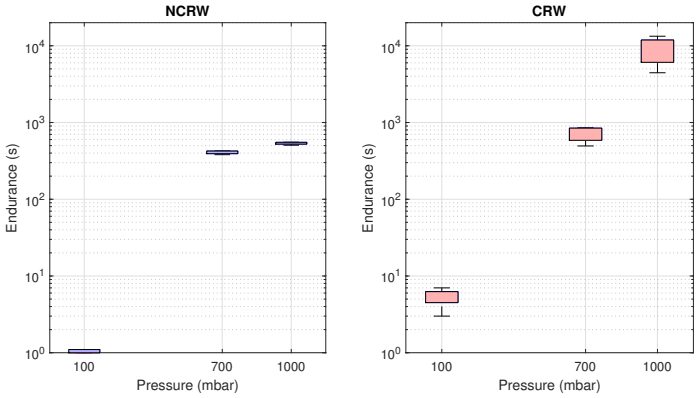

Figure 4.2: Endurance times of NCR and CR wires under 1080 V_{pk} 100 kHz SiC-converter bipolar 2-level waveform for various pressures.

Results of the PDIV, as displayed in the Weibull charts of Fig.4.1, show little variation between the two versions of the wires. Hence, an improvement in the inception voltage by the corona resistance might, as expectable ruled out. Indeed, no macroscopic dielectric property that impacts the inception voltage is usually altered significantly with the addition of nanoparticles.

The results of five samples per condition for the endurance tests of the NCRW and CRW wires are illustrated in Fig. 4.2 as boxplots. The test were conducted as described in section 3.2.3. The data have also been fitted in a Weibull distribution and the tenth percentile (B10) of the distribution obtained is summarized in Tab. 4.1.

As the ratio of the stressing voltage and PDIV is the same for the two wires, the performance boost given by nano-fillers can be easily assessed for any voltage level without any additional calculation. As expected, a performance increase can be observed in the endurance times from nano-filled materials at any pressure level. The striking observation is that as the pressure decreases to the levels of airline qualification the endurance times drop to values in the

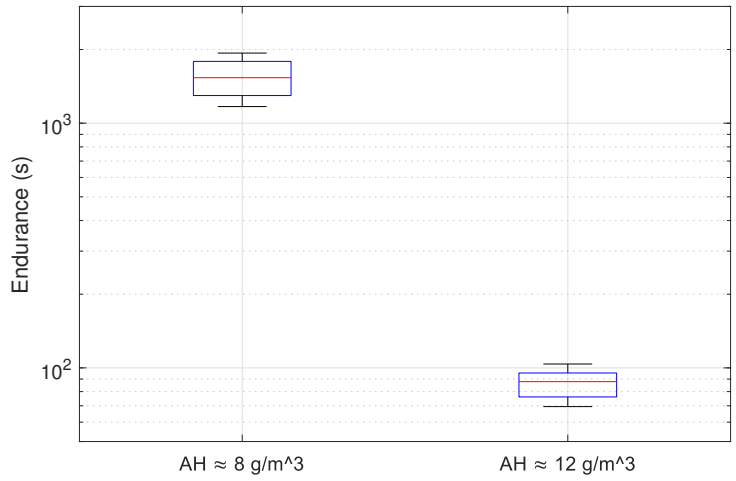

Figure 4.3: Impact of moisture content (as absolute humidity) on the endurance times of wires subjected to bipolar converter waveforms at 150 mbar for stressing voltages equal to 756 V_{pk}.

order of seconds, wherein is negligible difference between CRW and NCRW samples. It must be reminded that the critical condition under exam is the one representing an approximation of the worst case for real operations for future bus DC. Otherwise, for terrestrial altitudes, a significant reduction of the endurance times is recorded at for 3000 m, envisaging problems also for the automotive sector. At sea level altitudes the reduction is far from the critical values observed for the aircraft systems.

Additionally, it should be highlighted the increase in the endurance of CRW samples comes also with a wider variance, showing a larger in-homogeneity of the corona resistance capability of the wire, for all the pressure levels. This can also be noticed in the much lower β of the Weibull distribution in Tab. 4.1.

A change in the discharge mechanism as the pressure decreases can be deduced by a simple visual inspection of the samples during the tests. At room pressure the discharge is visible only in a completely dark environment and discharges are clustered at some spots. At 100 mbar the discharge is visible even in daylight and appears to cover the entire length of the specimen. It is hypothesized that as the pressure drops, the PD mechanism shifts from streamer-like to pseudo-glow-like discharge.

4.1.2 Air-Moisture Content Impact

The role of moisture content has been singled out clustering results for CRW samples obtained in different days, when relative humidity was variable. The endurance tests were conducted as described in section 3.2.3, with 5 specimens

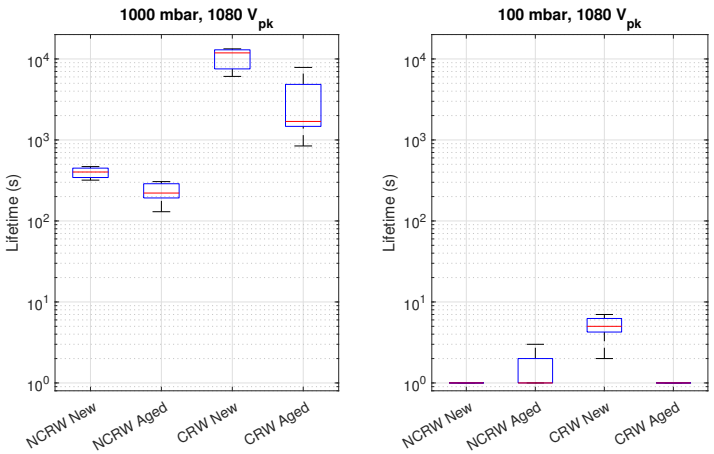

Figure 4.4: Endurance times of pristine and aged wires under 1080 V_{pk} SiC-converter bipolar waveform at 1 bar and 100 mbar.

per condition. The pressure was set to 150 mbar and the voltage to 756 V_{pk} (around 40% higher than the PDIV of the wire). The tests have been executed under the 2-level bipolar voltage produced by the SiC inverter discussed in section 3.2.6. The switching frequencies was set to 50 kHz and the rise time to 200 ns.

What can be clearly seen in the Fig. 4.3 is that moisture content has a dramatic effect on the reduction of endurance times, reducing the times over one order of magnitude as the water quantity increases from 8 g/m^3 to 12 g/m^3, values corresponding roughly to 35% and 50% of relative humidity at 25°C and 1000 mbar.

Likely, the polymer chain physically eroded by the electron bombardment reacts with the water molecules. The reaction causes polymer chain scission, further increasing the degradation ratio and explaining the accelerated failures [110].

4.1.3 Aging Impact

Pristine samples from the NCRW and CRW batches were aged with a single aging cycle with a duration of 340 h, at a constant isothermal stressing condition of 230°C (30°C higher than the thermal index of the enamel), placing the specimen in a ventilated oven. Endurance tests were performed on 5 samples for unaged and aged samples at pressures of 1000 and 100 mbar, under the same conditions discussed in the section 4.1.1. The results are reported in 4.4, as boxplots.

Aging appears to impact the variance of the results, further increasing the spread of the endurance results. More importantly, the tests at ambient pressure show that the endurance of the CRW samples drops of 85% after aging compared to the NCRW that drops of 60%. At 100 mbar, endurance

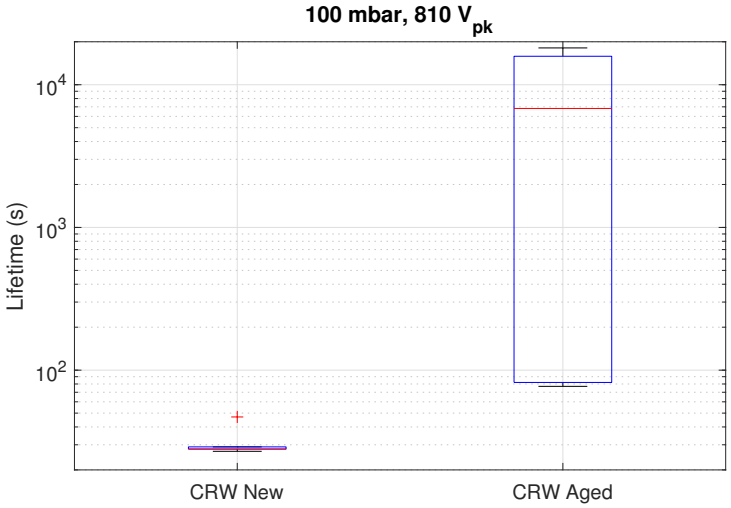

Figure 4.5: Endurance times of pristine and aged wires under 810 V_{pk} SiC-converter bipolar waveform at 100 mbar.

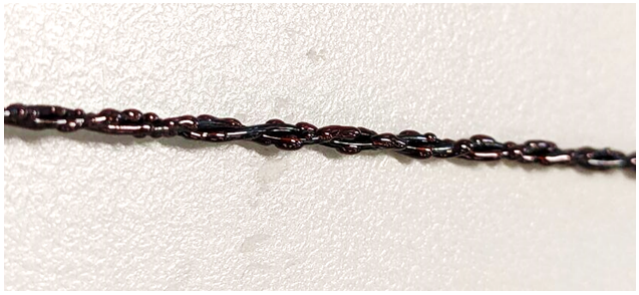

Figure 4.6: Picture of the swollen insulation of a thermally aged corona-resistant wire after PD bombardment.

is too brief to perform a similar estimation. The results obtained simply emphasize the ineffectiveness of CR materials in these conditions, especially after the materials aging.

Reducing the stressing voltage to 810 V_{pk}, as observable in Fig. 4.5, led to higher lifetimes in the order of minutes. Unfortunately the values achieved still remaining incompatible with the operation. Furthermore, strangely longer failure times were achieved by the thermally-aged corona-resistant materials compared to its unaged version. The finding could be explained looking at failed sample (Fig. 4.6), that presents a swollen and dark insulation. It is possible that carbonized by-products released by the enamel were able to suppress the discharge in the sites where PD were more active. At any rate, these conditions of the insulation are too concerning regarding its mechanical integrity and capability to operate in the motor to consider this behavior as a positive result. Ultimately, aging seems to play an important role in further reducing the capability of the materials to resist PD activity.

4.1.4 Converter Voltages Impact

To estimate the impact of the WBG-converter waveforms on the reduction of the endurance times under partial discharge comparative tests with high frequency AC voltages, different rise times and various voltage levels have been carried out at reduced pressure. Eventually, life curves have been computed.

The voltage range explored has been selected to represent a next generation drive system (800 and 1000 V), or even present 540 V drive systems that allow for DC bus transients. Indeed, the bus system of an aircraft is sometimes designed to operate at higher voltage levels for a fraction of its operation time.

The stressing voltages to be applied to the samples correspond to the turn-to-turn stresses appearing on a machine where overshoot at the terminals appears. These tests consider the worst case for a bipolar 2-level converter, where all the jump voltage (2/3 of the phase-ground voltage) drops on the first turn of the insulation, and the first and last and turn lay adjacent. Examples of such set of voltages are:

- 756 V_{pk}, corresponding to the stress produced by a bus DC of 540 V when the overshoot at the terminals is 100%
- 700, 840 and 1120 V_{pk}, corresponding to the stress produced by a bus DC of 800 V, when the overshoot at the terminals is respectively 25%, 50% and 100%
- 700, 875, 1050 and 1400 V_{pk}, corresponding to the stress produced by a bus DC of 1000 V, when the overshoot at the terminals is respectively 0%, 25%, 50% and 100%

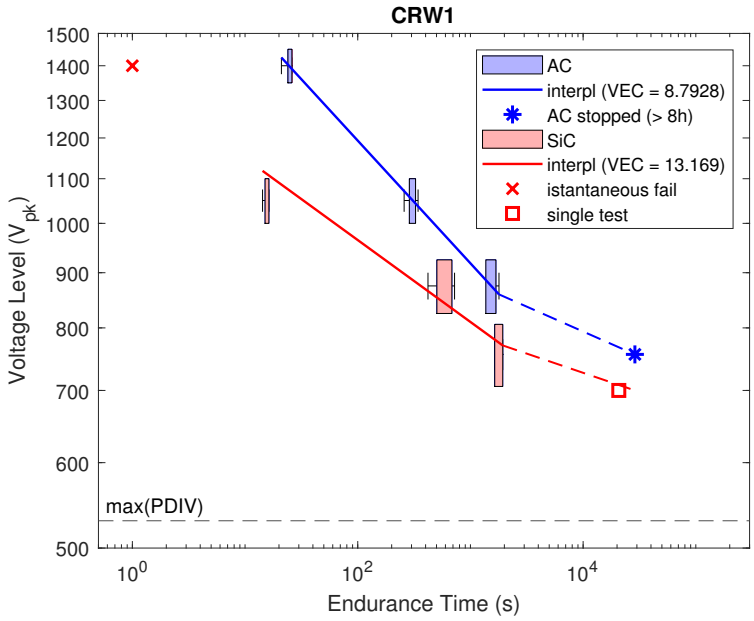

Figure 4.7: Endurance times of CRW corona resistant wires at various voltage levels (boxplots) and life lines estimations, at 150 mbar.

Fast Switching Waveforms

Comparative measurements with a sinusoidal and square-shaped source were performed with the same fundamental frequency of 50 kHz at 150 mbar. The pressure selected corresponds to a cruising altitude of 13.5 km, the typical maximal working altitude for airliners, despite the qualification altitude being set to 100 mbar [109][77].

Endurance tests were performed at 700, 756, 875, 1050 and 1400 V_{pk} according the procedure of 3.2.3. For tests in AC, a sinusoidal resonant power supply (described in section 3.2.6) was used. In pulsed conditions, the SiC inverter of section 3.2.6 was employed, set to generate a bipolar 2-level waveform with rise time of 200 ns. The inverter waveform presented an overshoot factor of 10%. Temperature and humidity were monitored before each test and the results here shown have been collected for the temperature and absolute humidity ranges of 20–25°C and 8–10 g/m3 (corresponding to 35–45% RH at 25°C, 1 bar).

Six samples were tested for their endurance in each condition, according to the procedure of section 3.2.3. For tests longer than 5 h only one point was collected and for tests longer than 8 h the measure was stopped. A preliminary measurement of the PDIV was carried out to verify whether the voltages applied during endurance tests were sufficient to incept PD in the twisted pairs. A conventional 50 Hz sinusoidal supply was used for this scope.

As illustrated in Fig. 4.7, tests run in AC resulted in longer lifetimes, when compared to the results obtained when using a pulsed supply, as also

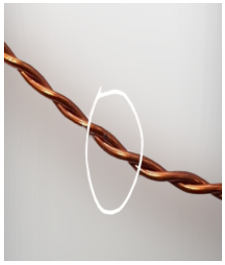

(a) Pitting, test performed at 875 V in AC.

(b) Burnt, test performed at 1400 V in AC.

Figure 4.8: Failure mechanisms typologies.

previously observed by other authors [111]. Tests in AC at lower voltages were censored after 8 h of endurance, and none of the tested specimens failed within such period. This confirms that the degradation rate on insulation systems due to PD activity is increased when voltage waveforms with fast slew rates are applied.

To extrapolate the time to failures for other voltages than the ones investigated, results were further processed fitting an inverse power law, often used to model life of an insulation [40]:

$$L = A * V^{-n} \tag{4.1}$$

where L represents the time to failure (the life of the material), V the applied voltage, n the Voltage Endurance Coefficient (VEC) and A is a proportionality factor.

As the stressing voltage peak increases, the higher electric field in the air causes a higher number of ionization and excitation events, generating larger electron avalanches and higher PD magnitudes. Consequently, the damage per unit time increases and the erosive power due to DEA process is enhanced accordingly. A closer inspection of the results seems to indicate that when the stressing voltage is reduced, the VEC decreases. Depending on the voltage level, two different regions might be envisaged, corresponding to high and moderate degradation rates (thus high and low VEC, respectively) possibly linked to the variation of the discharge characteristics.

A partial confirmation comes from the visual inspection of the failed wires. Under sinusoidal waveforms the breakdown point is punctual (Fig. 4.8a) up to 1050 V and then at 1400 V the discharge transits to a more dispersed activity that also appear to thermally degrades the insulation (Fig. 4.8b). Differently, for the converter waveform the transition occurs earlier, between 756 V and 875 V. This does not match exactly with the variation of the VEC reported in Fig. 4.7, but shows that above a certain threshold the energy of the discharge is enough to generate heat to burn the enamel.

An analysis of the surface temperature of the twisted pairs was carried

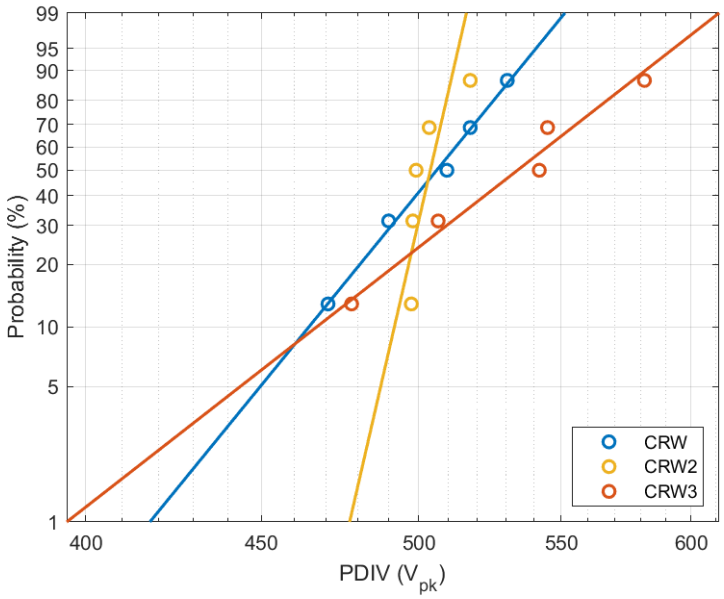

Figure 4.9: Weibull plots for PDIV of the CR wires under comparison (under AC sinusoidal 50 Hz voltage).

out using a thermal-imaging camera (see section 3.3.1) at 1000 mbar. The procedure was performed only at ambient pressure, since the thermal camera operates with wavelengths in the range 7.5 μm to 13 μm while the fused silica windows in the vacuum cell do not transmit radiation with wavelength above 4 μm. It was observed that below the PDIV the temperature of the specimens did not increase significantly, while with discharge incepted and the voltage set to 1080 V, the surface temperature was 62°C, over 40°C above the ambient one. It is likely that at reduced pressures the phenomenon is greatly enhanced, the burning is a marker of such hypothesis (temperatures around 300°C can be indirectly assumed). The observation might helps justifying the short endurance time recorded, as the plasma that compose the discharge activity clearly increases in energy as the pressure diminishes and the voltage increases.

Comparative of different CR Materials In the same identical test condition of Fig. 4.7 tests have been performed on CRW2 and CRW3 samples, in an attempt to generalize the results for different CR technology implementations by various manufacturers. The two share a similar PDIV to CRW wire, as Fig. 4.9 shows.

Indeed, as clear from the comparison of Fig. 4.10 with Fig. 4.7, the discussion made for CRW can be generalized for all wires sharing similar diameters. The numbers obtained for these wires are similar to the ones of CRW, suggesting that the findings are a good representation of the current

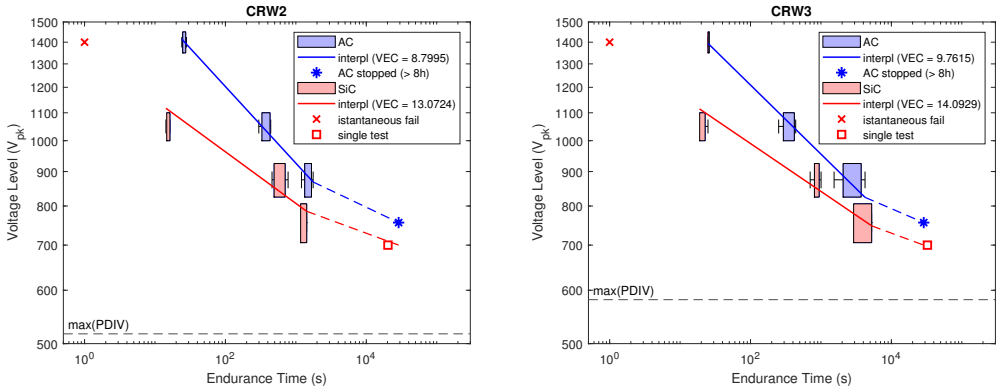

(a) CRW2 (b) CRW3

Figure 4.10: Endurance times of corona resistant wires (CRW2 and CRW3) at various voltage levels (boxplots) and life lines estimations, at 150 mbar.

Wire type	Pressure	Rise time	$PDIV_{pk}$	$PDIV_{DC}$	Photons per second
NCRW	1000	12	880	732	$(1–2)\times10^5$
NCRW	1000	237	797	780	$(1–3)\times10^4$
CRW	1000	12	881	731	$(1–2)\times10^5$
CRW	1000	237	787	770	$(1–3)\times10^4$
NCRW	100	12	555	424	$>1\times10^6$
NCRW	100	237	421	411	$>1\times10^6$
CRW	100	12	558	426	$>1\times10^6$
CRW	100	237	433	422	$>1\times10^6$

Table 4.2: PDIV results for CRW and NCRW, comprehensive of the detected photons repetition rate.

CR technology.

Rise Time Impact

Under converter voltage impulses, PD pulse magnitude increases as the voltage pulses get steeper, and their frequency content is shifted to higher frequency ranges [65], increasing the degradation rate of the insulation system. Besides, it is possible that the large frequency content has an influence on the PDIV itself. PDIV and endurance have been investigated when shortening the rise time for CRW and NCRW wires.

Experimental results of PDIV measurements with different rise times on NCRW and CR samples can be found in Tab. 4.2 for 1000 mbar and 100 mbar, that also reports the photon repetition rate. Test were carried out on five samples under the voltage of the SiC converter of section 3.2.6, with the procedure of section 3.2.2. The experiment were conducted at 100 kHz

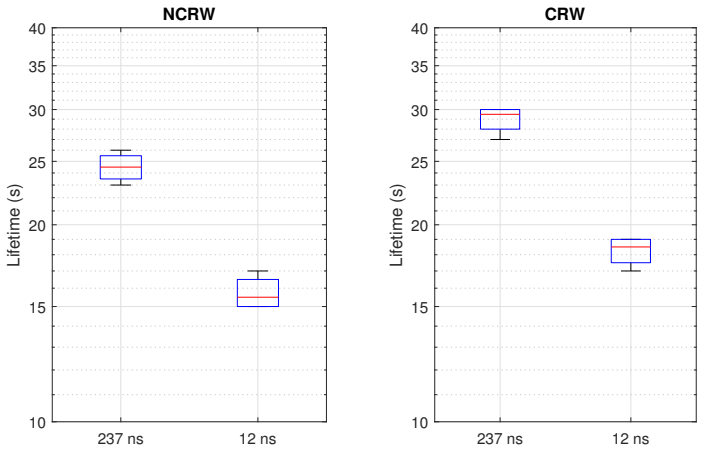

Figure 4.11: Endurance of twisted pairs, NCRW and CRW, for waveforms with same peak value but different rise time.

of switching frequency. When the rise time is decreased from 237 to 12 ns, PDIV levels increase from about 790 V_{pk} to 880 V_{pk} for both NCRW and CRW materials. This positive result, however, can be possibly explained considering that two conditions must be met in order for PD to incept: (a) a minimum voltage must be provided that can produce a field greater than the ionization field in the medium, and (b) a starting electron must become available. Both conditions may not be met in the very brief time at which the waveform is at its peak. A thorough analysis of the process is postponed to the following chapters. Anyway, a higher peak value of the PDIV may be attained as consequence, as the increase of the DC bus voltage increases the duration of the periods at which the waveform is above the inception field level. Indeed, the DC bus voltage at inception has the opposite trend, varying mildly or worsening as the rise time decreases.

It is worthwhile noting from the results at atmospheric pressure that the photon count rate is higher for tests with faster rise times, increasing of an order of magnitude from 10^4 to 10^5 photons per second. This finding corroborates the idea that once the discharge is started the number of carriers released in the avalanche is linked to the peak of the voltage waveform and not the DC bus level. For this reason, subsequent experiments with different rise times were performed at the same peak voltage. At reduced pressure the saturation of the detector does not enables the same comparison.

The following endurance test results shown in Tab. 4.3 uncover the consequences of fast switching on endurance. The data were collected at 100 mbar according the procedure of section 3.2.3 on five samples per condition, under the voltage waveform from the SiC-converter of section 3.2.6. The converter produced 2-level bipolar voltage switching at 100 kHz with a peak of 840 V. The results demonstrate that, although testing at a lower DC bus voltage,

Material	Pressure	Applied Voltage		Rise time	Life		
					α	β	B10
	(mbar)	(V_{pk})	(V_{DC})	(ns)	(s)	(-)	(s)
NCRW	100	840	825	237	23	25	22
NCRW	100	840	700	12	15	16	14
CRW	100	840	825	237	27	30	27
CRW	100	840	700	12	17	19	16

Table 4.3: Weibull fit parameters for the endurance of twisted pairs under waveforms with different rise times. Test conducted with same peak value on NCRW and CRW samples at 100 mbar.

the use of modern WBG semiconductors, reduces significantly the life of the insulation (in these results by around 50%), exacerbating the problematic.

A life curve at low pressure (100 mbar) for the most extreme converter conditions achievable (100 kHz of switching frequency and 12 ns of rise time) has been traced from the experimental data of Tab. 4.4, in Fig. 4.12. In this regard endurance tests have been carried out at 1120, 840 and 700 V under bipolar 2-level voltages.

The CRW and NCRW wires share similar values of endurance time within the voltage range explored, which are too short to guarantee operation in presence of PD activity. The results clearly show that in the harshest MEA conditions, considering transient voltages or next-generation DC bus levels (800 and 1000 V) CR wires can hardly assist the insulation designer.

4.1.5 Summary

Key Findings

- Under combined conditions of higher altitudes and SiC-waveforms stresses (square waveform, bipolar, 2-level, 12 ns of rise time and 100 kHz of switching frequency, $1080V_{pk}$) CR wires behave more similarly to non-CR ones. At 1000 mbar (0 m) CR endurance is more than tenfold non-CR, at 700 mbar (3 km) is around the double at 100-150 mbar (13-15 km) the same.
- Waveform with shorter rise times (higher overshoots) cause higher degradation rates, at the same peak value. The same happens under converter waveform compared to AC ones (with same frequency and peak value).
- Three different CR wires showed comparable results.

Material	Pressure	Applied Voltage	Rise time	Life		
				α	β	B10
	(mbar)	(V_{pk})	(ns)	(s)	(-)	(s)
NCRW	100	1120	12	1	∞	1
NCRW	100	840	12	16	23	15
NCRW	100	700	12	155	13	131
CRW	100	1120	12	6	14	5
CRW	100	840	12	19	24	17
CRW	100	700	12	192	15	165

Table 4.4: Endurance times Weibull distribution fitting parameters for various voltage levels and the harshest condition (at 100 mbar stressed by a bipolar 2-level voltage featuring 100 kHz of switching frequency and 12 ns of rise time).

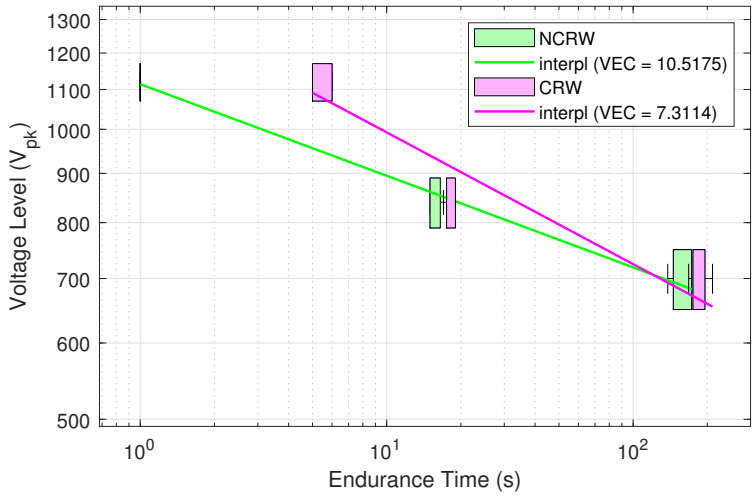

Figure 4.12: Endurance times at various voltage levels (boxplots) and life curves estimation for neat (NCRW) and corona resistant (CRW) wires, for the harshest condition (at 100 mbar stressed by a bipolar 2-level voltage featuring 100 kHz of switching frequency and 12 ns of rise time).

Figure 4.13: Picture of the Litz wire sample.

- In the mentioned conditions, the moisture content appears to reduce the endurance times of one order of magnitude.

4.2 Partial Discharge Endurance on High Performance Multistrand Wires

In this section the endurance of non-corona-resistant enamels for high performance traction motors is tested. The capability for insulation to withstand PD activity at voltage levels near the PDIV is investigated and quantified, to understand if a machine featuring organic insulation can allow the presence of discharges for a limited amount of time (i.e. during transients). Test featuring waveforms approximating the real turn-turn stress completed the campaign. The analysis provides the margins that the insulation designer can expect from the organic materials with thicknesses around 50 μm, typical of multistrand wires (i.e. Litz wires).

Samples

Twisted samples were obtained twisting two stranded Litz wire together. The Litz wire is composed of 12 enameled sub-conductors, each with a diameter of 0.35 mm and featuring a GR3 insulation. A picture of the specimen is in Fig. 4.13.

4.2.1 Temperature Effect

Endurance tests were performed at room temperature (25°C), 120°C and 180°C for five specimens in each condition, according the procedure of Sec. 3.2.3. The SiC converter of section 3.2.6 was used to feed the samples with a voltage exceeding the sample PDIV of 5% for each temperature. The bipolar 2-level stressing voltage waveform featured 250 ns of rise time and 50 kHz of switching frequency.

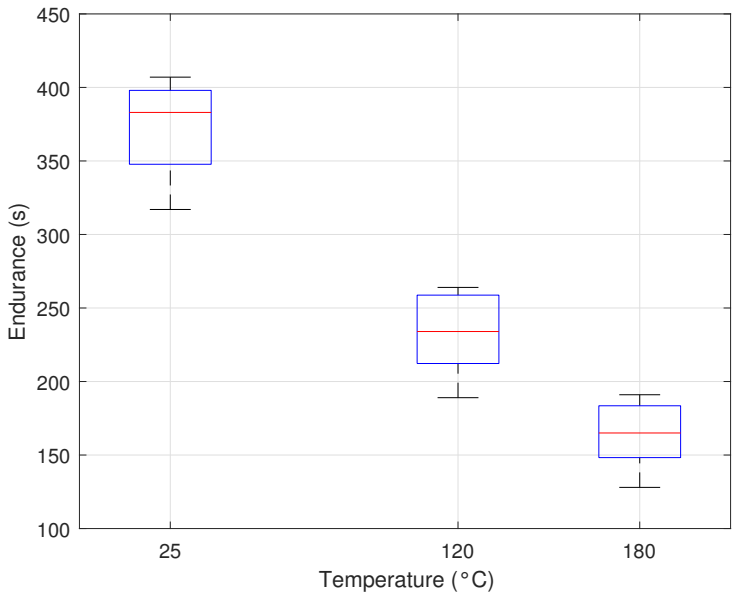

Figure 4.14: Endurance at voltages 5% above the PDIV, as trend of the temperature.

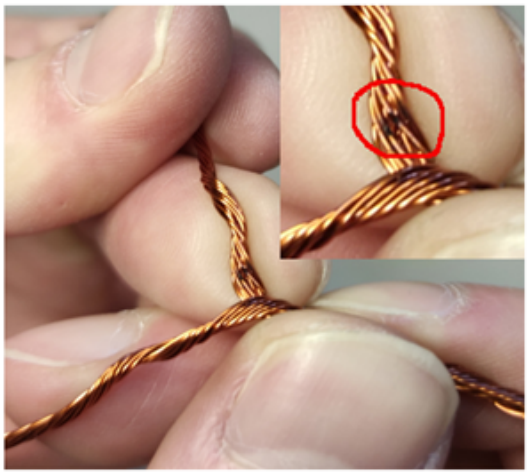

Figure 4.15: Picture of the failure site, caused by puncturing of the insulation by PD.

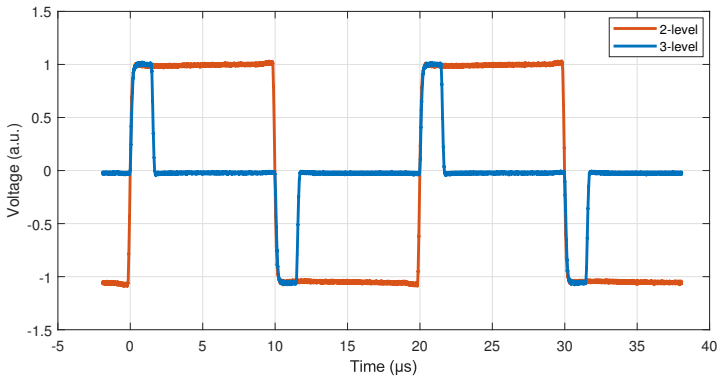

Figure 4.16: Two-level and three-level waveforms produced by a SiC converter employed for PD endurance tests.

Figure 4.14 shows the gradual decrease of endurance as the testing temperature increases. What stands out is the overall brief time to failure of the samples. The material analyzed proved to be very sensitive to the presence of PD, as the time to failure remains in the range of minutes even at room temperature with minor overvoltage with respect to the PDIV.

During the tests, temperature monitoring of the specimens using an IR thermal-imaging camera (section 3.3.1) revealed a gradual increase of surface temperature after PD initiation (e.g. just before the breakdown the samples tested at 180°C reached a temperature of 195°C). The heat generated increases more rapidly approaching the failure, possibly indicating an exacerbation of the discharge degradation ratio. To verify that the leading breakdown mechanism was electrical rather than thermal, the specimens were tested with a voltage marginally lower than the PDIV at 180°C. PD absence was checked though UHF detection. The samples did not reach breakdown even after hours, as no appreciable increase in temperature was recorded, ruling out thermal instability breakdown mechanisms. Also, after PD erosion, the failure site of the specimen was easily detectable (see Fig. 4.15).

In light of the measurement it can be asserted that the minor overvoltage is sufficient to incept the discharge along the whole sample and not only in the spots corresponding to the weakest points of the insulation.

4.2.2 3-level Waveform Impact

The turn-turn electrical stress generated in the stator of the machine by a converter reaches its maximum at the flanks of the phase-to-ground square voltage waveforms, as mentioned in Sec. 2.2.1. The best approximation of such stress for testing the insulation is a 3-level bipolar square wave voltage, instead of the typical used 2-level one. The positive and negative parts of the waveform correspond to the positive and negative flanks, respectively.

The endurance time under such waveform was surveyed and the result

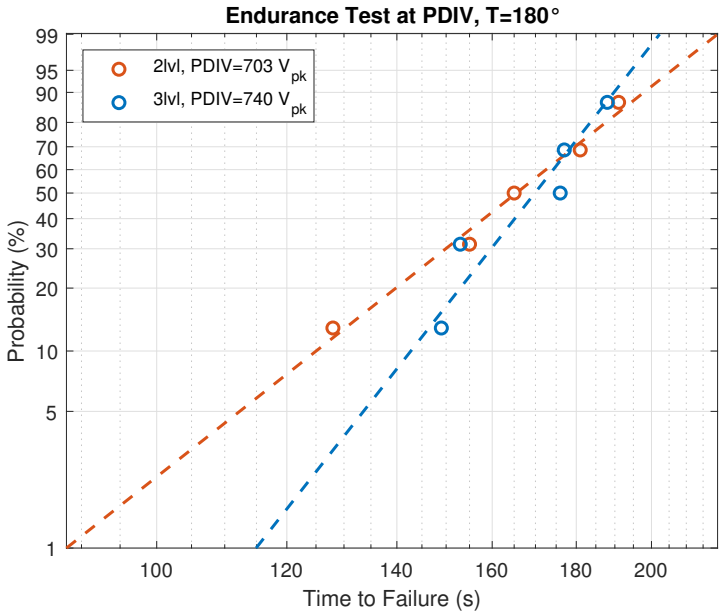

Figure 4.17: Comparison of the endurance times obtained for 2-level and 3-level waveforms.

compared to the one obtained for a more standard 2-level waveform. The SiC-converter of section 3.2.6 was employed, operating with a switching frequency of 50 kHz and around 250 ns of rise time for both configurations and a pulse width of around 1.5 μm for the 3-level configuration. A snapshot of the waveforms is recorded in Fig. 4.16. Tests were performed raising the voltage up to the PDIV, monitoring the discharge presence with an UHF detector (using a log-periodic antenna and the spectrum analyzer of Sec. 3.2.7). When PD incepted the voltage was further increased of 5% and the timer for the endurance time to PD was started, according to section 4.2.1. Test were conducted at 180°C temperature on 5 specimens per condition.

The PDIV in the two experimental conditions differs, with the 3-level waveform inception taking place at 37 V higher than the 2-level (703 V vs 740 V). A detailed investigation regarding the phenomenon is postponed for later chapters (Chap. 5, Sec. 5.1.1). Despite this difference in the stressing voltage, no great difference was recorded between the endurance times for the two scenarios. At voltages in proximity of the PDIV the repetition rate and magnitude of the discharges is the lowest, as the field is just sufficient to generate the electron avalanche [112]. Thus, the mere mild variation of the stressing voltage might not be sufficient to cause any appreciable difference in the endurances.

For square-shaped waveforms most discharges tend to appear at the voltage flank of the voltage reversal, while their occurrence on the voltage plateau is limited by the residual charge of the previous discharge activity, as the charge diffusion processes take some time [113]. The combination of this phe-

nomenon with the aforementioned one, provides a framework for understanding the similarity between the results for the 2-level and 3-level voltages.

4.2.3 Summary

Key Findings

- Litz wires (non-CR) fail in minutes under PD activity produced by SiC-waveforms (square waveform, bipolar, 2-level, 250 ns of rise time and 50 kHz of switching frequency) at voltages slightly above the PDIV (+5%).
- PD activity at operating temperature (180°C) reduce the endurance to 1.5 min (one third of room temperature values).
- Employment of 3-level waveforms more similar to real T-T stresses do not significantly change the lifetimes recorded.

Chapter 5

Partial Discharge Inception Voltage

This chapter illustrates the investigation on the partial discharge inception voltage in various models of a rotating machine. The impact of the new generation converter waveforms on the discharge inception will be explored. The contribution given by the impregnation resin in this new context will be assessed. The evolution of the inception voltage of the insulation subsystem will be evaluated as the degradation of the material progresses due to aging.

Designing a machine so that it never presents partial discharges during its lifetime appears to be the best choice in the MEA and EV contexts, also in light of the results of Chapter 4. This approach follows the philosophy of the standard IEC 60034-18-41. The failure criterion of the insulation becomes the inception of discharges, and consequently the inception voltage becomes the most important parameter to ensure the reliability of the machine.

In this context, it is crucial to know what factors influence the PDIV and its trend under aging stresses. Experimental tests were carried out on models of T-T, P-P and P-G insulation in an effort of expanding the current body of knowledge and determine which phenomena originate PDIV changes.

The results will be detailed in the chapter, but their discussion in a broader perspective will be performed in Chap. 6.

5.1 Turn-Turn Insulation Models

The reliability of the rotating machine is oftentimes dominated by the probability of inter-turn insulation failure. The voltage surges produced by power electronics converters increase the electrical stress due to overvoltages associated with reflections at motor terminals and uneven turn voltage distribution. Accordingly, the factors that impact the PDIV value in the inter-turn must be unveiled to achieve the maximum reliability of the system.

In this section the effect on the microscopic level of WBG-converter waveforms on T-T sample is analyzed. By impact at the microscopic level is meant how the characteristics of these waveforms (e.g. frequency, duration, rise time) impact the inception voltage. The investigation was carried out also for thermally aged specimens.

Moreover, in this scenario the evaluation of the impregnation resin/varnish performance becomes critical. The classical functions of electric motor impregnation resins are to improve the mechanical stability of the winding, enhance heat exchange, and protect the stator from the ingress of contaminants. In the past, due to the mild electric stress they had to withstand, they were designed having a variety of targets besides electrical withstand properties including e.g. viscosity, heat exchange, safety, and environmental protection. For long, this was not a problem, as they were subjected to limited electrical stress levels. Today, the new context is pushing the need for improved dielectric properties, especially in ways to improve the PDIV.

5.1.1 Real Turn-Turn Stresses Impact

As previously mentioned, the stress generated in the stator of a machine by a converter reaches its maximum at the flanks of the phase-to-ground square voltage waveforms (Chap. 2). These voltage waveforms can be approximated by a 3-level square wave voltage; with the positive and negative parts of the waveform corresponding to the positive and negative flanks, respectively. Silicon inverters have rise times in the order of hundreds of nanoseconds, SiC can be as short as tens of nanoseconds. Correspondingly, the 3-level voltage waveforms that approximate the turn-to-turn voltage can have an extremely low duty cycle and differ largely from the square wave voltage normally used to infer the PDIV.

It is crucial to investigate the PDIV of insulation models as the T-T stressing voltage approaches the real in-operation one, to take into consideration possible further PDIV reduction that undermine the machine reliability or possibly to take advantage of higher PDIV to increase its performances. Thus, test were carried out according to section 3.2.2 using optical PD detection and a SiC-converter (sec. 3.2.6).

Three-Level and Short Width Waveforms

Samples

Both twisted pairs of round enameled wires and litz wires were used for the tests:

- Twisted pairs produced in accordance with [91] were used for the tests, out of 0.56 mm grade 2 round enameled wire. To guarantee the homogeneity of the process a custom-made machine was used.

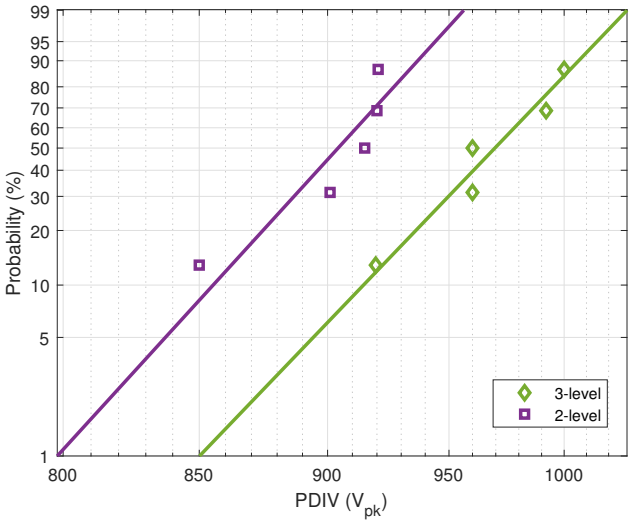

Figure 5.1: Weibull chart of the PDIV of twisted pairs under 2-level and 3-level waveforms.

> For the wires dimensions selected the standard prescribes twisting the winding wires with 12 rotations while applying a load of 7 N.
>
> - The same specimens of Sec. 4.2 were employed. They are twisted samples obtained twisting two stranded Litz wire together. The Litz wire is composed of 12 enameled sub-conductors, each with a diameter of 0.35 mm and featuring a GR3 insulation.

First, the analysis of the impact of a 3-level waveform compared to a 2-level one was performed. PDIV tests were carried out on five twisted pairs for each condition. The two voltage waveforms employed share the same rise time (around 20 ns) and switching frequency (100 kHz). The duty cycle set for the 3-levels waveform is 50 % so that the voltage is applied for 2.5 μs each half-period, compared to 5 μs for the 2-levels. The results are reported in a Weibull chart in Fig. 5.1, that shows that the PDIV of the 3-level waveform is 60 V higher than the one for 2-levels and that the shape parameter (β) of the distribution is similar indicating homogeneity in the measure for the two cases. During these tests, two different kinds of PD activity were recorded: an intermittent one and a continuous one where PD activity is never stopped once incepted and characterized by a higher number of photons released. An example of such photon activities is given in Fig. 5.2.

A similar kind of intermittent PD activity was already reported for unipolar waveforms [114], with PD activity coming in burst. During this campaign the phenomenon has been observed for 3-levels waveform. An intermittent behavior might be facilitated by space charge deposition due to undetected PD of low magnitude. After the first PD pulses, a residual charge is left in the local point of discharge on the enamel surface. The deposited charge diffuses

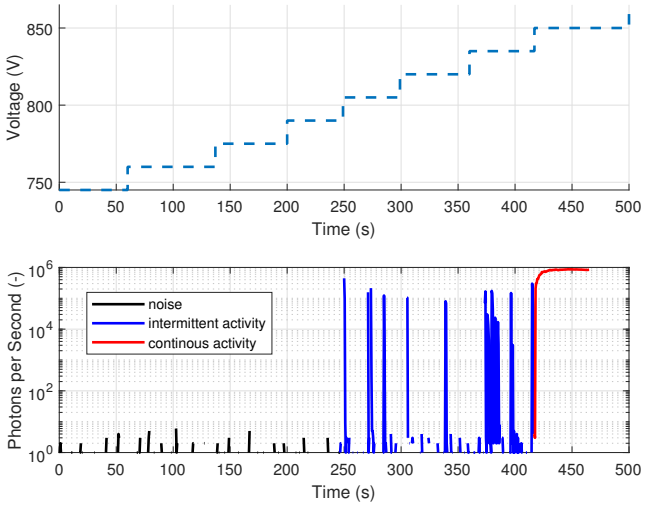

Figure 5.2: Intermittent and continuous PD activity regions as voltage was increased, for 3-level waveforms.

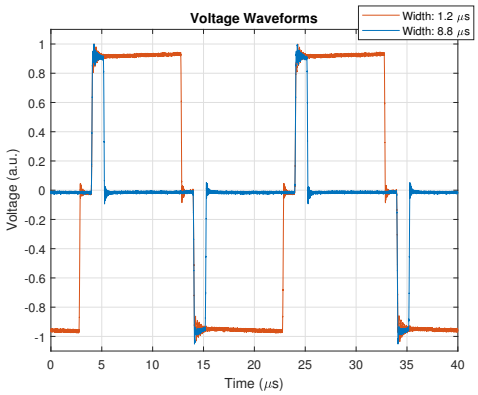

Figure 5.3: Three-level waveform voltages, with different duty cycles of 12% and 88% (pulse width of 1.2μs and 8.8μs respectively each semi-period).

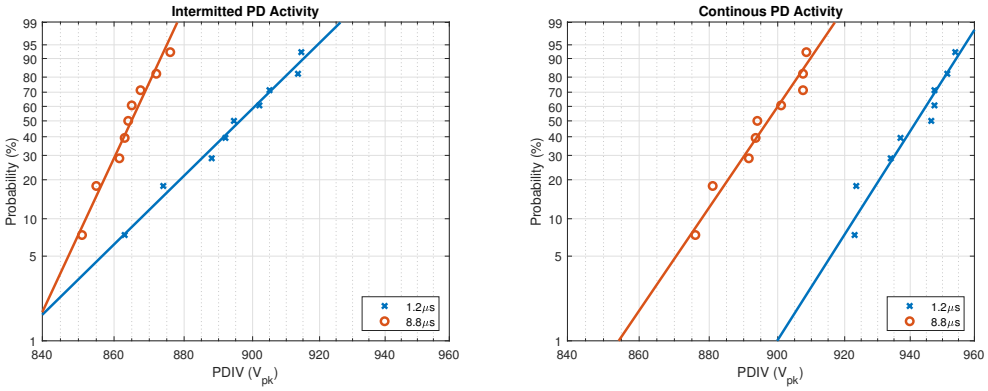

(a) PD inception for intermittent activity

(b) PD inception for continuous activity

Figure 5.4: Weibull chart of the PDIV of twisted pairs under 3-level waveforms with different duty cycles (pulse widths of 1.2μs and 8.8μs).

in the proximity and alters the local field distribution which may suppress the next discharges, especially in presence of small surface defects or dust-like particles. As such, the surface diffusion and conductivity properties play an important role. Additionally, tests repeated 24 h and 48 h after the first ones for some of the already tested specimens (not reported here for the sake of brevity) revealed that the intermittent activity could not be incepted again, and the only one recorded was the continuous. This latter finding reinforce the idea that small defects on the surface of the material may be the sites of the early discharge activity and that during the discharge such defects are smoothed or removed so that the following inception happens at higher voltages. It is likely that the continuous activity appears at a different location on the sample than the intermittent one, with the latter that disappears according to the processes already discussed [115][113]. The larger voltage jump present with a 2-level converter may explain the absence of intermittent discharge behavior in such condition, as the probable increase in the magnitude of the PDs may already eliminate in the first discharges the defects and trigger directly the continuous activity. A detailed comparison of the two kind of PD activity at the inception level between 2-levels and 3-levels waveform was not performed.

Following the findings, it has been chosen to record the inception of both kind of activities. The goal was to understand if the difference noted is attributable to the halved jump in the voltage or the shorter pulse width, so a waveform sharing the same jump voltage has been used. Eight samples were tested with two 3-level voltages sharing the same rise time (around 70 ns) and switching frequency (50 kHz), but with different duty cycles, respectively of 12% and 88% (voltage is high for 1.2 μs and 8.8 μs respectively each semi-period). The waveforms are illustrated in Fig. 5.3.

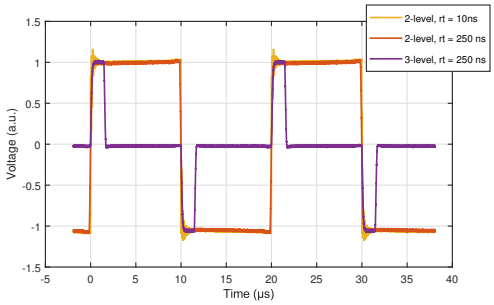

Figure 5.5: SiC-converter waveforms, 2-level (with different rise times) and 3-level.

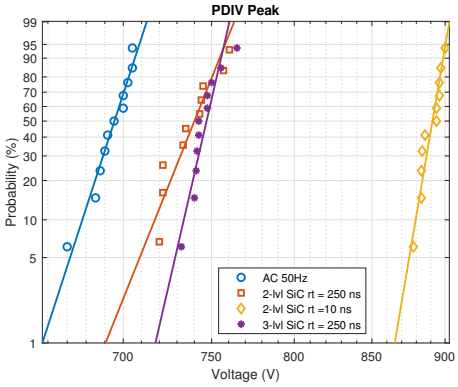

(a) PDIV in peak.

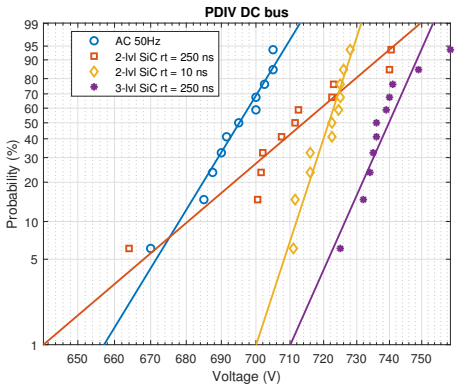

(b) PDIV in bus DC (the plateau of the voltage waveform). AC is still reported in peak.

Figure 5.6: PDIV for different waveforms, in Weibull charts.

Figure 5.4 report the Weibull charts for the PDIV recorded for the intermittent and continuous activity. In both, discharges are incepted at lower voltages for the waveform characterized by a longer impulse width. Specifically, by 30 V for the intermittent activity and by 55 V for the continuous activity (considering the 10th percentile of the PDIV probability). In sight of this outcome, the higher PDIV values recorded for 3-level short width pulses (lower that 2.5 μs) are almost certainly attributable to the short time under voltage. The shape of the voltage waveform seems less important since both 2-levels and 3-level waveforms with longer on-times reveal PDIV up to 7% lower.

The results were confirmed with tests on litz wires. The PDIV was measured under four different waveforms on four batches of ten samples. The waveforms employed are: AC sinusoidal 50 Hz, 2-level SiC-produced waveform 50 kHz with a rise time of 10 ns, 2-level SiC-produced waveform 50 kHz with rise time of 250 ns and 3-level SiC-produced waveform 50 kHz with rise time of 250 ns and pulse width of 1 μs. The three waveforms produced by the

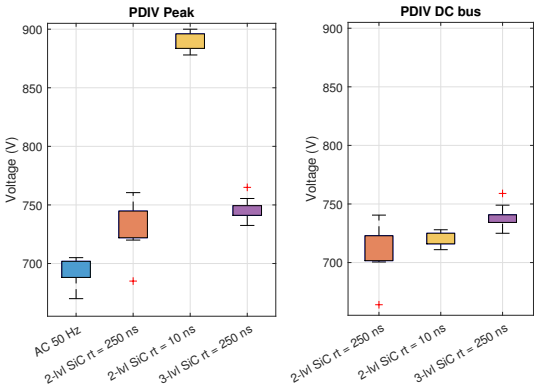

Figure 5.7: PDIV for different waveforms, in boxplots. Same results of Fig. 5.6.

converter are illustrated in Fig. 5.6. Waveforms with 250 ns of rise time have a minor overshoot (making the V_{pk} and V_{DC} similar) while the one with 10 ns of rise time has an overshoot of around 15%.

The PDIV data collected are represented in two Weibull charts of Fig. 5.6 and in the boxplot of Fig. 5.7, with the results expressed relying on the peak of the waveform or its plateau (DC bus). The 2-level waveform with 10 ns of rise time had the highest inception voltage in peak, 30% higher than AC, but much more similar to all the others when the DC bus voltage is considered. The 3-level waveform (on-time of 1 μs) compared to the 2-level (on-time of 10 μs) had a PDIV around 20 V higher. The two waveforms share the same rise time and hence same overshoot, excluding the effect caused by fast oscillations. As general framework, in terms of peak, the faster are the voltage transients the higher is the PDIV recorded.

From first principles PD events can appear when (a) the field in the air gap between the wires is high enough to ionize the air molecules and (b) a seed electron is present to initiate the electron avalanche process.

Regarding (a), a reduction in the electric field for shorter-width pulses or fast oscillating voltages of the overshoots may be attributed to delays in the field transfer to the surface of the enamel (and the air between the wires) due to polarization processes in the solid insulation. Regarding (b), a lower probability of having a starting electron during short duration pulses causes higher recorded inception voltage as the voltage is not kept constant indefinitely but is raised after a given time step. This means that the PDIV of longer and shorter pulses would eventually coincide statistically only for the lowest percentiles of the recorded values distribution. A statistical delay time of some microseconds is in line with results in literature for spark gaps [116][117]. The results obtained must be explained in light of these mechanism. A more detailed analysis will be presented later on, in section 6.2.1.

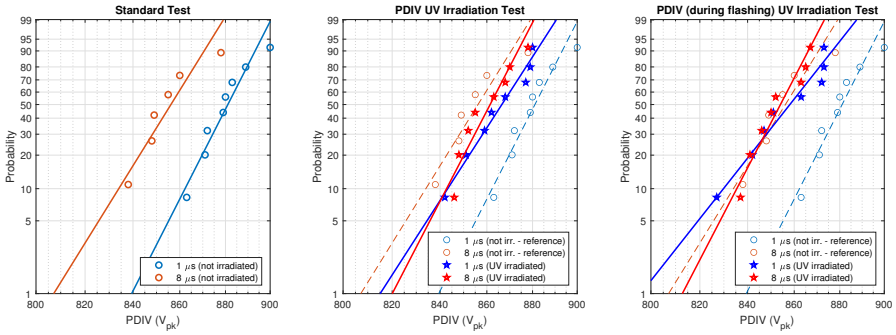

Figure 5.8: PDIV, intermittent activity, for standard (left) and irradiated (centre, right) tests under 3-level pulse. PD detected excluded inside the UV flashing time window (centre) and included (right).

5.1.2 PDIV in Presence of Artificially Generated Seed Electron

While both the reduction of field in the air and the absence of a seed electron can appear simultaneously, the latter can reasonably happen in times shorter than 5 μs. Instead, for the higher PDIV obtained for waveforms with large overshoots than for waveforms free from oscillations, the explanation might come from dielectric phenomena, as the time scale of the overshoots is a few ns which might be comparable with the relaxation time of the dielectric.

Experiments were carried out trying to generate artificially the first electron by means of UV light, similarly to what has been done in [118][119] with X-rays in an effort to distinguish the two contributions. A nano-pulsed ultraviolet lamp, with wavelength down to 220 nm, was used to irradiate the samples while subjected to voltage and measure their PDIV, as explained in section 3.2.4. It is very likely that such irradiation source is not able to generate any electron by photoionization in the air, but is anyway capable of exciting the molecules of the gas and polymer, possibly generating an electron in proximity of the polymer surface (photo-emission in polymers has a threshold of 3 to 3.5 eV [120], while the photons energy from the UV lamp tops to 5.6 eV).

The results are shown in Fig. 5.8. PD intermittent activity was measured in two detection scenarios, excluding the PD signals collected while the lamp was flashing and including also those pulses. PDIV differs slightly, being a little lower for the latter. The most important insight gained from the data collected is that when irradiating the samples, the inception voltage under short width pulses becomes almost identical to the one subjected to longer pulses. This value is in turn equal to the one under longer pulses not irradiated. This is good evidence in favor of the seed electron absence hypothesis. The same result is obtained if the continuous PD activity is monitored, with only the low percentile values following the trend (Fig. 5.9).

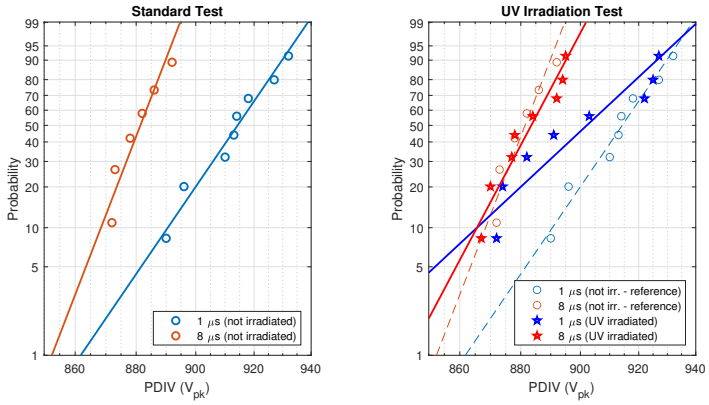

Figure 5.9: PDIV, continuous activity, for standard (left) and irradiated (right) tests under 3-level pulse.

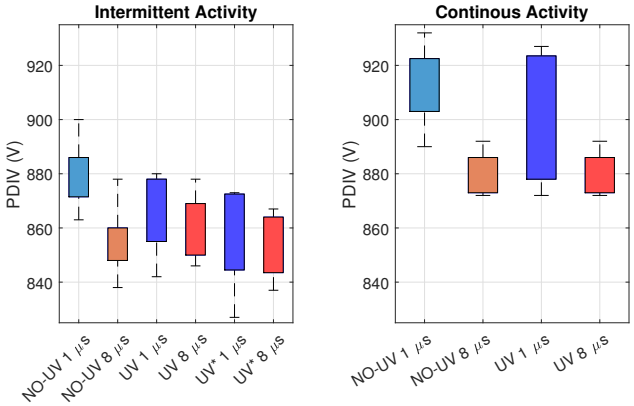

Figure 5.10: PDIV, intermittent and continuous activity, for standard and irradiated tests under 3-level pulses. (*: measurements with PD detection also during the flashing stage)

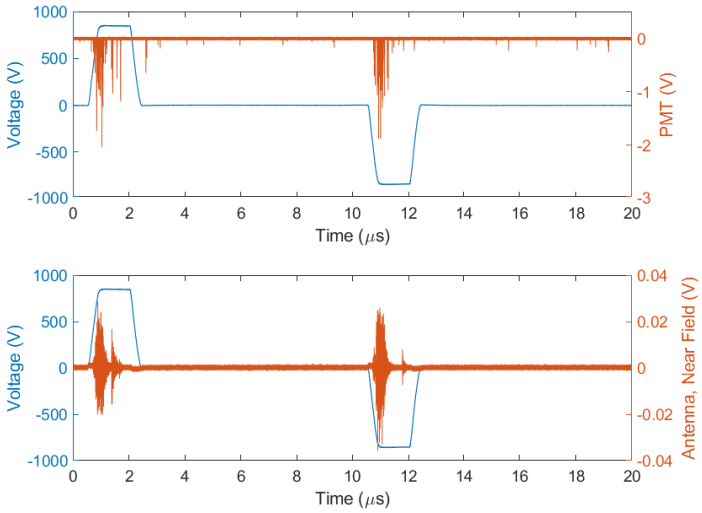

Figure 5.11: PD pulses collected after UV-irradiation, optically and electrically.

A comparison in boxplots instead of Weibull charts is in Fig.5.10, for easier comparison (but less statistical detail).

Locate the first ever PD pulse was not possible. Nonetheless, locating some of the consecutive PD pulses or their envelope was attempted. From their observation (Fig. 5.11) it is clear that when the discharge appears, does so in the first part of the waveform, further dismissing hypothesis on delays of field transfer and excluding that time lag for discharge formation play any role.

A similar approach was followed to explore the behavior of the insulation during the fast oscillations that occur during overshoot. In this case, PDIV under the same waveform with rise time of 7 ns and switching frequency of 50 kHz was compared in the presence and absence of UV radiation. The lamp flash was tuned to appear at peak voltage. The results show that there is no difference, not even statistical, between the two conditions, suggesting that the role of the first electron is not determinant in this case. However, it should be taken into account that in this experiment the time under radiation is reduced compared with that previously, with only 50 μs of irradiation time per step above the V_{DC} (compared to 500 μs of the previous experiment), leaving room for further investigation with longer times.

Overall, the results seem to indicate that higher values of PDIV recorded for short width pulse (with a time scale in the order of microseconds) could be attributed the time-lag for the seed electron appearance, while the higher values for highly overshooted waveforms (time scale of tens of nanoseconds) should be attributed to some different phenomena. Dielectric polarization is considered and discussed as the cause in Sec. 6.2.1.

While in these experiments the voltage differences recorded are in the or-

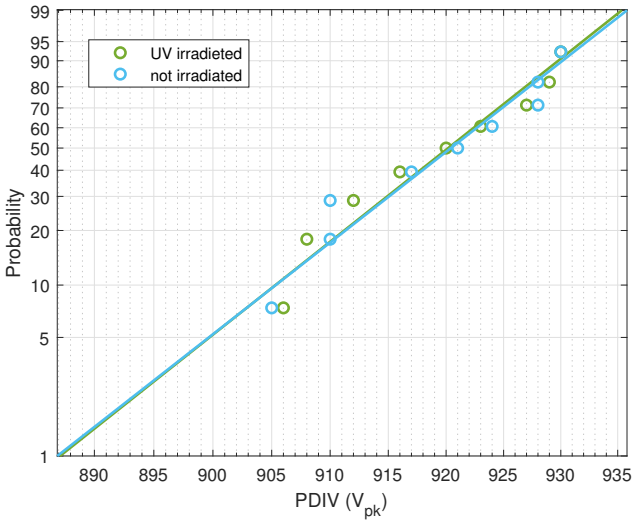

Figure 5.12: PDIV under UV irradiation and not, for a highly overshooted 2-level waveform.

der of 30–60 V, much larger values could be expected when transitioning to waveforms with pulse widths in the tens of nanoseconds (rather than microseconds), such as those produced in the interturn of a machine fed by a SiC-converter. This emphasizes the importance of the study.

5.1.3 Temperature Impact on Impregnated Samples

Experimental analysis of twisted pairs is required to assess whether impregnating resin work as intended when PDIV improvement is the target.

Samples

Tests were performed on twisted pairs and their impregnated version. The samples were produced in accordance with [91]. For the wires dimensions selected the standard prescribes twisting the winding wires with 12 rotations while applying a load of 7 N.

Three different enameled magnet wires were used (denominated Wire A, Wire B, Wire C), all of them featuring polyester/polyester-imide basecoat and a polyamide-imide overcoat, grade 2 insulation and a diameter of 0.56 mm. The impregnated version of the samples was manufactured with dip and bake technology using a resin suspected of having problems at high temperatures. The resin is undisclosed due to confidentiality agreement.

A fourth enameled wire (Wire D) and its impregnated version were used for comparative tests. Wire D is a grade 2, 0.63 mm diameter with polyester/polyester-imide basecoat and a polyamide-imide overcoat. It was impregnated using a different resin based on polyester-imide.

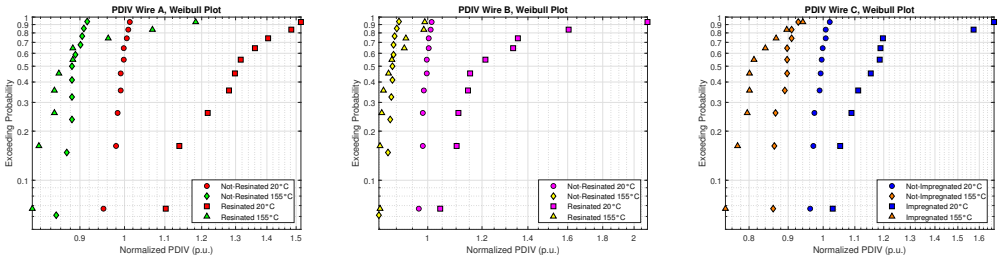

(a) Wire A. (b) Wire B. (c) Wire C.

Figure 5.13: Weibull chart of the PDIV for impregnated wire with undisclosed resin suspected to have problems at high temperature, and correspondent not impregnated wires. Measurements at room temperature and 155°C.

> All the materials are suitable for class 200 insulation systems.

Test of PDIV and PDEV were carried out on ten samples of the Wires A, B and C at room temperature (RT) and high temperature (155°C). Measurements were performed at 50 Hz with an AC sinusoidal source (Sec. 3.2.6) and conventional PD detection system (Sec. 3.2.7).

Whatever the wire among A, B, C the impregnation resin helped improve the PDIV and the PDEV at RT, as it can be observed in the Weibull charts of Fig. 5.13 and in Fig. 5.14. The results show that the PDIV of impregnated wires (circular markers) are substantially larger than the ones measured on conventional non-impregnated wires (diamond markers). However, the better performance is not consistent, with some samples having PDIV and PDEV 1.7 times the base value and others only of some percent points, indicating a large variance of the results. Furthermore, for the impregnated samples a regression line does not fit properly the Weibull distribution. In sight of this, the minimum value recorded for a group of 6 to 10 samples is often a better indicator, being around the value of the 10th percentile of the distribution. This might be the best option for evaluating the performance of the resins and summarizing the results found.

The Weibull distribution not being able to properly model the PDIV data of the impregnated wires indicates the in-homogeneity of the sample manufacturing, that causes the formation of two macro categories of specimens, better and worse impregnated TPs with different PDIV distributions. Impregnation in TPs is a process where the thickness of the resin layer covering the sample is not easily controlled, contrary to the deposition of enamel on the magnet wire. This may explain the bimodality of the collected distribution.

When the same samples are tested at elevated temperature (155°C), the non-impregnated TPs perform better than the impregnated ones. Impregnated samples not only have a mean drop in the PDIV larger than the non-impregnated, but the drop is so large that the actual PDIV is sometimes lower than the non-impregnated sample. Tests at RT were repeated after the ones at

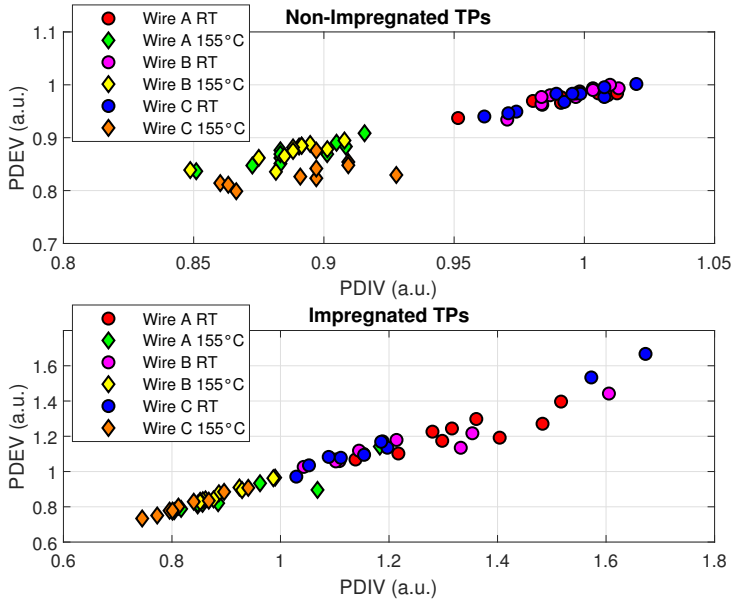

Figure 5.14: PDIV and PDEV of the three wires impregnated with a resin suspected to have problems in temperature, impregnated and not, at room and high temperature.

high temperatures, obtaining the same results as before. Thus, it was assured that the chemical structure of the resin did not suffer a permanent change.

As comparative, 6 samples of the Wire D were tested for the PDIV at RT and 140°C. The results are reported in Fig. 5.15. A comparison of the trends under temperature of this resin with the previous one highlights that the resin used for D is better: when the temperature grows the impregnated samples still outperform the non-impregnated ones. However, the PDIV drop in percentage remains larger.

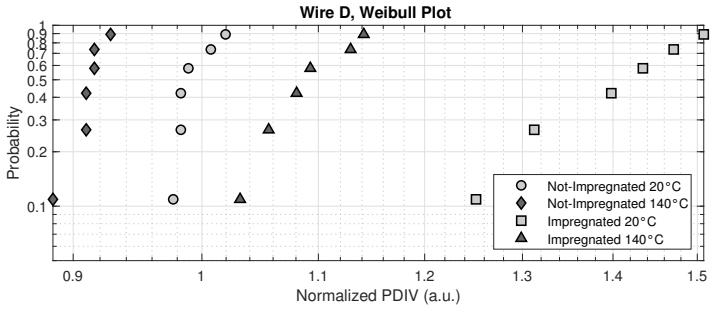

Figure 5.15: Weibull chart of the PDIV for a wire non-impregnated and impregnated with a non problematic resin. Measurements at room temperature and 140°C.

5.1.4 PDIV and Dielectric Parameters Correlation

Manufacturers of electric motors need guidance in the selection of the impregnation resin that guarantees a PDIV high enough for their application. Comparison of different resins is a steppingstone in the design of machine insulation and critical behaviors already observed for some resins must be avoided. Also, combination of enamels with nano-additives and resins could lead to unforeseen effects. This section explores the results of combining three enamels and resins and endeavors to evaluate (a) possible effects of nano-filled wires and resins combinations and (b) the impact of the dielectric permittivity of such resins on the PDIV of impregnated samples. Particular attention is paid to PDIV when the operational temperature rises and exceeds the glass transition temperature (T_g) of resin. Dielectric spectroscopy measurements, PDIV measurements, and FEM simulations have been performed in this attempt.

Samples

Three different enameled wires with the same diameter were impregnated each with three different resins. The wires, featuring grade 1 insulation and a diameter of 1 mm were manufactured twisting the wire 10 times according to [91]. All of them have thermal index of 200°C and an estimated T_g above 240°C. The wires have been name coded as:

STD Enameled wire featuring a polyamide-imide overcoat.

CR1 Nano-filled version of STD.

CR2 Alternative nano-filled version of STD.

The dip and bake technology was used for the impregnation of the samples. The three resins used have been name coded as:

UP Single component unsaturated polyester-imide resin, volatile organic compounds free. Thermal index of 200°C. The resin has a viscosity in the range 900–1500 mPa $*$ s and estimated glass transition temperature below 110°C.

EP Single component modified epoxy resin, with thermal index 180°C. The resin has a viscosity in the range 2500–3500 mPa $*$ s and estimated glass transition temperature around 120°C.

HD Single component epoxy resin, with thermal index 180°C. The resin has an estimated glass transition temperature around 90°C. The resin has a viscosity in the range 1300 mPa $*$ s

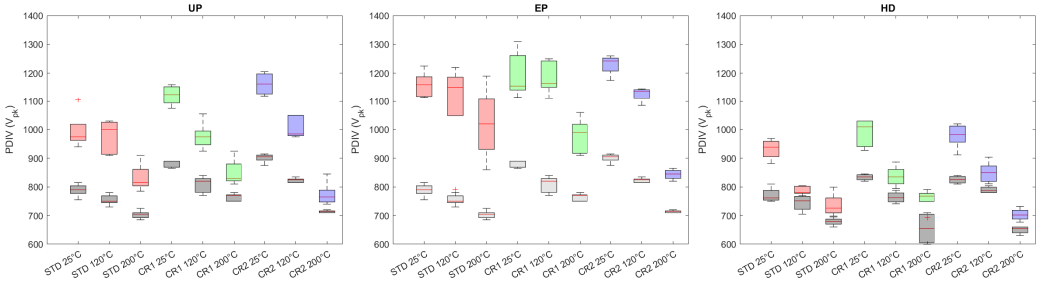

(a) UP resin (b) EP resin (c) HD resin

Figure 5.16: PDIV results in boxplots for non-impregnated wires (gray) and impregnated (colored) with three enamels for each resin at different temperature (25°C, 120°C and 200°C).

> The resins have an estimated coefficient of linear thermal expansion of 70×10^{-6} K^{-1} below the glass transition temperature and 180×10^{-6} K^{-1} above it.
>
> Flat samples of each resin were obtained from a 1 mm thick slab, to be used for dielectric spectroscopy measurements.

PDIV measurements were performed at room temperature with controlled humidity (25°C, 40% RH) inside a climatic chamber and at high temperature (120°C in climatic chamber and 200°C in oven) without a humidity control. A conventional PD detection method (section 3.2.7) and AC sinusoidal source (section 3.2.6) were employed, carrying out the test as described in Sec. 3.2.2.

The results from Fig. 5.16 show that for any temperature the PDIV of impregnated samples is always higher than the corresponding PDIV of non-impregnated sample. The combination of different resins with enamels featuring different CR technologies did not raised any issue, as no critical behaviors were recorded, even above the thermal index of some of the materials. More so, from the cross analysis between all the resins it appears a clear hierarchy of them, that is independent from the testing temperature. EP performs better than the UP, while HD is the worse performing one.

The difference of PDIV recorded for re-tests carried out on samples in the same conditions and of the same typology (e.g. test on non-impregnated TP) raised some doubt on the descriptive potential of the results. This is thought to be caused by an uncontrolled hidden parameter, possibly the moisture content in the air. The moisture could impact the results affecting the avalanche formation in the discharge mechanism or by changing the surface conduction of the solid dielectric and its permittivity, as different resins have different hygroscopicity characteristics. Pre-treatments in a vacuum oven (6 h at 50°C and low pressure) or in ventilated oven (2 h at 150°C) have been attempted to single out the phenomena in play, without success. Also, due to samples fragility, manipulation and re-test may play a role in the PDIV variations.

The general hierarchy of the resin highlighted is unlikely affected by the

limitations drawn, while a finer comparison becomes problematic. Given so, another set of less secure observation may be traced. In absolute values, both the samples having CR enamels seems to perform slightly better than the STD, having slightly higher inception voltages for both impregnated and not samples. Normalizing the results to the values at 25°C enables to observe that across all the resins, the PDIV drop in percentage at 200°C seems larger for the CR2 wires (range from -27% to -36%) compared to CR1 (range from -8% to -28%) and STD (range from -5% to -26%). At 120°C the drop is more homogeneous for all the wires typologies (from no reduction to around -20%). The outcome is difficult to interpret, especially in sight of the uncertainty of the results.

Overall, larger drops of PDIV have been recorded for the impregnated samples than for the non-impregnated ones as temperature increased. The reduction of PDIV at high temperatures can be explained by two phenomena (a) the reduction of the air density and (b) the modification of the electric field distribution in the air gap surrounding the insulation [64][121]. Considering (a), increasing the temperature at constant pressure reduces the number density of the gas, leading to larger mean free paths for collisions between free electrons and gas neutral molecules. Electrons can thus be accelerated over longer distances and gain more energy. As a result, for the same voltage, the number of ionization events per unit length increases. Alternatively, lower voltages are required to incept PD. The modification of the electric field distribution, (b), can be caused by the variation of the real part of the permittivity and/or the thermal expansion of the solid insulation. Due to the large range of possible values for both the permittivity and the thermal expansion coefficient, the variation of the field distribution may have different intensities: from negligible effects to major alterations of the field, possibly altering the site of the discharge events. Preliminary tests have been carried out at reduced pressure, to achieve an air density equal to the one at higher temperatures. This ensues that the pure density-reduction effect can be evaluated and then compared to the combined one appearing when the temperature is increased. The examination has been performed at 120°C and 750 mbar that is the equivalent pressure, calculated keeping constant the p/T ratio. For unimpregnated TPs, PDIV did not differ significantly. For impregnated samples, with any of the resin under evaluation, the PDIV drop at the equivalent pressure was milder than the one at 120°C, indicating that the processes of (b) are very likely adding up and further reducing the measured values. Hence, the non-impregnated sample PDIV decrease may be attributed entirely to the air density reduction, as the permittivity of the enamel hardly changes in the temperature range (Tg>240°C) and thermal expansion of the enamel may be considered negligible (0.3%, with an estimated enamel thickness variation of 0.1 μm). For impregnated twisted pair, the analysis is more difficult.

Figure 5.17 reports the real and imaginary parts of the resins permittivity at different temperatures, from dielectric spectroscopy results. Due to the

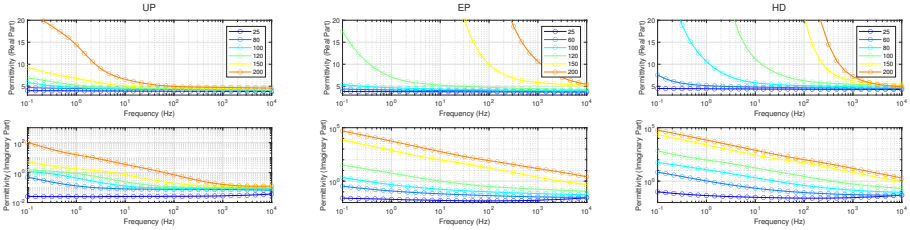

(a) UP resin (b) EP resin (c) HD resin

Figure 5.17: Dielectric spectroscopy results for the permittivity (real and imaginary part) of 1 mm thick resin sample.

considerable sample thickness, a voltage of 100 Vrms was applied to the 10 mm diameter circular sample to increase the dielectric analyzer sensitivity (as described in section 3.3.2). At room temperature the relative permittivity of the three resins is quite stable in frequency, with values of 3.7 for UP, 3.8 for EP and 4.5 for HD. As the temperature approaches the glass transition temperature of each of the resins a rapid increase of the permittivity is noticed. This change occurs more gently for the polyester resin (UP), starting at 100°C. The change occurs strongly for the epoxy resins, between 60°C and 80°C for HD and between 100°C and 120°C for EP. The temperatures values at which the transition occurs are coherently with the estimated T_g from the manufacturer. Some doubts remain on the measurement procedure above the T_g, since the sample softens, and its thickness can be reduced due to the mechanical actions of the electrodes. Indeed some of the extreme permittivity values reached seem unrealistic.

Nonetheless, similar PDIV and permittivity trends have been found by other authors [122], confirming that the observations are not limited to materials here under exam.

Figure 5.18 reports the sample capacitance and dissipation factor for twisted pairs manufactured out of CR1 wire (impregnated and not). The samples were connected to the dielectric analyzer (measured as described in section 3.3.2) to measure the capacitance between the two twisted wires, applying a 3V rms voltage waveform. The measurement was performed inside an oven and the dielectric parameters were recorded after 30 minutes from temperature stabilization. For the non-impregnated ones, it can be observed that the capacitance is scarcely influenced by the temperature. Contrarily, for all the impregnated samples important changes in the capacitance are detectable, especially above the T_g of the resin. For all the materials the trends are like the ones observed for the permittivity, as the dielectric response is apparently dominated by that of the resin. Even if doubts may be raised on the exact value of the permittivity of the resins due to the mentioned spectroscopy measurement limitations, the high correlation between capacitance and permittivity values visible in Fig. 5.19 demonstrates that the values recorded on

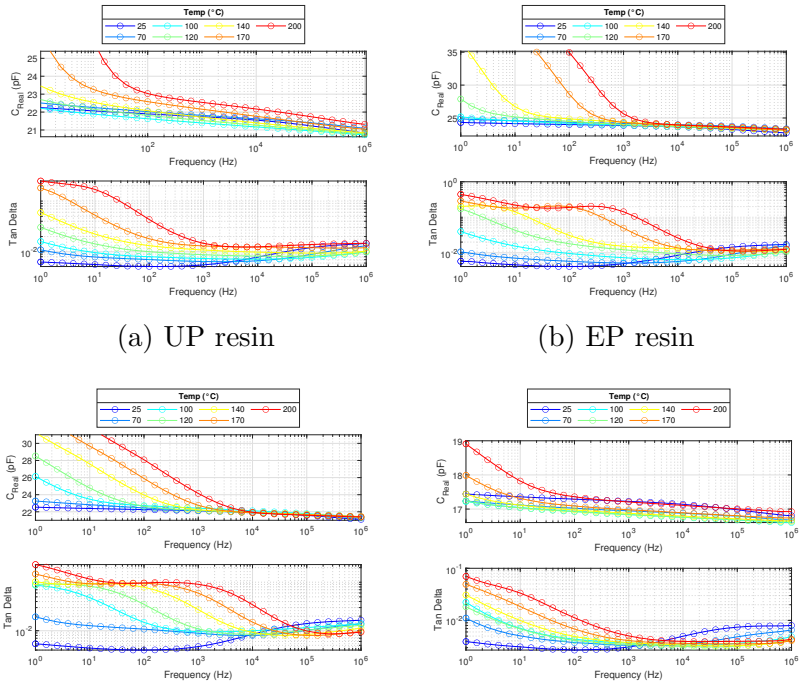

(a) UP resin

(b) EP resin

(c) HD resin

(d) Not impregnated

Figure 5.18: Capacitance and dissipation factor of the TP specimen impregnated with different resins or not impregnated, obtained through dielectric spectroscopy.

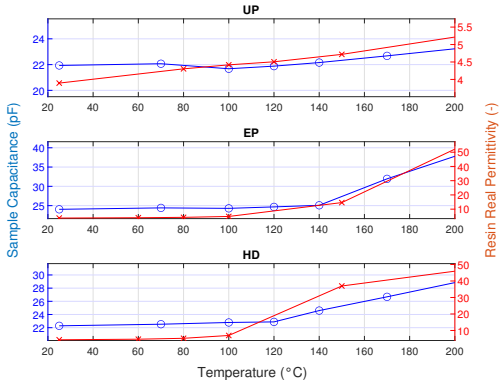

Figure 5.19: Variation of sample capacitance and resin real part permittivity in temperature, at grid frequency (50 Hz), for the three resins under exam.

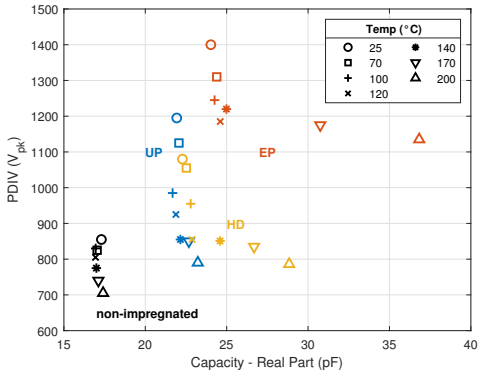

Figure 5.20: Correlation between sample capacitance and PDIV, as the temperature varies.

flat samples are not far from the real ones, at least for the grid frequency and that the capacitance change is almost fully attributable to the variation of resin permittivity (even if expansion phenomena are likely happening).

So, considering the thermal expansion coefficients provided by the manufacturer, the resin should thermally expand up to 3% when the temperature reaches 200°C. The conductors' thermal expansion is an order of magnitude smaller (0.3–0.4%). Considering a 1 mm diameter wire and hypothesizing a resin thickness of 40 μm, the resin layer thickness increases to 42 μm and the copper diameter to 1.004 mm. Using a 2-dimensional FEM model of the twisted pair, if the only change associated with temperature is the material expansion, hence keeping both the relative permittivity of the enamel and the resin equal to 4 the estimated increase of the capacitance is negligible (<1pF). Expansion is negligible for the capacitance variation.

In an attempt to correlate the PDIV results with the permittivity of the resin, PDIV tests have been performed following dielectric spectroscopy tests on a single specimen for each resin. The results are reported in Fig. 5.20. The graph clearly shows that is not possible to find a single regression line across all resins and for temperatures above and below the T_g. Anyway, the thickness of each resin is unknown and is very likely the factor that clusters the results of different resins in different regions. The previously mentioned resin hierarchy, here observable again, is very likely caused by the thickness of material deposited in the impregnation phase. This is partially coherent with their reported viscosity, having the EP as the most viscous and as consequence the one where the material deposited is thicker. Furthermore, if the temperatures above and below the T_g are treated separately, two different regression lines might be traced. Indeed, above the T_g as the capacitance of the sample varies largely the PDIV keeps varying with a slower ratio. This is clearer for the epoxy resins, that present a bigger variation of permittivity values. Overall, the investigation shown that resin thickness is the major contributor to the PDIV and that variation of the permittivity appears to modify

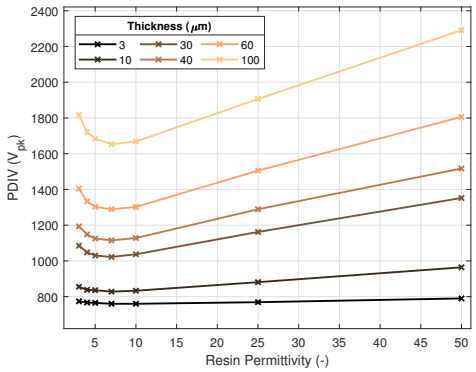

Figure 5.21: PDIV prediction thought Schumann based criterion.

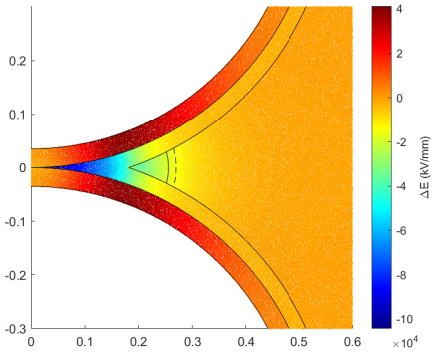

Figure 5.22: 2D model of a twisted pair section. Difference of the electric field distribution when the resin permittivity is increased from 3 to 50 (thickness of resin layer 30 μm, enamel permittivity 4). The critical line of the discharge (solid line) moves to the left (dashed line).

the results only marginally.

Finally, a modeling of PDIV trend as function of temperature was attempted. Using a simple air density proportional model $PDIV(T) = PDIV(T_0) * T_0/T$, the predicted reductions are 24% at and 37%, greatly overestimating the measured ones (for a non impregnated samples are 10% at 120°C and 14% at 200°C). Prediction using a more sophisticated tool based on the Schumann criterion (K=6) and using ionization swarm parameters derived using Bolsig+ was applied, its description is in Sec. 3.4. Eventually this approach led to inconclusive results for impregnated samples, as too many parameters including the thickness of the resin were unknown. Nonetheless, the model was employed to carry out a sensitivity analysis to the thickness and permittivity, to better understand the impact of both parameters. Results are in Fig. 5.21, obtained considering a constant air density (1 bar and 25°C). The results reinforce the idea that the resin thickness is the most impactful parameter in determining the inception voltage. In Fig. 5.22 can be observed

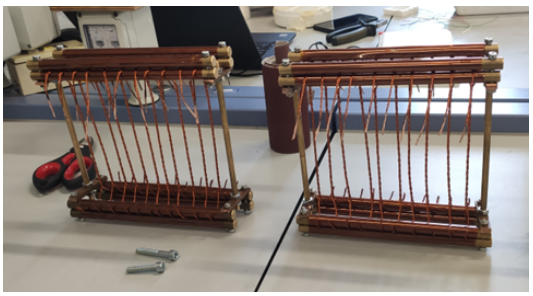

Figure 5.23: Sample holders, for aging samples of the Litz wires avoid mechanical stresses.

how the substantial change of the resin permittivity mostly varies the field inside the solid enamel insulation and marginally the one in the air. During the attempt it was highlighted the extreme importance of the geometry of the point in the wires' contact proximity. From the figure is evident the limitation of the design of the region where the wires contact, here modeled with a cusp. Some experiments have been carried out rounding the cusp, but ultimately this does not impact the inception voltage, unless the curvature starts to cover the area where the critical discharge lines appear. Geometrical variations in the area, possibly coming from thermal expansion, could alter significantly the PDIV.

In summary, the results achieved through a combination of PDIV tests, dielectric spectroscopy tests and FEM-simulation appear to indicate that resin design should aim at maximizing its coating effectiveness by controlling the viscosity, adhesion, and thermal expansion coefficient.

5.1.5 Converter Stresses on Thermally Aged Samples

In a previous section (Sec. 5.1.1) it has been shown that different features of the voltage waveform cause different values of PDIV. It is not clear if when aging start to degrade the insulation the effects recorded get exacerbated, mitigated or remain in place with the same magnitude. Especially, the impact of very fast transients on impregnated samples could vary as function of time under thermal stress.

Impact of Waveshape on Enameled Aged Samples

The first step in understanding the combined impact of converter waveshapes and aging is to the study of the trend of PDIV for enameled only sample, the simplest model of the turn-turn insulation. For this reason, specimens were fed with different voltage waveforms.

> **Samples**

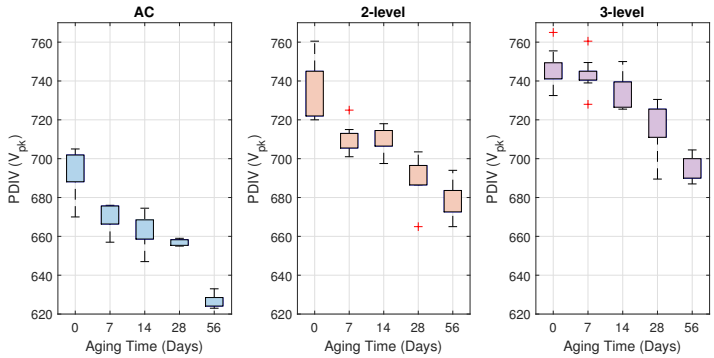

Figure 5.24: PDIV results for the Litz wires in boxplot as the aging progressed, for three different testing waveforms.

> Samples of twisted litz wires, identical to the one produced in section 4.2, were arranged on holders for being aged. Five holders, ten samples per holder, were realized to be isothermally aged in a ventilated oven at +30°C of their thermal index (220°C). Each was aged for a different time. The longest aging time was 56 days corresponding to around 1350 h. Half of the specimens in each holder was tested under AC voltages first and then all the specimens were tested under SiC converter produced waveforms.

The samples were subjected to AC 50Hz sinusoidal voltage and SiC-converter produced waveforms. The two converter weaveforms used had a 50 kHz of switching frequency and no overshoot, with rise times of 200 ns and 100 ns for a 2-level and 3-level one respectively. The three level waveform had a pulse width of 1.5μs.

The results, illustrated in Fig. 5.24 show a steady decline of the PDIV, similar for all the waveforms under exam. The PDIV decline remains contained under the 10% even for the longest aging time. Comparison of the PDIV of samples for the different waveforms shows that no particular variation takes place across the three voltage waveforms.

Impact of Waveshape on Impregnated Aged Samples

It has been shown that a well-designed resin can help increasing the PDIV. Yet, the evolution of the electrical withstand properties under converter voltages as the resin-enamel insulation materials degrade due to aging could deviate from the trend under industrial AC voltages. Indeed, dielectrics are dynamic systems and their dielectric permittivity shows a dependence on frequency as polarization contributions cease to occur above some critical frequencies, where the converter voltage could have significant energy.

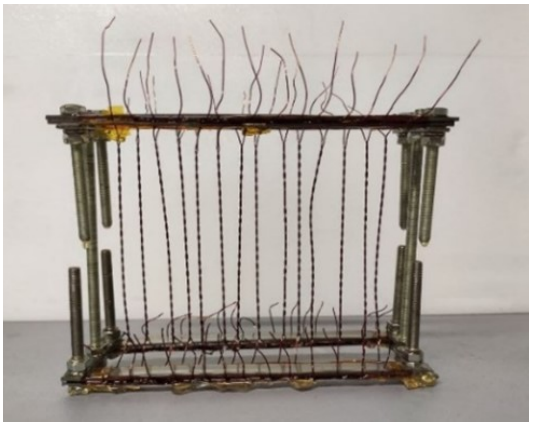

Figure 5.25: Sample holders, for aging samples of the impregnated enameled wires, to avoid mechanical stresses.

Samples

Two TP sets (non-impregnated and impregnated) manufactured using a grade 2 polyester/polyester-imide basecoat and a polyamide-imide overcoat wire were realized. The wire featured a diameter of 0.56 mm, so the specimens were twisted with 12 rotations while applying a load of 7 N, in accordance with [91]. The impregnation was performed through dip and bake process with an unsaturated polyester resin. Each set was aged up to 56 days (1300 h) in sub cycles of 7 or 14 days at a temperature of 230°C (+30°C than the thermal index of the materials), as suggested by [92].

Two main aging cycles were carried out:

- On single TPs not held by any structure, both impregnated and not-impregnated versions, 10 samples each, subjected to consecutive thermal aging and diagnostic cycles. The same samples underwent the tests with different voltage source at all the aging times, up to 56 days of aging.
- On impregnated TPs, hold in a structure (Fig. 5.25) to limit the mechanical stress. Four holders with 14 TPs each were manufactured, seven to be tested for each voltage source. Three holders underwent 10, 20 and 30 days of thermal aging respectively and the fourth was kept unaged. After the aging the diagnostic cycle was performed. No sample has been tested more than once, thus excluding the possibility of PDIV drops caused by damage of previous PD activity.

In the diagnostic cycle, PDIV on the same samples was tested under AC sinusoidal voltage with conventional PD detection (Sec. 3.2.7) and under converter-generated bipolar square voltage waveform (Sec. 3.2.6) at a fre-

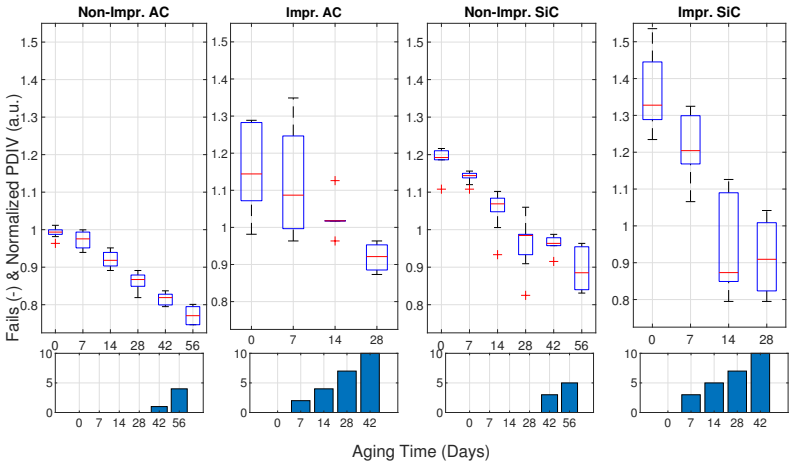

Figure 5.26: PDIV results for the non-impregnated and impregnated TP in boxplots as the aging progressed, in AC and under SiC-converter waveform. Results are reported scaled to the values of non-impregnated un-aged AC samples. The number of cumulative fails is reported below each graph.

(a) Cracking of aged sample, embrittled by the aging.

(b) Burnt region after short circuit due to PD erosion.

Figure 5.27: Pictures of failures of impregnated twisted pairs.

quency of 10kHz and rise time of 8 ns.

The results collected for the PDIV have been illustrated with boxplots in Fig. 5.26, with all the values scaled to α of the Weibull distribution for the un-aged non-impregnated set. The figure also provides the cumulative number of samples failed. Indeed, it was not possible to continue the tests after 42 aging days for the impregnated samples due to their failure. After only 7 aging days, insulation adhesion problems and embrittlement were already observed. Figure 5.27a is an example of that, the enamel is missing at the terminal parts of a twisted pair. The sample was not subjected to any specific mechanical test but just handled to connect it to the test fixture for PDIV measurements. A moderate mechanical stress was enough to crack the insulation and expose the copper, indicating the extreme brittleness.

For non-impregnated TPs the PDIV (peak voltage) values under SiC volt-

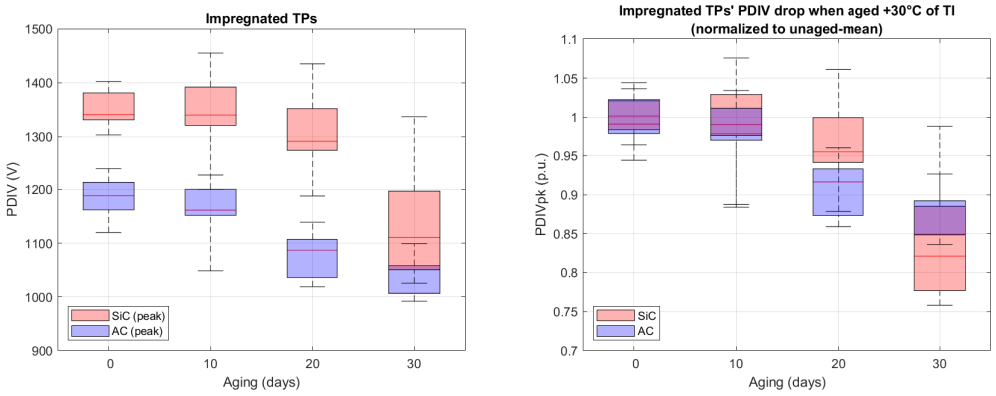

(a) Absolute values. (b) Normalized to the un-aged mean.

Figure 5.28: PDIV trend in boxplots as aging progresses for impregnated samples fed by AC and SiC-converter waveforms.

age are greater than the ones in AC, for any aging time, result coherent with previous studies and is related to the large overshoot of the SiC impulse voltage (Sec. 5.1.1). Contrarily, impregnated TPs perform better under converter voltages only when they are pristine. As aging progresses, the PDIV obtained using the SiC converter becomes lower than the one using AC voltage waveforms.

To exclude the impact of handling and the impact of damage from previous PD activity, the investigation was carried out on a second set of impregnated wires. The same frequency of 10 kHz and rise time of 8 ns were employed. Ambient conditions inside the test cell were monitored and kept controlled to minimize the impact of ambient conditions on the PDIV. Temperature and relative humidity were set to 25°C and 40% with an accuracy of 1°C and 5% respectively.

Figure 5.28a illustrates the PDIV drop under the two stressing voltages. It should be highlighted that at 30 days of aging the distributions of PDIV for sinusoidal and converter waveform starts to overlap, whilst this does not happen earlier. The results have been normalized to the mean of the unaged samples, in Fig. 5.28b, in the effort of highlighting the sole effect of the aging. So, while it is difficult to highlight a precise trend of the decline for the mean value, the decline of the minimum value recorded for each distribution is clearer. Because the weakest link of the chain determines the reliability of the whole system in insulation systems, a selected percentile in tail of the distribution should be used for comparisons.

Let us define with the term high frequency the region of the spectrum above 50 Hz where the spectral energy of the converter voltage waveform is non-negligible. With thermal aging, de-polymerization and oxidation phenomena might vary the resin real permittivity so that it is larger at high frequencies compared to 50 Hz. Therefore, for SiC voltage waveforms, the permittivity

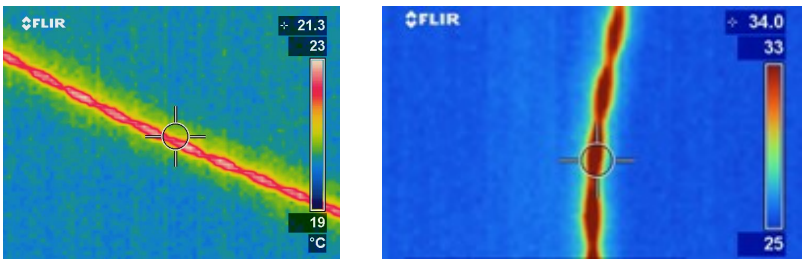

(a) 540 V_{DC} (b) 825 V_{pk}

Figure 5.29: IR imaging of TP fed with 100 kHz converter waveforms.

mismatch between air and solid would be larger, leading to comparatively higher electric field in the air. This would eventually lower the PDIV, as lower voltages are needed to produce the same electric field in the air and explain the difference recorded. Other possibilities such as the change of the sample geometry (chance caused by a shrinking of the insulation) or the increase hygroscopicity of the resin would likely affect the PDIV in the same manner for the two waveform types and do not set up a valid description [121][123]. Factors like the sample mechanical fragility, relative humidity and impact of previous discharge activities have been limited by the latter test design. Indeed, this test with specimens supported in a frame shows lower PDIV drop for both AC and square waveform.

Alternatively, an increase of the resin imaginary permittivity in the high frequency region could increase the temperature of the sample and reduce the PDIV by temperature effect. This was investigated indirectly with IR camera acquisitions. Samples were subjected to voltages lower than PDIV and the surface temperature recorded, measurements were repeated for three specimens. The temperature of non-impregnated TPs subjected to 100 kHz square waveform did not rise above the ambient temperature. On the contrary, the temperature of impregnated TPs increased 4°C above the room temperature (stressed at 540 V_{DC}) and 9°C (stressed at 825 V_{pk}), independently from the aging time. Acquisitions are reported in Fig. 5.29. Since doubts existed on the reflectivity of the resin in the IR range, acquisitions were repeated for a lower switching frequency (10 kHz). In these latter tests, none of the samples displayed a significant temperature increase. Thus, a convincing explanation is that the heat is generated by the dielectric losses, that at a given frequency they can be estimated per unit volume as:

$$p = 2\pi f E^2 \varepsilon"(f) \tag{5.1}$$

The phenomenon was found to be observable even for pristine samples, so contributing from the start to the reduction of the PDIV and in a wider view the aging and lifetime of the machine.

Samples of the un-aged and aged resin have undergone preliminary Fourier Transformer Infrared Analysis (FTIR) tests, to roughly estimate the chemical

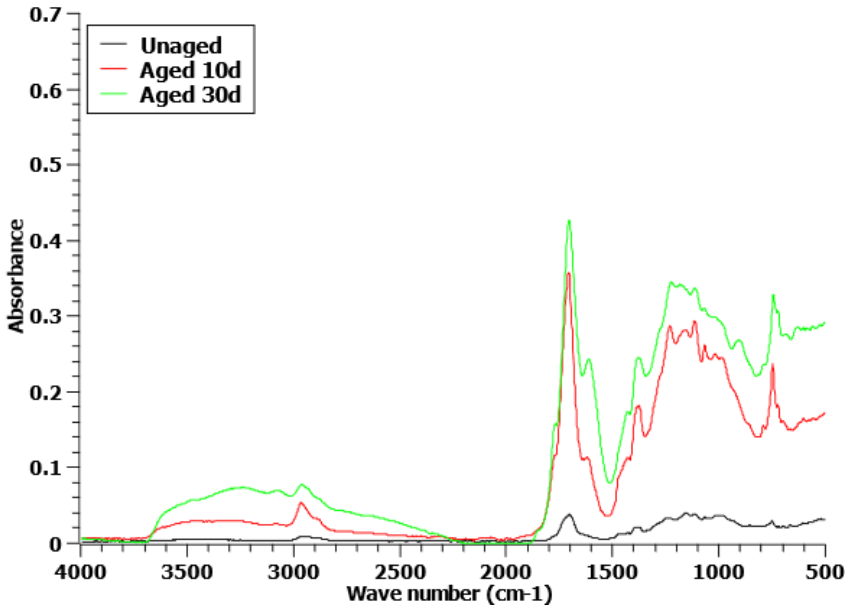

Figure 5.30: FTIR of unaged and aged samples or resin.

changes of the resin, Fig. 5.30. The acquisitions hints the formation mainly of anhydrides (peak at 1752 cm^{-1}) and carboxylic acids (peak at 2971 cm^{-1}) other than an increased moisture absorption (large band at 2300-3700 cm^{-1}) According to literature, the formation of anhydrides comes from the oxidation of methylene in the α-position of ester groups, most likely due to a radical attack of the C-H bonds [124]. Radicals at high temperatures like the one of the accelerated thermal aging (230°C) originate from the thermolysis of the polymer backbone, while at lower temperatures much more similar to the operating ones (150°C), the thermal degradation of hydroperoxides is the radical source [125]. Unfortunately, the analysis does not provide enough information to complement the treatment of the mechanisms discussed.

As a side note, in all the charts of the impregnated samples can be observed that the results are quite dispersed, especially if compared to what is usually found in non-impregnated samples. As mentioned earlier the impregnation in TPs is a process where the thickness of the resin layer covering the sample is not easily controlled. Manufacturing technique and viscosity of the resin impact the process. Unfortunately, this factor partially hinders the trend analysis.

Combined Impact of Aging and Pressure Reduction

The same kind of twisted pair wires were impregnated with a different polyesterimide resin (Voltatex 4201) and were tested at reduced 100 mbar pressure and compared to the values at standard atmospheric pressure (1000 mbar), under the same test conditions as before. The results, shown in Fig. 5.31 are this

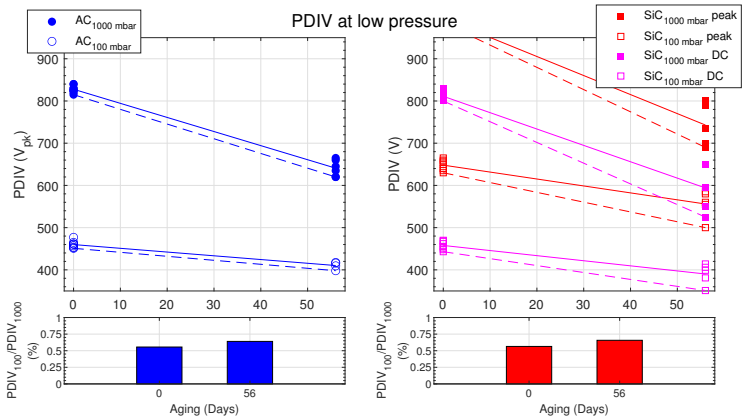

Figure 5.31: Twisted pairs PDIV drop as function of aging, reported for atmospheric and reduced pressure (100 mbar).

time illustrated using both V_{pk} and V_{DC} for the SiC-converter voltage. The results at atmospheric pressure reaffirm what has already been mentioned. But comparing the data with those obtained at reduced pressure shows that the percentage reductions in PDIV due to aging at low pressure are smaller. While at high pressure the PDIV drops over 20% at 1000 mbar, the drop is 10% under AC and 15% under converter at 100 mbar. This can also be evidenced by the ratio of the two PDIVs, shown in the graph below of Fig.5.31, that increases as the samples age. An explanation of the phenomenon will be given in Sec. 6.2, complement with other results.

5.1.6 Summary

Key Findings

- 3-level waveforms with short-width pulses (<2.5 μs) shown PDIV up to 7% higher than longer width ones.
- PDIV (in peak) under converter generated waveform has been recorded to be always higher than under industrial 50 Hz voltages (even up to 30%).
- In presence of artificially generated electrons (by UV-irradiation) the PDIV differences for short-width pulses has been canceled. The same did not happen for high-overshoot waveforms.
- The existence of resins causing PDIV lower than un-impregnated samples at operating temperature has been recorded.
- Combination of PDIV tests, dielectric spectroscopy tests and FEM-simulation appear to indicate that coating effectiveness is the most

important parameter for PDIV maximization.

- PDIV tests at temperatures higher than the glass transition temperature of resins (where permittivity greatly increased) did not reveal enhanced PDIV drop.
- Impregnated T-T models (but not enameled-only ones), showed accelerated PDIV drop if measured under SiC-waveforms (-24% vs -16% after 700 h at +30°C of thermal index). Nonetheless they did not drop below the values measured in AC.
- Significant dielectric losses were recorded only for impregnated T-T samples under square waveforms (+9°C on the surface at 100 kHz, no increase at 10 kHz).
- PDIV drops after aging were lower when measured at 100 mbar (-10% compared to -20% after 1300 h at +30°C of thermal index).

5.2 Complete Insulation Models

The action of the various stresses that contribute to the deterioration of a stator windings is certainly not new, as extensive literature exist on the aging processes. However, in the new context brought by WBG converters, parts previously subjected to only moderate stresses now have to withstand significant electric fields. On these portions of the insulation, the effect of converter electrical stresses material on degraded materials is unclear. In addition, the established accelerated aging test processes need to be supplemented with stresses representative of operating conditions for the automotive and especially MEA sectors to properly model the useful life of the materials. An analysis of the PDIV behavior under (a) WBG-converter waveforms and (b) degradation cycles typical of transportation sector on models of machine insulation would be essential to understand the peculiar critical issues.

The study permits to understand what knowledge gained in the study of T-T systems is transferable to P-P and P-G systems.

Motor insulation models (motorettes) complete of all the insulation materials and representative of the geometry of the stator, were employed in the attempt to study both the converter impact and MEA characteristic aging on the P-P and P-G. These models are representative not only of turn-turn isolation but also of phase-to-phase and phase-to-ground isolation.

Samples

Motorettes with two coils have been manufactured. Their insulation system, in thermal class 200°C is composed of:

Subsystem	AC 50 Hz			Converter 300Hz		
	α (V)	β (-)	B10 (V)	α (V)	β (-)	B10 (V)
P-G	1779	18	1576	2340	9	1848
P-P	1264	13	1065	1794	24	1642

Table 5.1: Weibull fitting parameter for the PDIV results of motorettes under AC and converter stresses.

- Rounded wires enamel: grade 2 insulation on a 0.56 mm of diameter. The insulation is composed of a basecoat in THEIC-modified polyester or polyesterimide and overcoat of polyamide-imide.
- Slot insulation and phase insulation in the slotted region: NKN, Nomex-Kapton-Nomex with thickness of 250 μm
- Phase insulation in the end-winding: Nomex 110 μm
- Impregnating resin: Voltatex 4201 polyester-imide, monocomponent
- Bandaging: Nomex AA 52083-C-A

In an attempt to better understand the PDIV mechanisms for the P-P and P-G systems, also un-impregnated slot mockups have been manufactured. Their inception voltage has been measured and the tool of Sec. 3.4 has been used to analyze the inception values.

5.2.1 Converter Waveforms Impact

An analysis of the motorette PDIV behavior under converter waveforms is essential to understand the critical issues peculiar to subsystems containing layers and liners and to understand if the knowledge gained in the study of turn-turn systems is transferable to phase-phase and phase-ground ones.

Samples

The motorettes described in the chapter introduction have been used. Testing of the P-G was achieved connecting both coils to the high voltage with the frame grounded. Testing of the P-P was achieved connecting to the high voltage to the top coil and the ground to the bottom one, while the frame was insulated from the ground.

The test were carried out with a full-bridge Belke source (Sec. 3.2.6), with a rise time of 100 ns, overshoot factor of 16% and switching frequency of 300 Hz, the waveform is visible in Fig. 5.32. Five samples were tested

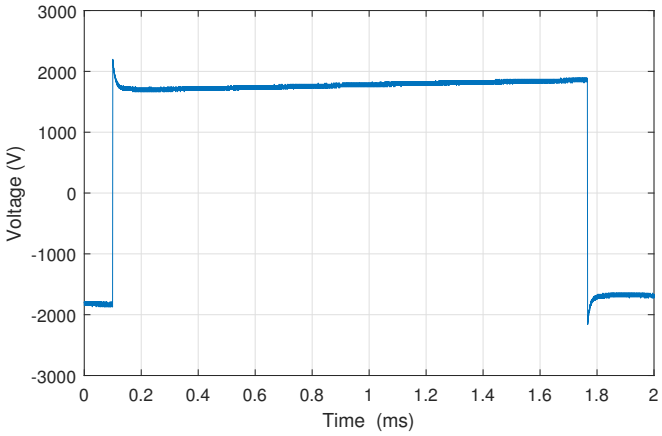

Figure 5.32: Bipolar 2-level waveform with 100 ns of rise time and 300 Hz of switching frequency used for the PDIV tests of motorettes.

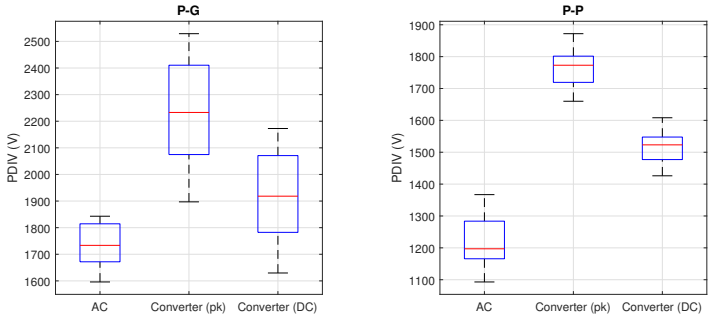

Figure 5.33: PDIV of P-P and P-G insulation subsystem for motorettes stressed in AC and under 2-level bipolar converter voltages.

per condition following the procedure of section 3.2.2.The PD were signal was detected with an HFCT and probed to an oscilloscope. High pass filtering was used to eliminate the converter noise. Optical detection was also attempted, using the same PMT described in Sec. 3.2.4. The results are reported in Fig. 5.33 and Tab. 5.1.

Again, the $PDIV_{pk}$ under converter waveform is higher than for AC waveforms. If instead the DC bus of the converter is taken into account similar values are obtained for AC and converter voltages for the P-G. Of all the measurements, only one sample out of five for the P-G and two out of five for the P-P were detectable optically, as discharges here can happen inside the slot, out of the photo-multiplier line of sight.

Despite fewer experimental activities carried out on P-P and P-G models, it appears that similar conclusions to those obtained for T-T models can be derived. The phenomena identified as responsible for the increase in PDIV in the T-T (i.e. statistical lag of first electron and field reduction from dielectric relaxation) continue to have a physical role in this context as well. One difference lies in the fact that in P-P and P-G pulse widths hardly are expected to go below few microseconds, as that would mean that the corresponding switching frequencies are approaching the megahertz. On the other hand, overshoots are ever-present and the possible effect of electron absence and air field reduction seem enough to explain the results obtained also in this context.

5.2.2 Phase-Phase and Phase-Ground Inception Prediction

In an attempt to better understand the PDIV for the P-P and P-G systems, un-impregnated slot models have been manufactured. Their inception voltage has been measured and the tool of Sec. 3.4 has been used to analyze the inception values.

Samples

Two types of samples were designed, observable in Fig. 5.34, for modeling the phase-to-ground and the and phase-to-phase insulation respectively. Different insulation layers have been used for manufacturing the samples.

- **P-G models** Metal frame and polyamide enameled wire separated by an insulation layer. The wire used features a grade 2 insulation and 0.63 mm outer diameter.
- **P-P models** A PVC frame hosted two coils of polyamide enameled wire separated by an insulation layer. The wire used features a grade 2 insulation and 0.63 mm outer diameter.

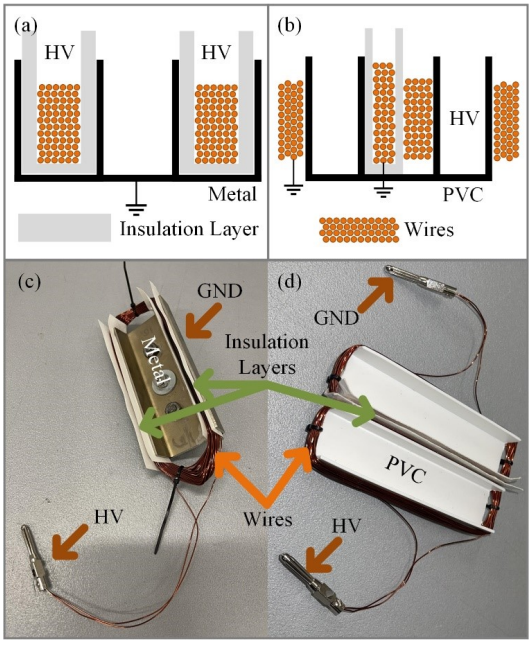

Figure 5.34: Un-impregnated motorette samples and their connection schemes.

> Four types of insulation layers were used in the tests: Kapton polyimide film with a thickness of 50 μm, Nomex insulation paper with a thickness of 80 μm, and two Nomex-Mylar-Nomex (NMN) insulation paper with thicknesses of 190 μm and 240 μm.
>
> The coils were manually wounded in the slot mockup. To ensure a tight contact between the wires and the insulation layers and between the insulation layers and the slot mockup, each set of magnet wires was wound at least 40 times in the phase-to-ground model and at least 20 times in the phase-to-phase model. Insulation strips (PVC at room temperature, and insulation papers with a thickness of 1100 μm at high temperature) were used to compress the coils between them or against the slot mockup.
>
> Their simulation models are in Sec. 3.4.2.

PDIV tests were carried out at room temperature, with relative humidity ranging between 35% and 40%. Test were carried out also at 180°C for the P-G models only. Three samples were tested in each condition, according to Sec. 3.2.2 using the sinusoidal source of Sec. 3.2.6 and conventional PD detection (Sec. 3.2.7). The connection scheme can be observed in Fig. 5.34, and the results in Tab. 5.2.

Fitting the distribution for a set of only 3 experimental values would not be statistically accurate, so the lowest recorded value was chosen to represent each of the conditions. This choice is also in line with the selection of the lowest percentiles to summarize the properties of insulation, as the reliability of the insulation chain depend on the one of the weakest point. For each

Types	Insulation Layer	T (°C)	$PDIV_{pk}$(V)		
			S1	S2	S3
P-to-P	Kapton Film (50 μm)	25	1175	1200	1175
	Nomex paper (80 μm)	25	1275	1275	1275
	NMN paper (190 μm)	25	1700	1700	1700
	NMN paper (240 μm)	25	1950	1925	1925
P-to-G	Kapton Film (50 μm)	23	950	925	950
	Nomex paper (80 μm)	23	1000	975	975
	NMN paper (190 μm)	23	1350	1375	1350
	NMN paper (240 μm)	23	1525	1450	1450
	Kapton Film (50 μm)	180	800	775	775
	Nomex paper (80 μm)	180	800	800	800
	NMN paper (190 μm)	180	925	925	925
	NMN paper (240 μm)	180	1150	1150	1125

Table 5.2: PDIV experimental results for P-G and P-P models, in AC for various insulation film typologies and thicknesses.

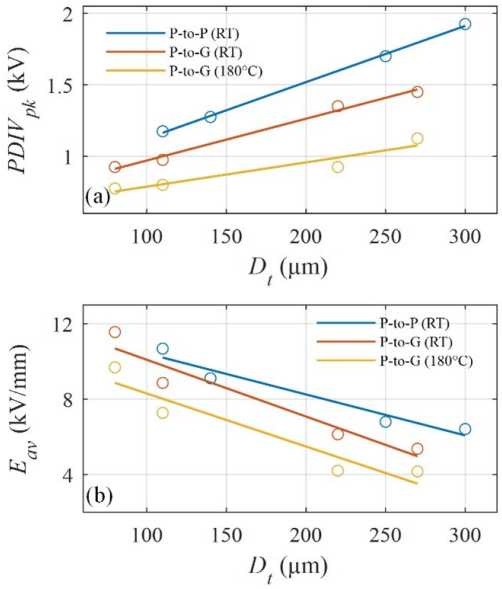

Figure 5.35: Correlation between the PDIV and average field in the insulation, as function of the total insulation thickness.

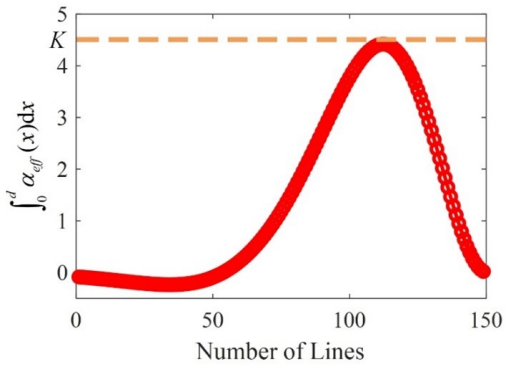

Figure 5.36: Constant K value along the field lines, at PDIV.

experimental condition the total insulation thickness D_t (sum of wires and layers insulation) and the average field

$$E_{av} = PDIV_{pk}/D_t \tag{5.2}$$

were calculated, to obtain a series of fitting curves, in Fig. 5.35. The average field E_{av} and total insulation thickness relationship appears to be non-linear. Otherwise, the PDIV seems to be linear function of the thickness. The curves show that a direct prediction of PDIV starting from the only insulation thickness could be possible. Although, these curves can be used only to some extent as criteria for insulation design, having a significant deficiency in their applicability for different materials, sizes and especially geometries. Indeed, they don't share the same slope coefficient.

It has been thought to improve the prediction using a tool based on Schumann criterion, described in Sec. 3.4. Previous studies showed that prediction of twisted pairs PDIV with a vast range in insulation thickness and wire diameter was possible through the Schumann criterion, relying on a single value for Schumann constant ($K = 6$) [64][82].

A calculation of the constant K of the phase-to-ground and phase-to-phase insulation models was performed for the room temperature values, using the procedure described in Sec. 3.4.2. Values obtained from dielectric spectroscopy tests have been used for the permittivity values used in the simulation.

Starting from the PDIV, the field distribution was calculated a value K has been found for any of the field lines, like Fig. 5.36 represents. The maximum of those values is the one that produces the highest number of critical carriers, hence the candidate for the PD inception.

The values obtained are in Tab. 5.3. Figure 5.4 illustrate those values as function of the total insulation thickness. The constants K of insulation models made of insulation papers (Nomex papers and NMN papers) is relatively stable, and in average 3.58 for the P-G and 4.76 for the P-P, across the materials and the thicknesses. The values for Kapton films are much larger than

Types	Insulation Layer	Dt (μm)	K
P-to-P	Kapton Film (50 μm)	110	8.65
	Nomex paper (80 μm)	140	4.91
	NMN paper (190 μm)	250	4.67
	NMN paper (240 μm)	300	4.69
P-to-G	Kapton Film (50 μm)	80	7.79
	Nomex paper (80 μm)	110	3.54
	NMN paper (190 μm)	220	3.51
	NMN paper (240 μm)	270	3.70

Table 5.3: Constants K of different models at room temperature, obtained starting from PDIV experimental data.

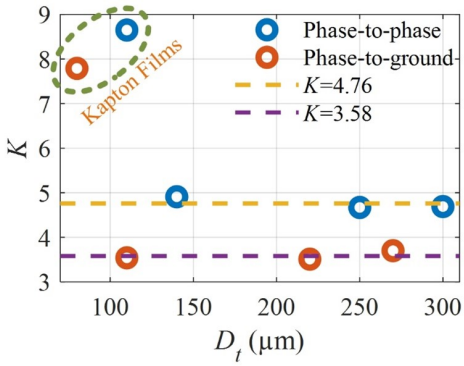

Table 5.4: Constant K value along the field lines, at PDIV.

Insulation Layer	Dt (µm)	Predicted $PDIV_{pk}$ (kV)	Measured $PDIV_{pk}$ (kV)	Error (%)
Nomex paper (80 µm)	110	0.74	0.80	-7.50
NMN paper (190 µm)	220	0.92	0.925	-0.54
NMN paper (240 µm)	270	1.03	1.125	-8.44

Table 5.5: Prediction of PDIV for the same sample geometries at 180°C.

those of other models. This may be due to the fact that the Kapton film is thinner and softer, which could lead to the difference between the simulation model and the actual geometries. Since insulation papers are more often used in the manufacture of motors, the high values of constants K of insulation models with Kapton films can be ignored.

The value $K = 3.58$ has been used to predict the PDIV, for the samples tested at high temperature, as recorded in Tab. 5.5, with errors inside the 10%. Clearly, this set of measurements is insufficient to evaluate the goodness of fit, being too small and not differentiated. However, it is the first step on which a more detailed study can be built.

The analysis performed shows that a simple predictive approach for the PDIV of P-P and P-G is possible, capable of modeling different insulation materials and thicknesses with a single value of the Schumann constant. The method presents some limitation, relying on a model of the geometry that could be not fully representative of the reality (e.g. for the Kapton films). Moreover, the wire thickness has been kept constant to exclude a factor from the analysis. Further tests should be carried out including various enamel thickness to prove that the calculated K remain constant. Nonetheless, given the encouraging results, the values presented can be used as first evaluation tool for the occurrence of discharges in these two types of insulation models and the described methods used as starting point for a more detailed study.

5.2.3 Thermal Aging Cycles for MEA Application

The goal of the experiments was to understand the PDIV trend for motorette models undergoing aging cycles, with a particular focus for the MEA conditions.

The procedure mimics a qualification procedure for a single aging temperature under IEC standards ([92] and [39]), with modification relevant for the MEA sector. To the classical aging technique described in the standards a special temperature-shock procedure and airliner vibration stresses were added. The temperature-shock procedure implemented is simulating the motor startup at high altitude temperatures (-65°C), causing a fast thermo-mechanical variation. The vibration profile applied to motorettes is the one

typical of airliner missions. Also, to understand the performance degradation of the insulation in a more realist scenario the evolution of the PDIV at 100 mbar as aging progressed was monitored.

> **Samples**
>
> The motorettes described in the chapter introduction have been used. Testing of the P-P was achieved connecting to the high voltage to the top coil and the ground to the bottom one, while the frame was insulated from the ground.

Motorettes sets underwent an aging cycle, until failure. The aging cycle used is divided in two sub-cycles:

1. Aging sub-cycle, subdivided in:
   (a) Thermal aging, carried out at 230°C (+30°C of the lowest thermal index among the materials) in a ventilated oven. The thermal cycles last 7 or 14 days. Initially, shorter cycles are used to monitor closely the reduction of PDIV.
   (b) Moisture absorption, where motorettes are exposed to 60°C/80% RH in a climatic chamber for 48 h, similarly to what prescribed by [92].
   (c) Vibration stressing, for duration of 1 hour, with a vibration profile characteristic of aircraft stress. The motorettes are mounted so that the motion occurs at right angles to the plane of the coils so that the coil ends are excited to vibrate as they would under radial end-winding forces in an actual motor, according to [92]. A modal shaker is employed to generate the vibration profile.
   (d) Thermo-mechanical shock, subjecting the samples to a quick temperature jump of 185°C. Motorettes are positioned in the climatic chamber at -65°C, a 40 A current is fed for 30 s, until the copper reaches 120°C.
2. Diagnostic sub-cycle, where diagnostic test are performed. Partial discharge tests were performed raising the voltage up to the PDIV. This differs from the standard [39], that prescribe a PD proof test rather than a PDIV test. In the P-P and P-G the PDIV was tested in AC, in the T-T through a surge generator (Schleich MTC2). Pre-conditioning was applied to the T-T of the motorettes to stabilize the PDIV/RPDIV [94]. The specific test setup for each subsystem are described in Sec. 3.2.

Two different sets of motorette underwent different versions of the aging cycle:

Set A Underwent the full aging-cycle, but with only a subset of 3 motorettes undergoing the vibration testing.

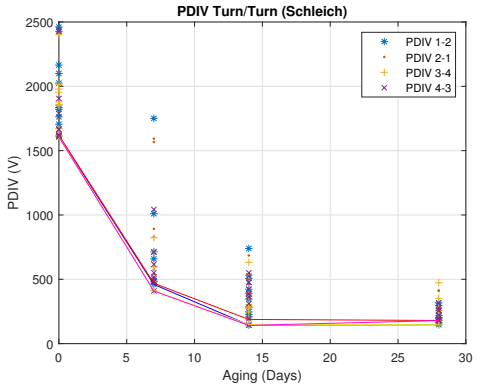

Figure 5.37: T-T PDIV trend as aging progressed. Dramatic drop detected after only 7 days of aging.

Set B Skipped the moisture absorption, vibration and thermo-mechanical shock, underwent the thermal aging only. PDIV was also measured at reduced pressure (100 mbar) in addition to the ambient pressure. Turn-turn PDIV detection was not possible at reduced pressure for the limitation of the instrument.

Turn-Turn

PDIV and RPDIV tests were performed at each aging cycle through a Schleich MTC2-6kV (Sec. 3.2.5). Figure 5.37 shows a sharp decline of the PDIV (for the motorettes Set A). Very similar results are obtained if the RPDIV is plotted instead. This decline was not an artifact of testing, as PD could be heard and often visually observed in the sample end-winding. Despite the different aging cycles, motorette Set B behaved in a very similar way.

The drop is incompatible with any operation and could not be explained solely by effect of thermal aging, as the results of Sec. 5.1.5 are obtained for the same wire and impregnation resin of the one here analyzed and show a moderate decrease of PDIV. Pre-conditioning (subjecting the motorettes to 10 pulses at 2.6 kV just before the test) was ruled out, as control specimens undergoing the test without it did not show any improvement.

It was suspected that the interaction of the thermal degradation by-products of the different dielectrics composing the insulation system of the motorettes could lead to accelerated degradation of the wire insulation (enamel and/or resin) due to chemical incompatibility. To prove that, a thermal cycle (14 days at +30°C of the minimum thermal index among the materials, according to [92]) and consecutive PDIV tests on twisted pairs were carried out using sealed tubes (the same kind used for UL testing [126], Fig. 5.38) containing different materials. Two different tubes were used:

- Tube containing impregnated and non-impregnated twisted pairs with the liners, bandages and sleeving used to assemble the motorettes.

Figure 5.38: UL Tube used for the chemical compatibility analysis, with materials to be tested inside.

Tube	Breakdowns (out of 5)		Tot:
	Impr.	Non-Impr.	
w/ Materials	3	4	7
w/o Materials	1	0	1

Table 5.6: Failures of TP aged in sealed tubes with or without other materials, for chemical compatibility analysis.

- Tube containing impregnated and non-impregnated twisted pairs only.

The PDIV of both the impregnated and not-impregnated twisted pairs from the two tubes were comparable. However, the samples aged in the presence of liners, sleeving and bandaging reported a staggering breakdown ratio, as almost every sample short circuited immediately after PD inception. On the contrary, those aged without other materials did withstand PD activity without breaking down. A comparative table is Tab 5.6.

This phenomenon was further investigated with optical analysis at the Scanning Electron Microscope (Sec. 3.3.4). The twisted pairs aged in the presence of the other dielectrics did present increased degradation (Fig. 5.39) and cracks (Fig. 5.40).

It is speculated that aromatics solvents (as benzene and toluene) were released during thermal aging from the sleeving pipes (SIGI - Favier 15C, silicone-braided fiberglass, class 250°C) used to protect the terminals of the motorettes. The sleeving was blamed for the damage, as it presented an acrid smell after thermal aging. Thus, the drop in PDIV and RPDIV could be ascribed to a chain of events, starting from the release of solvents that weakened the insulation during the thermal aging, followed by crack formation due to voltage conditioning and handling of the terminals. This consequently caused the strong PDIV reduction. The experience shows that it is crucial to

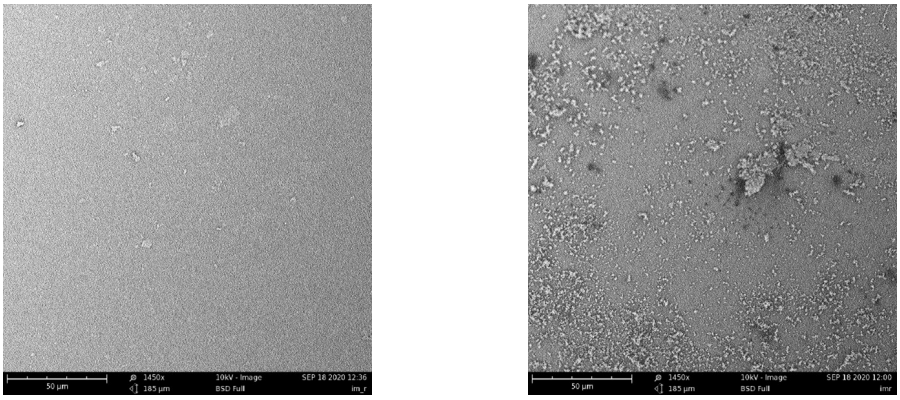

(a) Without materials. (b) With materials.

Figure 5.39: SEM picture of the surface of impregnated samples aged with or without other materials.

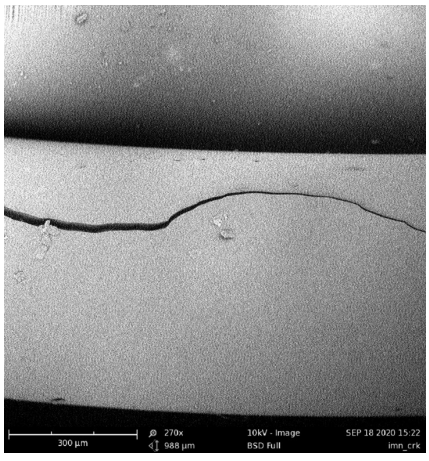

Figure 5.40: SEM picture of a crack on the surface of an impregnated sample aged with a chemical incompatible material.

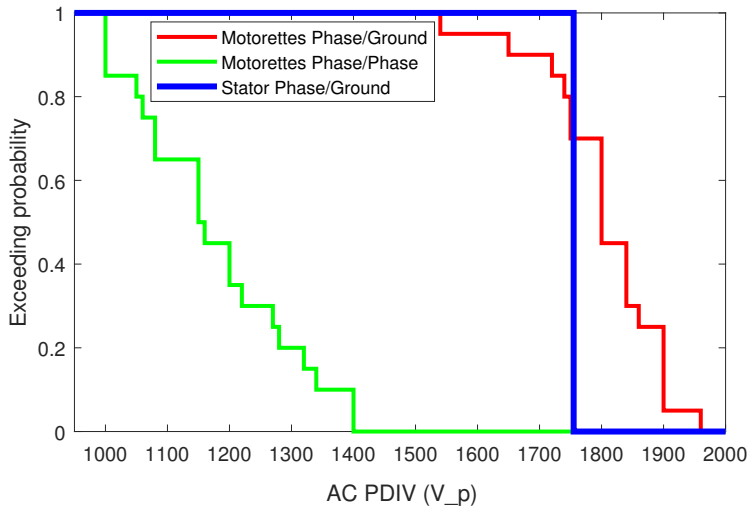

Figure 5.41: Comparison of PDIV values for the stator and its models (motorettes), before any aging.

screen out those material that are not able to work properly together, possibly by thermal tests performed in a sealed environment.

Furthermore, the experiments shows that the T-T PDIV of more complex samples like motorettes do not differ much from the simplest one, like twisted pairs samples. The PDIV range recorded for the unaged motorettes with the pulse generator match with the peak-peak value of the PDIV recorded for the impregnated TPs with the same wire and resin (Sec. 5.1.5).

Phase-Ground and Phase-Phase

The P-P and P-G of the motorettes were tested under AC voltage, in each diagnostic sub-cycle. A comparison with the values before aging obtained for the complete stator (featuring an inaccessible star point, so that only P-G can be tested) shows that the motorettes results tends to be centred around the value found for the stator, as illustrated in Fig. 5.41. The results obtained for the motorettes after each aging cycle are summarized in Fig. 5.42a and Fig. 5.42b, reported as peak of the voltage. For Motorettes A, the tests were stopped after the coils started to move within the slots, at 84 days of aging. For Motorettes A, the tests were stopped at 70 days as the P-G of all motorettes was short circuited.

The P-G PDIV does not exhibit a monotone trend, as after a first decrement starts to increase (both sets, A and B). This phenomenon could be attributed to a reduction of the permittivity of one of the components of the P-G subsystem. Since the impregnation resin has been tested with twisted pairs (Sec. 5.1.5) and did not show the same behavior, the Nomex paper is the most probable candidate for such variation. On the other hand, P-P

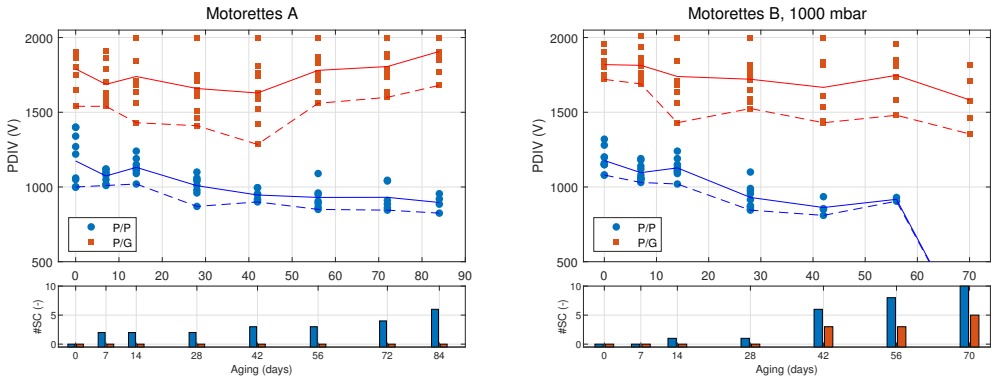

(a) Full aging cycle and ambient pressure diagnostic only.

(b) Thermal only and low pressure diagnostic.

Figure 5.42: PDIV trends (P-P and P-G) and cumulative sample fails for motorettes subjected to different aging cycles.

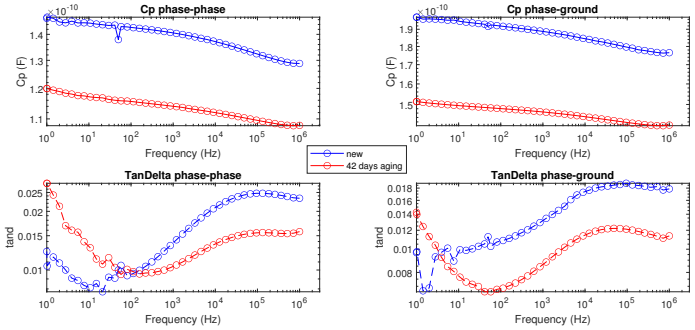

Figure 5.43: Dielectric spectroscopy of the P-P and P-G subsystems of a motorette, prior and after aging.

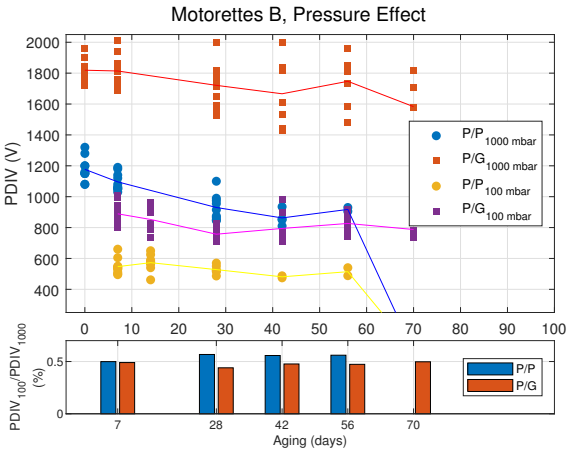

Figure 5.44: PDIV trends (P-P and P-G) at atmospheric pressure and reduced pressure (100 mbar) as the aging progresses, and their ratio below.

insulation shows a monotone decline, with a PDIV that is much lower than P-G. The lower values recorded are not surprising as the thickness of the insulation is much lower compared with the P-G one. Dielectric spectroscopy tests performed on the entire samples, show that after aging the capacitance of the motorette decreased, more for the P-G than for the P-P, as illustrated in Fig. 5.43. Although the change in capacitance reflects both the geometry and dielectric proprieties variation, this result seems to be in agreement with the hypothesis that it is the permittivity that changes, especially in light of the results in section 5.1.4.

Comparing the results obtained for the two motorettes sets, A and B, shows that the extra conditioning steps (moisture and thermal-shock) did not impact significantly the PDIV. This result must be taken with care. It indicates that these stresses do not cause degradation of the insulation in the short times they are applied at any stage of the model's life. However, they have not been applied continuously as aging factors, and it is very likely that applied continuously they contribute to system degradation or PDIV reduction. Dedicated tests are needed to demonstrate the magnitude of their impact.

The cumulative number of short circuits recorded as aging progresses, illustrated in Fig. 5.42a and Fig. 5.42b, stands out. The suspicious high number of failures could be linked to the previously described chemical compatibility issues. Anyway, it is interesting to observe that tests at reduced pressure led to a higher failure rate for both insulation sub-systems. Indeed, only motorette set B underwent tests at both atmosphere and reduced pressure. This observation is further evidence for the increased danger of low-pressure discharges.

A comparison of the PDIV results for 100 mbar and 1000 mbar is in Fig. 5.44. The PDIV drop at reduced pressure is about 50%, with the P-P being

constantly higher (56%) and the P-G starting from a lower value and increase continuously. The outcome is very interesting for two different reasons. First, this number is similar to the value measured and modeled for T-T in [64][82]. This indicates that despite the differences in the field distribution for the geometries of the different subsystem, general rules of technical interest may be found. Second, what has been reported in section 5.1.5 for twisted pairs seems to hold also in P-P and P-G insulation systems, where the ratio of the PDIV at reduced and atmospheric pressure overall appears to increase as the aging progresses. This peculiar result will be further discussed in Sec. 6.2.1.

5.2.4 Summary

Key Findings

- Similarly to T-T models, in P-P and P-G of motorettes the peak PDIV under converter waveforms was found to be higher than the value under AC voltages.
- A single modeling Schumann coefficient (K) for each P-P and P-G geometry was found to fit different materials and insulation thicknesses, similarly to what done in other studies for T-T models. This is the first step towards the creation of dedicated PDIV simulation tools.
- Materials incompatibilities caused a dramatic T-T drop and breakdown ratio. The event likely originates from the creation of cracks from aromatics solvents release.
- Extra conditioning steps to simulate aeronautic stresses (moisture, thermal-shock and plane-vibration profile) did not impact significantly the PDIV.
- PDIV drops after aging were reduced when measured at 100 mbar (milder than for T-T models).

Chapter 6

Insulation Coordination and Qualification

This chapter discusses from a broader perspective the experimental results obtained and uses the insights garnered to improve reliability through insulation coordination and qualification.

Insulation coordination is the practice of designing the various insulation system components, in a coordinated manner and in relation to the stresses and the environmental conditions [127] [128][91]. The challenge can be met with varying degrees of depth, dependent mainly on the degree of the research maturity.

Ultimately the goal of the insulation specialist would be to design the system with a statistical/probabilistic approach, where a quantitative evaluation of the failure risk is assessed through the knowledge of the subjected stresses and the related degradation processes as a function of time. In such way, the insulation systems of the rotating machines is designed with a given statistical failure probability (hence also a given reliability), both for the intended life and for a given single mission profile. In the best case scenario the equipment is designed with predictive maintenance in mind, having its condition monitored during the operation or at certain check-points by means of non-destructive diagnostic tests.

Unfortunately this approach is far from being implemented and before the challenge could be met, many research gaps should be tackled. Rotating machines life prediction has a significant level of complexity, caused by the vast variety of stresses and the possible defects in materials or manufacturing, even for the classical AC stresses and industrial environments [129]. Such complexity makes difficult to isolate the single phenomena and create multi-stress degradation models.

Furthermore, electrification in automotive and aeronautic sectors is relatively immature. The sectors strive for maximum performances with reduced weight and size, pushing for higher power density in the motor-converters chain. Simultaneously they present challenging mission profiles and critical

environments. In the race of next-gen bus DC voltages, customers' needs are often above manufacturers' capabilities, and only a comprehensive multidisciplinary design approach avoids production of complete unreliable machines or costly oversize ones. Nowadays, the target for the insulation design is to minimize the risk of failure mainly improving the weakest point of the insulation and demonstrate that a machine can operate as intended with sufficient margins under a defined mission profile within the specified lifetime. This latter task is satisfied with a representative qualification [44]. In the path to meeting these demands, new knowledge is built that could be used in the future for a more statistical design approach.

Several are the recognized routes to failure for a machine [44]. To reduce the complexity of the goal, the most important design and environmental factors governing the failures specific from the use of WBG-converters and in the MEA environment have to be isolated. This methodology, historically embedded in the dielectric community, is called elsewhere physics-of-failure and relies on the idea that the dominant failure site and mechanism drive the entire machine reliability, since in the failure probability chain is the weakest link that determines the overall reliability [130][131].

For low-voltage rotating machines to be used in electrification of transportation it is clear that the PD inception is the main phenomenon that determines a drop on the insulation reliability [132][48], and it is more so evident after the test campaign performed. The weakness of T-T; the extreme voltage rise times, on-times and switching frequencies; and the reduced pressure are the main contributing factor to the unreliability of motors in the electrification sector. This justified the set of measurements performed.

The life estimation of the equipment then comprises two clearly separable stages, before PD inception and after PD inception. For the first, to compute a life estimation means to evaluate the PDIV evolution as the aging takes place. When the electrical stress overcome the PDIV threshold, the life estimation transitions to the second and becomes a matter of endurance time under PD estimation. Hence, in this study was pivotal to evaluate both, how the PDIV is impacted by the peculiar voltage stress features of WBG-converters and by the aging processes, and as secondary instance evaluate the degradation processes that take place while the discharge is active in the real operating conditions. That has been done in Chap. 5 and Chap. 4, respectively. The results obtained are discussed within a comprehensive framework in this chapter, and are used to establish a conduct to design and qualify a transportation motor with reliability as core requirement.

6.1 Lifetime in Case of PD Inception

When PD are incepted a series of physical and chemical phenomena contribute to the polymer degradation. Corona resistant (CR) winding wires feature

polymeric materials filled by inorganic micro- or nano-particles, able to withstand PD degradation for some time are sometime presented as a solution. While they proved their efficacy in the more standard industrial application, findings of Chap. 4 should be a wake-up call for insulation designers of next generation aircraft.

The endurance times at low pressure and next-gen bus DC voltages showed values incompatible with operation, with lifetimes in the order of seconds the most extreme conditions (100 mbar, 1000 V_{pk}, 100 kHz). The reason of this behavior is ascribed almost entirely to the reduction of the pressure. During a discharge process, electrons gather their energy by accelerating through their mean free path, λ , which is the average distance that an electron can travel without collisions with neutral particles. With mean free path increasing of a factor of ten from the pressure reducing from 1000 mbar to 100 mbar, the average energy of the electron population $\langle w \rangle$ increases by a factor of ten as well, according to:

$$\langle w \rangle = \lambda e E \tag{6.1}$$

When the electron energies are in excess of the bond energies of the insulation (typically 3-4 eV for C-C and C-H bonds), the electron bombardment on dielectric surfaces causes erosion by Dissociative Electron Attachment (DEA). Accordingly, the damage sustained per unit time increases with the number of impacting electrons (N, proportional to the magnitude of the discharge) times the fraction of electrons with kinetic energies above the bond energy (F). Hot electrons having energies of 10–15 eV can cause both dissociative electron attachment and ionization, those with energies in excess of 15 eV ionize the molecules of the solid and propagate within the solid losing about 9 eV at each ionization [133]. This leads a single electron to break multiple bonds resulting in a superlinear dependence of the degradation rate on $N * F$.

The energetic levels of the electrons population of the PD, w, which is effectively a non-equilibrium cold atmospheric plasma, approximately fit to a Druyvesteyn distribution function [134][135]:

$$f(w) = 1.23 * \left(\frac{w}{\langle w \rangle^3} \right)^{1/2} * exp\left(-0.55 * \frac{w}{\langle w \rangle}^2 \right) \tag{6.2}$$

This means that even a population characterized by a value of $\langle w \rangle$ lower than the minimum energy necessary for DEA degradation is capable of inducing some damage, since a fraction of its population is going to have a sufficient energetic content to trigger DEA. As the pressure reduces, the distribution flattens, as is shown in Fig. 6.1. Electrons having larger energies increase.

The shift toward higher energies for the electron as the pressure reduces has been observed using optic emission spectroscopy [89] and provides a partial explanation for the very short PD endurance time observed at low pressures, for both standard and CR winding wires. It is unclear whether this mechanism

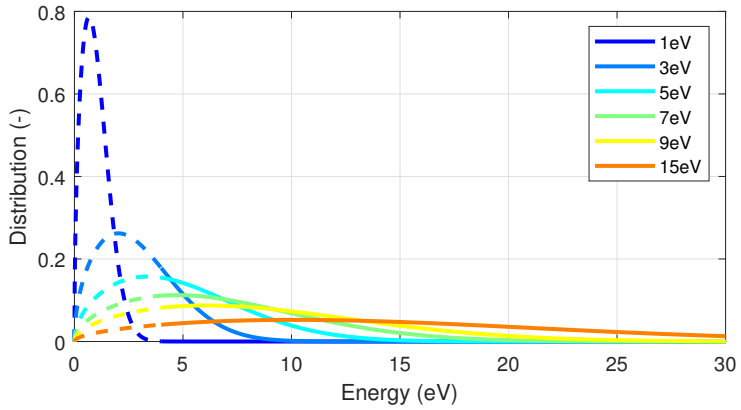

Figure 6.1: Distribution of the electrons' energetic content, for different mean energies. The lines are solid in regions where the energy is enough to start DEA events, dashed elsewhere.

leads to a highly accelerated etching of the polymeric matrix only or if also the chemical bonds of the inorganic materials or the inorganic-organic interphase that are too strong to be broken by high-pressure PD are now accessible (energy bonds in mica are above 100 eV).

A clue comes from the recorded variation of the voltage endurance coefficient for higher values of voltage and lower levels of pressure. The increased degradation recorded might be an indication that an energy threshold (dependent both on the field and the pressure) has been crossed, beyond which extra degradation processes of inorganic materials are activated. The hypothesis is that above this pressure-voltage threshold, the average electron energy is so large that energetic electrons capable of breaking the inorganic chemical bonds (or the bonds between the inorganic nanoparticles and the host polymeric matrix) are abundant. These highly energetic electrons justify the comparable breakdown times of CR and non-CR materials.

The experiments showed that also environmental factors play a major role, with humidity decreasing the endurance times by one order of magnitude probably by the addition of chemical degradation, worsening the scenario.

It appears, therefore, that the only way to design a machine to operate in an MEA (non-pressurized) environment is to have the equipment operate in the absence of discharge for its entire life (i.e., with a Type I design).

The context is less problematic for the automotive sector. CR technologies may help the designer, even if a more detailed analysis of their efficacy under WBG-converter waveform has to be assessed. Indeed, it was observed also by other authors [111], that PD activity under converter voltages is harsher than the one under AC, even if voltage and frequency are the same. Measurements of endurance times of non-CR Litz wires at atmospheric pressure and various temperature under modeled T-T converter pulses reminded that operation with PD activity incepted for organic only materials is not possible, even for

DC Bus (V)	Perc. Time (%)	Operation ref. RTCA DO-160
564	79.6	
620	19.9	
692	0.27	abnormal transient
795	0.08	normal transient
842	0.03	abnormal transient

Table 6.1: Reference Voltage Levels for a MEA actuator.

the transients that may appear in the system. At voltage levels barely above the PDIV, the insulation system failed in matter of minutes.

Hybrid 60034-18-41/42 Design Approach For systems that present a non-constant voltage profile, like the one of Tab. 6.1, an hybrid design approach could be followed, designing the machine to be PD free for the normal operating voltage (the lifetime is determined by the time needed for the PDIV drops below the normal operating voltage or other degradation phenomena bring the insulation to failure) and to operate with PD incepted for the transients only.

The design for the insulation should be split in two separate branches. The overall lifetime of the machine becomes the lower between the one obtained under PD activity and the one assessed as usually.

The estimation of the lifetime under PD can be executed relying on cumulative damage laws, of which Miner's law is the simplest version. Cumulative damage laws sum the damage sustained at each stress level, provided that the percentages of time at the various stress levels are known.

The Miner's law, for k-levels of a given stress factor S can be expressed as:

$$\sum_{i}^{k} \Delta t_i / L_i = \sum_{i}^{k} p_i L / L_i = 1 \tag{6.3}$$

where Δt_i is the time under each stress level S_i and L_i the lifetime that would be achieved if only S_i is applied continuously, so that $\Delta t_i / L_i$ is the fraction of damage caused by S_i only. Then, p_i is the probability that $S = S_i$ (for the sake of simplicity, S is assumed to be a discrete random variable but could be a continuous one as well). The unknown term to solve for is L, the total life result of multiple stress levels application.

The life L_i can be obtained for all the stress levels from the experimental life curves of the insulation system, i.e., curves having the form $L = g(S)$ where g is an appropriate function. It is important to highlight, that several simplifications are necessary to apply Miner's law since the stress is not only

electrical (the PD erosion) but also thermomechanical: a unique model accounting for electrical, thermal, and mechanical would be necessary, but the testing costs and times for developing such a model are often prohibitive. In other words, determining the g function for accounting all the combination of conditions (e.g. environmental, degradation stage), that may also present synergies, is problematic.

Miner law could help assess roughly the lifetime achievable under PD-inception, while the design of the machine regarding the PDIV keeps following its own design rules. The g functions may reduce to:

- $L = \infty$ for all voltage levels where PD are not incepted.
- $L = A * V^{-n}$ (Eq. 4.1), the inverse power law, for all the voltage levels where PD are incepted. If the environmental factors have a significant impact on the degradation processes, then different life curves with their respective coefficients should be employed (e.g. temperature, pressure, humidity) for each major operating point.

Given the probabilities of each operating environmental point combined with the probabilities of each voltage level, the maximum lifetime achievable with the selected materials can be calculated resorting to the respective life curve model for each of those conditions.

Let us make an example considering a single life curve model. Consider an actuator for the MEA that operates with the voltage reported in Tab. 6.1 at 150 mbar, featuring in the T-T one of the CR enameled wire studied in Chap. 4, like the one with the life curve of Fig. 4.7. The wire has an AC PDIV around 520 V, and for the sake of the example we can consider to operate without PD activity incepted for all the non-transient voltages and PD incepted for all the transient voltages. An overshoot factor of 1.5 at the machine terminals and an important uneven voltage distribution of the voltage (70% of the jump voltage is considered, see Sec. 2.2.1), reasonable for the use of a SiC-converter. If the actuator is operated with a bipolar converter, Eq. 6.3 predicts a lifetime of 200 hours[1], surely lower than the time needed for the PDIV to drop below the nominal voltage due to aging. This lifetime is much less than the goal for transportation machines, even if the example considers current-generation voltage levels and sub-critical voltage stresses. The example demonstrate that this design approach is hardly employable at the lower pressures of MEA aircraft, at least for un-pressurized machines.

Conversely, the one described could be a feasible approach for motors in the automotive sector, relying on the longer endurance times of corona

[1] known the life curve, that for the wire under discussion is $L(V) = 62.53 * V^{-13.169}$, and the stress levels of Tab. 6.1, considering PD incepted only for V > 620 V then Eq. 6.3 becomes

$$1 = \frac{0.27 * L}{62.53 * 962^{-13.169}} + \frac{0.08 * L}{62.53 * 795^{-13.169}} + \frac{0.03 * L}{62.53 * 842^{-13.169}}$$

that has to be solved for L

resistant materials at sea level pressure. Here the lifetime obtainable considering the life curves of CR-wires (e.g. [75][76][136][137][138][139]) and voltage swings/transients in the range between 800–1000 V appearing for less than 1% of the service time results in values greater than the typical design of 10000 hours, thus operation in mixed PD regime may be evaluated. Due to the endurance times depending on the voltage with an inverse power law, the lifetime estimated is very sensitive to the variation of the voltage stresses to the predicted ones, both in terms of probability than in terms of voltage levels estimation. If this lifetime prediction method is applied, it is crucial to remember the uncertainty margins it carries.

Moreover, all the lifetime regression line estimation should be performed relying on the lowest percentiles for the endurance times collected, representative of the weakest portion of the insulation, to guarantee a conservative design.

6.2 Major Contributors to PDIV

The quantities that contribute to determining the value of PDIV become primary when its maximization is sought. An in-depth discussion following the results obtained is addressed here, divided mainly into three macro topics:

- The impact of converter waveforms on PDIV, with a theoretical analysis of the physical mechanisms that justify the findings.
- The importance of resin and the properties to be pursued for guarantee good performances.
- The peculiar characteristics of discharge inception in low-pressure environments and potential PDIV control measures.

6.2.1 PDIV under Realistic Converter Stresses

The (microscopic) effect of converter waveforms on the insulation has been explored more than once in literature, inquiring how the characteristics of these waveforms (e.g. frequency, duration, rise time) impact the inception voltage. The results are some times contradicting, as with increasingly short times rise times (typically associated with oscillations) and fast switching voltages some authors found increasing PDIV [64][65][66][67], while others found decreasing PDIV [68][69][70].

In Chap. 5, extensive measurements have been performed on many specimens, using waveform originating from fast switching sources. Tests were carried out on models of T-T in Sec. 5.1.1 and P-P, P-G models in Sec. 5.2.1. Of particular care was the approximation of the real T-T stress, using a short-width 3-level bipolar pulse. The results obtained are confirming and expanding the body of evidence supporting the findings of authors that

recorded higher PDIV for faster voltage phenomena (measuring voltage resorting to the peak of the waveform). The analysis performed here hopes to show how the results obtained are the most convincing, being justified by a theoretical description.

Discharge mechanisms typical of the inter-turn insulation system involve small air gaps, electrodes covered by dielectrics and mildly non-uniform electric fields. Today the criteria for determining the voltage levels leading to PD inception are not entirely understood [45]. Despite this, from first principles PD events can be incepted only when (a) the field in the air gap between the wires is high enough to ionize the air molecules and (b) a seed electron is present to initiate the electron avalanche process.

Larger inception voltages for the short-width or fast oscillating overshooted pulses (like the one recorded in Chap. 5) may be caused by the impossibility of fulfilling either or both of these conditions. These might imply that the electric field in the air is lower when using "fast" voltages or that the probability of starting electrons is so low that the PDIV is largely overestimated. On the other hand, lower inception voltages (recorded by other authors) indicate that some phenomenon is inhibiting discharge for the slower waveforms or aiding the discharge for the faster ones.

The results obtained under UV irradiation in Sec. 5.1.1 bring concrete and important evidence, to settle the argument and single out the phenomena affecting the PDIV inception. It is unlikely that many electrons would be produced by photo-ionization in the gas from the UV source employed, as its energy is not compatible with the ionization of gas molecules[2]. Anyway, UV-irradiation has been used successfully to reduce the time lag of the discharge in sphere gaps, irradiating the metallic electrodes [46][142][143][116]. In the emitted range of the UV lamp selected, photo-emission from polymer surface is possible (energy threshold is 3 to 3.5 eV) [120], hence electron can be generated directly on the material surface, available for being accelerated by the electric field, similarly to the experiments for the sphere-gap. Summarizing the observations from the test performed, square-shaped 3-level waveforms with 1 μs and 9 μs of pulse on-time respectively were recorded to have different PDIV, the former (shorter) up to 7% higher than the latter (longer). While irradiated, their PDIV drops to the same level of the non-irradiated longer-pulses case. This might be enough to demonstrate that the short times under voltage lead to a time lag for the first electron appearance.

When the seed electron is not artificially originated on the surface of the sample, it is unknown which process brings to its generation. The electron might be generated by background radiation in the air volume or on sample surface. If the electron is considered to appear in the air volume estimation

[2]Ionization of air requires energies higher than the ones developed by the lamp used, that tops to 5.6 eV. According to [140] the first ionization potential for molecular nitrogen and oxygen are 15.6 eV and 12.5 eV, respectively, corresponding to limit wavelenghts of 79 nm and 99 nm. Absorption of air in the UV range is reported in [141]

of its generation probability might be performed with Volume-Time theory, as performed in [144]. Alternatively, the electron could be freed from the surface of the polymer by de-trapping processes. Below the onset of field emission processes, the physical mechanisms that provide the seed electrons are unclear. Electrons on the surface of the material could be trapped electrons from previous events or could be provided by the electrode. Electron transport mechanisms within the bulk of the insulation material are not incompatible with the sourcing of the starting electron[3].

In addition, it is very likely that before the inception of the PD events, ionization takes place in sub-critical phenomena, perhaps Townsend-like PDs [146]. Such events do not cause significant degradation of the polymer surface, differently than streamer (or streamer-like) PD discharges which manifests important energy transfer. Nonetheless, the carriers so generated can reach the surface and cause different phenomena depending on the surface trapping mechanisms and the recombination speed. If the charges gets trapped, they can contribute to the enhancement of the field at the next field polarity reversal. Some evidence for charge deposited after PD inception show that deposited charge may remain present for up to 24 hours [113]. Indeed, both bulk or surface space charge accumulation can distort the field distribution [147]. Also, themselves can become the source for the seed electron. The presence of accumulated space charge does not helps to discriminate the difference of PDIV reported, neither explain the results of other authors.

Unfortunately, the time scale of all the mentioned phenomena are hard to estimate. In all these cases, an accurate prediction of the statistical fluctuations of PDIV is hindered by the limited knowledge of the discharge mechanism (consequently, of the most accurate criterion for streamer inception calculation), as discussed in [45].

Contrarily to what observed for the short-width pulses of 1 μs of duration, UV-irradiation did not provide any help in reducing the PDIV for waveforms with fast oscillating overshoots where the peak of the voltage was reached only for few nanoseconds. For this scenario, additional phenomena could take place. First, the formation time lag of the discharge may start play a role, depending on the length of the discharge path. In this instance the time needed for the discharge to become critical may be too slow, and the field

[3]Carriers mobility in the bulk of polymer materials is limited by the inter-molecular mobility (orders of magnitude lower than the intra-molecular one), due to the presence of traps [145]. Inter-molecular mobility is typically in the range 10^{-7}–10^{-14} $m^2V^{-1}s^{-1}$. From the mobility μ definition (concept not completely transferable to the polymers containing traps), the time t required for migrate a distance s under the electric field E is:

$$t = \frac{s}{\mu E} \tag{6.4}$$

Considering the figures of the inception of the discharge in a twisted pair (voltage of 800 V applied on an insulation thickness of 70 μm that has to travel for 35 μm) the electron can migrate from the electrode to the surface in times as short as 25 μs.

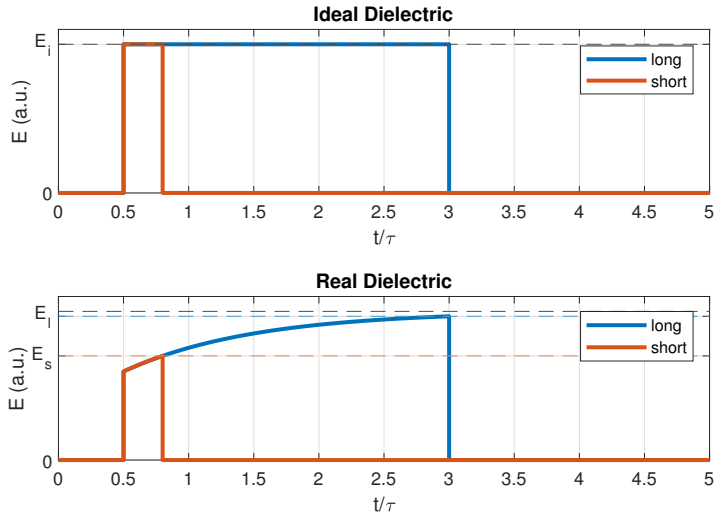

Figure 6.2: Electric field appearing in a selected point of the air gap for shorter and longer pulses in case of an ideal or real (Debye-modeled) dielectric.

removed before the gap short circuits.

An alternative and more sounding explanation could come from the polarization physics. When a voltage is applied to the dielectric (in this case the enamel or the enamel and resin compound) the buildup of polarization takes a finite time, that is the time needed for the dielectric dipoles to get aligned in the field-orientation opposing its direction. This is the basic description of the dielectric relaxation. Let us model the dielectric relaxation in its simplest manner, with a single relaxation phenomenon having a relaxation time τ and following the Debye polarization model.

Before the dielectric polarization takes place, the field inside the dielectric is higher, and so is the voltage drop inside the solid insulation. Of the total voltage drop from the metallic electrodes, in this scenario a smaller portion drops in the air. After the polarization takes place, the opposite happens, with the electric field in the solid reduced and higher voltage drop in the air. Figure 6.2 illustrates, for explanatory purposes only, the ideal value of the electric field that would appear in a selected point in the air considering instantaneous polarization phenomena for two pulses, one with duration much shorter than τ and the other comparable with it. The two pulses may represent a very short width square pulse of overshoot portion of the wave. If real polarization is accounted, the field would increase gradually in the selected point, reaching a maximum value of E_l for a long pulse (identical to the value reached for ideal polarization, but reached in a longer time) and a smaller value E_s for the short pulse. Only for pulses lasting longer than 3 times τ the same field as the ideal condition is reached.

Another way to describe the phenomenon is in the frequency domain. The dielectric permittivity drops as the frequency increases and if the same De-

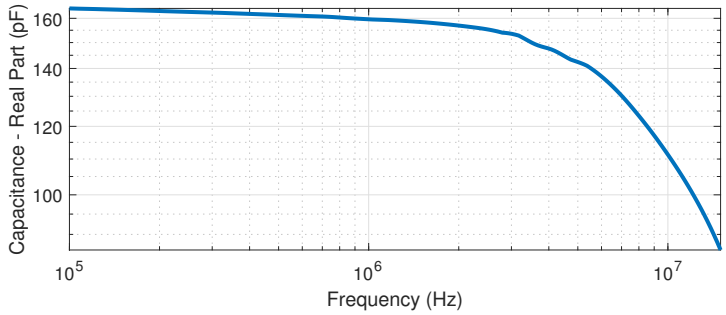

Figure 6.3: Dielectric spectroscopy of polyamide films in a broad frequency range, up to 15 MHz

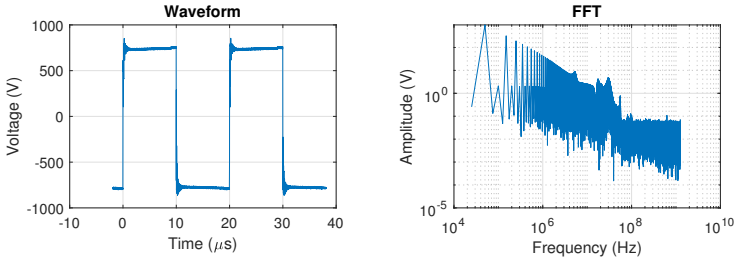

Figure 6.4: Converter waveform and its fast Fourier transform.

bye model is used with a single polarization, a single drop is centered at the characteristic frequency $f_{ch} = 1/\tau$. Two regions may be individuated with different ε values, above and below this characteristic frequency. Consider the interface between the solid dielectric and the air gap, without space-charge deposition. The field at the interface can be written (from Maxwell's Equations, especially from Gauss' Law $\nabla \times D = \rho$) as:

$$\nabla D = 0 \rightarrow \varepsilon_{solid} E_{solid} = \varepsilon_0 E_{air} \tag{6.5}$$

that results in

$$E_{air} = \varepsilon_r E_{solid} \tag{6.6}$$

For the high frequency harmonics of the voltage waveform (the ones describing the short rise time and following fast oscillations, $f > f_{ch}$) the $\varepsilon_r = \varepsilon_{hf}$ is lower and not contributing at the reinforcement of the field in the air as much as the frequency component. Evidence exists that such relaxation happens for the materials under investigation. Dielectric spectroscopy in a broad frequency range was performed with the instrument of Sec. 6.3 for polyamide films. Results are in Fig. 6.3 and shows a drop of permittivity starting from around 2 MHz, where the converter waveforms with overshoots have a significant energy (see Fig. 6.4).

If any space charge is present the description has to include the field generated by the charges, nonetheless, the principle of the phenomenon remains.

Concluding, transitioning to faster voltages (both in terms of rise time, oscillations, overshoots and frequency) appears to increase the PDIV, perhaps as a result of multiple phenomena. First of all, the statistical time lag for the seed electron appearance and then possibly the time required to transfer the field on the surface of the material due to dielectric phenomena. Thus, for testing an apparatus, if the voltage is reported with its peak, the sinusoidal grid-frequency testing voltage is likely the worst case for PD inception and no extra safety factors should be employed for considering the converter waveform features during the PDIV-oriented design. Testing with shorter pulses, similar to those generated in the T-T by WBG-converter with rise times down to tens of nanoseconds might provide even higher PDIV levels. However, the increases reported might not be fully exploitable by the insulation designer, due to their statistical nature.

6.2.2 Critical Role of the Impregnation Resin

As the reliability of the machine is oftentimes dominated by the probability of inter-turn insulation failure, impregnating resins play a key role, filling the cavities between the enameled wires in the slots and increasing the insulation thickness in the end-winding. Therefore, the reliability of the electric drive chain becomes dependent on the performance of the impregnating resins. This context is pushing the need for improved dielectric properties of varnishes and resins, able to improve the PDIV of the machine at all operating conditions.

The results of Sec. 5.1.4, obtained through a combination of PDIV tests, dielectric spectroscopy analysis and FEM modeling indicate that a variation of PDIV as temperature changes in impregnated samples of the turn-turn insulation is the result of several phenomena acting simultaneously. Both the air density reduction, the thermal expansion of the resin, and the modification of the field distribution from the permittivity change could impact the final value of the PDIV. Conversely, for non-impregnated samples only the air density reduction is deemed to play a role, due to the negligible variations of permittivity and thickness with temperature.

The impact of these phenomena is not equally important, as better performances in terms of PDIV increment for a selected resin can traced back to the thickness of the coating layer deposited on the enamel, with permittivity having an ambiguous effect and thermal expansion probably a negligible one. Indeed the comparative experimental activity between three resin was able to determine that despite all of the them were operating above their respective glass transition temperature, some with strongly increased dielectric permittivity compared to the one at room temperature, the PDIV reduction was not correlated to that increment. The results obtained in [121], where a correlation between PDIV and change in capacitance during thermal aging is present, are probably caused by a change in insulation thickness [148] and not by a change in permittivity. Therefore, not knowing a priori the trend of

the two parameters, the use of capacitance as a diagnostic parameter could prove problematic. The simulations performed for the composite enamel-resin system predict that when resin permittivity increases up to 2 times the enamel one, the PDIV diminishes. If the permittivity further increases, the electric field in the air is weakened, eventually leading to higher PDIV. For the enamel-resin composite, the resin permittivity variations appear to affect the PDIV to a lower extent than the enamel permittivity for the enameled only model [82][64]. Insulation thickness, on the other hand, keep its primary role. To improve the prediction model other steps are necessary. First, the section geometry of the sample obtained from sample sectioning is needed, with special care for the portion of insulation close to the contact of wires, were the resin layer is thicker and modeling is more complex. Second, a better understanding of the interaction between geometry and dielectric variations when the temperature exceeds the glass transition is required.

Moreover, some resins may present critical behaviors at higher temperatures. The results of Sec. 5.1.3 illustrate that some impregnating resins affect the PDIV at operating temperatures in a unfavorable way. In the worst case, the PDIV of the impregnated wires can be lower than that of the bare wires. This result can be partially explained in light of the analysis just carried out, but is unclear if the variation of the sole dielectric parameters can fully justify this behavior. The compound impact of permittivity increment and air density reduction have been estimated to reduce the PDIV about 15% according to preliminary simulation (with resin thickness of 50 μm and relative permittivity going from 3 to 5), while in this experimental scenario the drop is about 25%. More complex thermo-mechanical interaction should be investigated to understand the result. The observations mandate to screen out resins having a poor performance at high temperatures, for that simple tests on insulation models can be performed, comparing the PDIV of impregnated and non-impregnated specimens at room temperature and at elevated temperatures. The resins with unsatisfactory behavior should not be considered for WBG-converter-fed applications, like in automotive and MEA sectors.

The results of Sec. 5.1.5 suggest that as thermal aging progresses, the PDIV drops with an accelerated ratio under overshooted SiC impulse testing voltages compared to classical AC sinusoidal voltages. Indeed, while larger PDIV values were achieved for converter voltages for new samples, values recorded after 30 days at +30°C of the resin thermal index show that sample tested under AC and SiC waveforms share comparable values. Considering the absolute values of the measurements, the peak for AC still remains intermediate between the bus DC and the peak of the converter, with the latter approaching the AC values. This is illustrated in Fig. 6.5. An unsaturated-polyester resin was employed.

Regarding the higher PDIV values obtained for waveforms with the peak reached with fast oscillations the same considerations made in the previous section can be traced. In this scenario the analysis tends to favor explana-

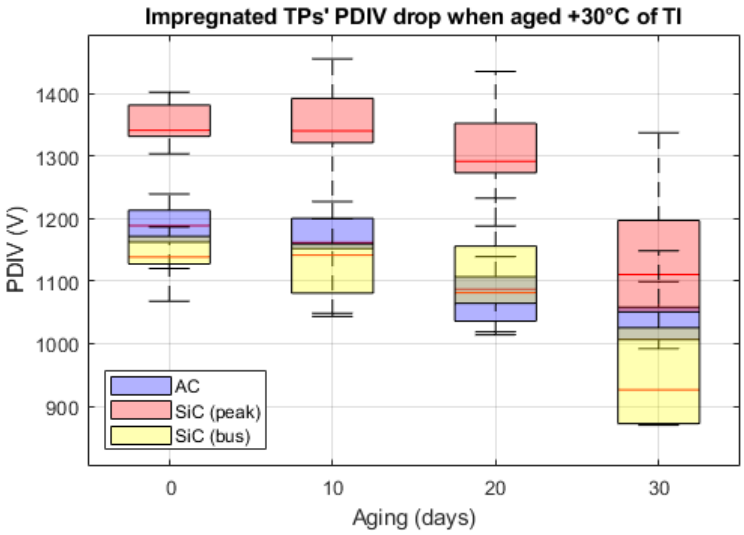

Figure 6.5: PDIV trends under SiC-converter and AC waveforms as the aging progresses. The values are reported both for peak and bus DC for the converter waveshape.

tion through dielectric relaxation phenomena taking some time. Under this assumption, it may be conjectured that with thermal degradation, the permittivity variation is not constant along all the frequency spectrum. After aging, in the high frequency portion of the spectrum where the converter has the frequency content associated to the fast oscillations, the permittivity could be greater than at low frequencies. That could be caused by oxidation processes not homogeneous along the frequency spectrum and chain scission processes that might reduce the low frequency permittivity. This could justify the trend, as more high frequency field would be pushed in the air in aged samples compared to pristine ones. However, the process would require a first electron available at the peak of the waveform for those fast transients, hypothesis conflicting with the other results obtained. In [149] thermal degradation of the resin showed an increase of permittivity and DC conductivity for the lower temperatures, that are the test condition here applied. The increased DC conductivity may help sourcing the starting electron. Possibly, investigation should be performed at higher temperatures, similar to the operating ones, where according to [149] the resin behavior reverses, with a strong degree both in terms of dielectric permittivity and DC conductivity.

The PDIV reductions obtained for unframed specimens are greater, with PDIV under converter waveform lower than under AC waveform. Samples were subjected to mechanical stress by handling (when already embrittled by thermal aging), and tested repeatedly after each thermal cycle (with AC being the first test). The failure rate of the specimen after the onset of PD activity was also higher. The outcome should not be attributed to the test voltage, as both handling and previous discharge activity deteriorated the

insulation. The result, however, is a reminder of the mechanical brittleness of unframed impregnated specimens, a condition similar to the one present at the end-winding of a stator. During the same campaign, a noticeable increase of temperature due to dielectric losses was recorded for all the samples fed by converter waveforms with frequencies of 100 kHz. The phenomenon was active also on pristine samples, contributing to the thermal aging from the beginning of the machine life.

Concluding, evaluating the performance of impregnating resin is a challenging operation. Testing impregnated twisted pairs remains an elusive task, with results that need be evaluated carefully and on statistical basis. Two major issues are indeed typical of these tests: a large variance of the experimental data associated with the randomness of resin deposition, and the brittleness of the insulation that demands for a very careful handling to prevent cracking the insulation. Overall, the thickness of the resin layer is the most important parameter to improve the PDIV. Hence, the material designers should concentrate effort maximizing its coating effectiveness by controlling the viscosity, adhesion, and thermal expansion coefficient. However, the two resin requirements (a) to fill the slots completely avoiding the formation of cavities and (b) reduce the flow of the resin in the end-winding when the stator is extracted from the autoclave for the curing in the oven, are at odds. On one hand, the viscosity of the resin should be low to avoid the first issue (a), on the other larger values helps the latter (b). Trade off solutions are needed. A possible solution is to use a low-viscosity epoxy resin suitable for double impregnation. Alternatively, it is possible to encapsulate the end-winding. This solution however increases the weight of the actuator.

Operating the resin above its glass transition temperature did not envisaged problems, and in light of the results obtained it is yet unclear how important is to control of the dielectric permittivity of the material. Anyhow, it becomes crucial to screen out materials that at operating condition perform worse than their un-impregnated counterparts.

6.2.3 Systems Operating in Aeronautical Conditions

Partial discharge inception voltage is greatly reduced in low-pressure conditions, typical of the aeronautic environment [88][150]. The drop of PDIV at 150 mbar from standard ambient condition has been measured to be around 50%, while the pressure reduction is about 85%. The reason for the PDIV reduction is that as the pressure decreases the mean free path traveled by the electron accelerated by the electric field is increases. Accordingly, the kinetic energy acquired by an electron in its path between collisions is greater and a smaller field is required to reach the ionization energies of the neutral air species [46]. The same mechanism drives also the PDIV reduction for higher temperatures, as both the temperature increase and pressure decrease determine a reduction of the air density, associated with the mean free path

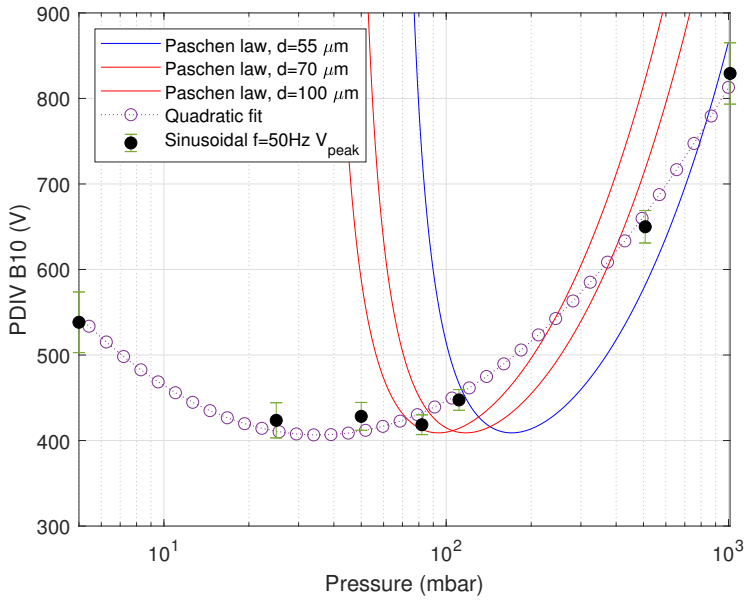

Figure 6.6: Experimental data fitted with a quadratic regression line [64] and with the Paschen law, for three discharge lines lengths.

increase. This leads to decreased inception voltages, in a Paschen-like fashion.

To this regard, Paschen Law cannot be used as direct tool for fitting the PDIV of the specimens, as a definite discharge length is not defined. Some tools have been realized to predict the PDIV using Paschen law, searching for the minimum voltage that satisfies the Paschen breakdown criterion for each of the field lines of a TP geometry [83][84][85]. The fit of the model to the experimental data depends on the selection of the coefficient for the Paschen law, that in turn depend on the gas material and the secondary emission coefficient of the electrodes. The Paschen law is founded on the Towsend breakdown mechanism, where electric field is constant, electrodes are not covered by any dielectric and secondary electron emission from cathode is fundamental to sustain the discharge mechanism. Despite some claims can be issued in favor of secondary electron generation from polymer surfaces [151][152][153], the knowledge on the topic is limited and it is unlikely that discharge events in dielectric bounded conditions are produced with a cathode feedback mechanism. Furthermore, studies show that the Paschen law deviates for gaps with lengths in the order of ten micrometers [104]. For these reasons its application might be less straightforward than expected.

It is worth understanding to what extent the mentioned PDIV reduction with pressure can be limited with the insulation coordination. For each winding wire diameter, three different insulation grades (grades 1-3) with increasing insulation thickness are available on the market [37]. Grade 3 wires are often the most suitable for inverter duty in a standard industrial environment. The increased performance in partial discharge prevention come with the cost of

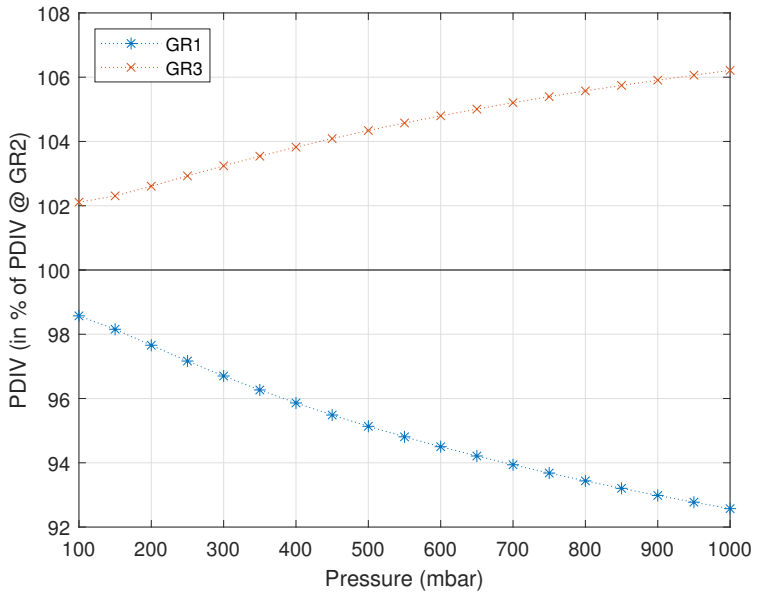

Figure 6.7: PDIV performance difference of GR1 and GR3 wires compared to GR2 wire, for the pressure range of interest for MEA applications.

a reduced slot fill factor, worsening the power density of the drive, that is oftentimes the main target to be achieved. Simulation of wires with the same diameter (0.56 mm) but different grades with the software of Sec. 3.4 were performed with variable pressures. The results are reported in Fig. 6.7, with values obtained with GR2 as the baseline. As the pressure decreases, the dependence of PDIV on the enamel thickness becomes less significant, PDIV at 150 mbar increases to 473 V with a GR3 wire starting from 438 V with a GR2 wire. The increase is limited to 38 V (8.7%) and might not be a turning point to improve the design.

This behavior can be explained inspecting the electrical field lines where PDs takes place (here indicated as critical field lines, CFL). The lengths of the CFLs as a function of the pressure are reported in 6.8. The CFLs follow approximately the reciprocal of the pressure. Assumed that the electric field is constant and normal both inwards and outwards the dielectric surface, then:

$$V = V_{gas} + V_{solid} = E_{gas} * l_{gas} + E_{solid} * l_{solid} \tag{6.7}$$

where E_{gas} and E_{solid} are the electric fields in the gas and in the solid respectively; l_{gas} and l_{solid} are the lengths of the CFLs in the gas and in the solid respectively.

The electrostatic partition of the voltage between the air and the solid insulation the voltage drop in the solid can be evaluated as:

$$V_{solid} \approx V * (1 - \frac{l_{gas}}{l_{solid}/\varepsilon_r}) \tag{6.8}$$

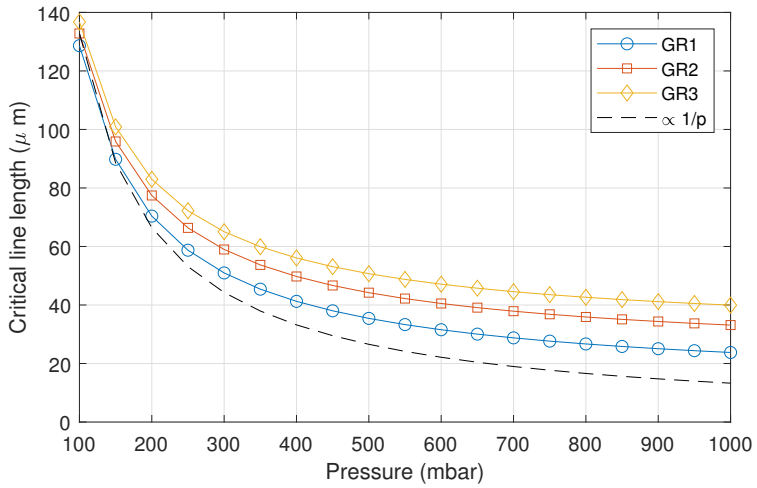

Figure 6.8: Evolution of critical field discharge line length as function of the pressure.

where ε_r is the permittivity of the enamel.

Known that $l_{gas} \approx k/p$, while the same does not happen for l_{solid}, the voltage drop in the solid insulation form Eq. 6.8 gets reduced as the pressure decreases, because the critical lines lengthen. Consequently, the role of the solid dielectric becomes less important at reduced pressures.

Sensitivity curves of PDIV to the enamel parameters have been traced from the same software and are illustrated in Fig. 6.9. The sensitivity to thickness and permittivity marked in the legend were evaluated respectively at the values of 2.7 of relative permittivity and 35 μm of thickness. Seemingly, the reduced sensitivity of PDIV to the enamel parameters makes less attractive using Grade 3 magnet wires. However, at the same time, it de-emphasizes the impact of aging on the reduction of PDIV over time, both in case of thickness reduction (as recorded in [148]) or as permittivity increases.

This analysis completely matches the experimental results obtained on aged T-T models (twisted pairs, both impregnated and not) in Sec. 5.1.5 and in aged P-P and P-G models in Sec. 5.2.3. The ratio between the PDIV at lower pressures and ground pressure increases as the aging progresses, determining an improvement for the insulation designer.

The remarks here noted demonstrate that in the typical aircraft operating condition, the insulation designer has even less tools to control the PDIV than usual. In this scenario, the stress reduction solutions are more effective than the ones that try to improve the insulation systems.

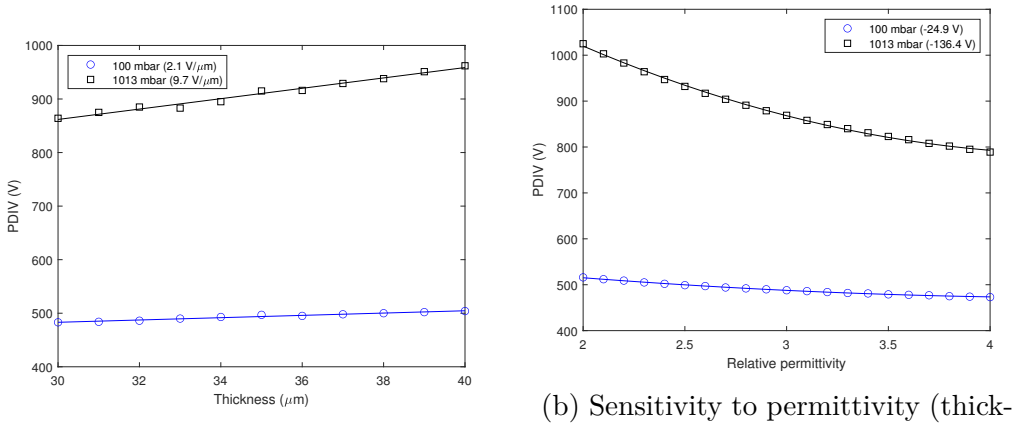

(a) Sensitivity to thickness ($\varepsilon_r = 2.7$).

(b) Sensitivity to permittivity (thickness = 35 μm).

Figure 6.9: Sensitivity curves of PDIV for a 0.56 mm wire with GR2 insulation.

6.3 PDIV-Based Design Approach

The summary discussion carried out, reaffirms the impossibility of operating the transportation drives in presence of partial discharge activity (with a possible exception for transient voltages at ground-altitude, with the already described hybrid approach). Therefore, the design approach to be followed is to make a PD-free EIS for its entire lifetime.

The Reference Operating Condition (ROC) is the set of operating conditions prescribed for evaluating the performance of a machine. The ROC for the insulation system should be the most challenging combination of environmental condition (usually temperature, pressure and moisture). For automotive sector an exemplifying ROC might be the operation in plateau regions of 3000 m altitude [154]. There representative operating condition might be a 700 mbar pressures, temperatures up to 180–200°C with relative humidity up to 60%. For the aeronautical sector the worst condition experienced is the one during the cruising, at altitudes where the pressure is about 200 mbar external temperatures from -60°C and -40°C with typically lower absolute humidity than ground condition. The hot-spot temperature inside the machine can be as high as standard industrial drives. Clearly the definition of a ROC is typical for each machine and its relative use case or mission profile. The target for the design of transportation motors drives would be maximizing the PDIV at the ROC while reducing the electrical stress applied. As previously discussed, the action is most critical for the turn/turn insulation.

PD inception might occur in service even if the new insulation system is PD-free. That is because as the materials are continuously subjected to the TEAM stresses, degradation phenomena alter the materials properties, typically worsening them. The relevant degradation phenomena acting on the PDIV have to be taken into account.

Summarizing the results of the tests campaign carried out on PD inception,

it has been observed that:

1. The features of converter waveforms do not reduce the PDIV compared to the more standard AC 50 Hz voltages, in fact at least for pristine samples they appear to raise them. Nonetheless, very likely the increase is not exploitable due to its statistical nature, originating from multiple phenomena including the time lag for first electron appearance.

2. Resins presenting poor performance in temperature (lower PDIV than non-impregnated samples) exists and should be screened out.

3. Operating a resin above its glass transition temperature, where the permittivity significantly increase did not lead to a critical PDIV drop.

4. Resin thickness appears to be the dominant parameter for PDIV improvement in the end-winding.

5. Resin cracks and embrittlement are common, due to different thermal expansion coefficients of the wire enamel and the impregnating resin. Also, chemical incompatibilities of materials may be the trigger of such degradation.

6. Thermal aging on impregnated samples causes larger PDIV percent drops under convert waveforms than under AC 50 Hz ones, but the absolute PDIV values of the former remains always larger than the latter. The phenomenon is not observed for non-impregnated samples.

7. Dielectric losses not detectable at 50 Hz may appear at converter frequencies, contributing to thermal aging from the start of the machine lifetime.

8. In low-pressure environments the role of solid insulation is de-emphasized. Increasing the insulation thickness might not provide significant improvements. Simultaneously materials aging phenomena are less relevant.

9. Rapid temperature variations (simulation of the start up at reduced temperatures, with a step of 185°C in 30 seconds) and subjection to aircraft vibration profile did not reveal issues when applied in aging subcycles (as a conditioning phase). Nonetheless, their contribution as aging factors has yet to be quantified.

They add to the previously known conditions that:

10. High-overshoots factors increase the magnitude of the stressing voltage.

11. Uneven voltage distribution in the windings, causes high potential difference between the turns (both inside the slot and at the end-winding)

12. Cavities between conductors can be present due to incomplete filling of the slots by the impregnation resin.

13. Delamination of the slot liners or phase separators might appear due to thermal stress and/or chemical incompatibility.

14. Misplaced or missing insulation films in the phase insulation (allowing winding wires from different phases to come in contact) can reduce the usual P-P PDIV to the T-T levels.

resulting in a framework where the combination of unprecedented challenging stresses, harsh environment and impossibility to operate with PD activity, set up PDIV targets difficult to meet.

Some of the findings are easing the constraints on the PDIV (1, 3, 6, somehow 8 concerning aging, and 9). Unfortunately the majority of them can still affect reliability. The issues that have been observed and should be mitigated or avoided can be mainly divided in four categories. Issues related to the choice of materials (e.g. 2, 4, 5, 7, 13), related to processing (e.g. 12), to manufacturing (e.g. 14) and outside of the sole insulation design control (e.g 10, 11, and 8). The first two should be tackled in the design phase. Differently, manufacturing problems should be solved by screened out by quality control on the complete stators.

The PDIV maximization can clearly be achieved by selecting optimal materials and geometries. Unfortunately that might not be enough, and a good design is not limited to that. The design of the insulation should be conducted in a comprehensive framework where the insulation properties (especially the PDIV) are coordinated with the voltage stresses and solutions are sought from both directions to achieve the best performances. Due to the challenging scenario, this comprehensive design approach is considered for the design route of the insulation. Some solutions identified to further improve inception voltage are then covered in the following sections (divided in two categories depending on whether they are applicable on the machine or the converter), while the steps to be performed during qualification will be discussed later on.

6.3.1 Proposed Insulation Coordination Route

A tentative preliminary electrical drive design is produced from the requirements of torque, speed, efficiency, heat dissipation and weight/dimensions (starting from the machine operation cycle or mission profile). The DC bus selection is part of this stage but oftentimes it is not a free parameter, being imposed by the system architecture. From the preliminary design of the drive, PDIV targets values should be assessed for any of the insulation subsystems (T-T, P-P, P-G).

A first design attempt for insulation material and geometries is performed, after the estimation of the voltages that will occur on each of the insulation

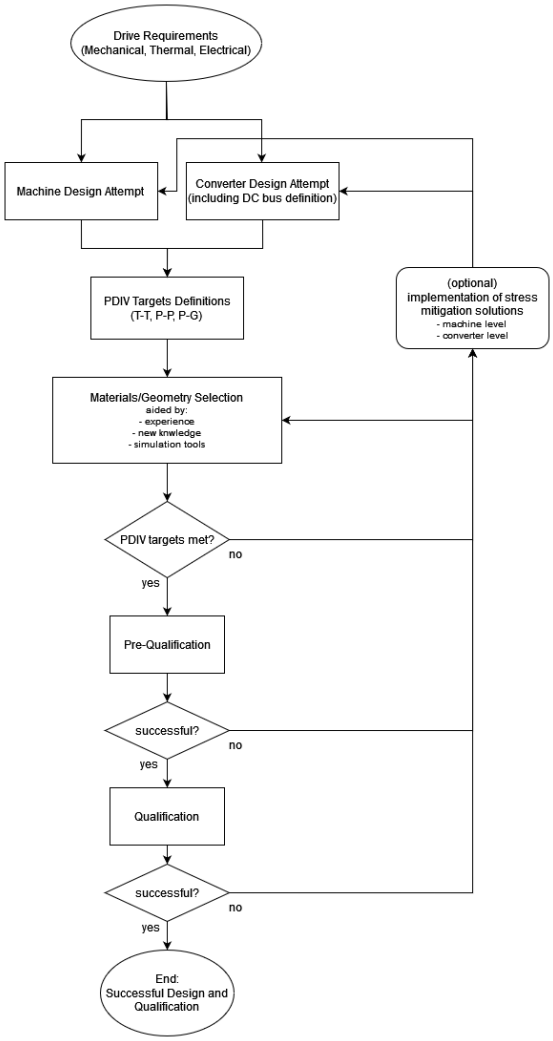

Figure 6.10: Insulation coordination proposed flowchart.

subsystems and the hot spot temperatures to be sustained. Materials and geometries should be selected to guarantee the proper PDIV margins compared to the qualification requirements and the specific environment and stresses to be undergone. For doing so, the recommendation of the standards (e.g. [127]) combined with the experience and up-to-date knowledge on the topic should be used. The designer should try to foresee this PDIV decrease with aging, by the knowledge of the relevant degradation processes.

Simulation tools might be extremely useful. In particular the most relevant might be:

- Voltage stress prediction tools, able to estimate the voltage in any of the insulation subsystem by modeling the overshoots at the machine terminals and the voltage distribution in the windings. Example of tools developed are: [62][155][156][157][158][159][160].
- PDIV prediction tools, for the estimation of the inception values starting from the geometries and material properties. Examples of such tools are the one illustrated in section 3.4, and the many that can be found in literature like: [82][83][84][85].

This is an iterative approach, where different materials and geometries can be evaluated until the PDIV targets are met. In case the requirements on the insulation system are excessively demanding, the overall drive design might be revised. The stress mitigation solutions of the following sections may be employed to increase the PDIV or reduce the stresses.

Once a satisfying design is obtained, pre-qualification of the materials to screen-out possible bad performing or incompatible materials is recommended. Then the qualification of the system can be performed, to prove that the design is able to withstand the voltage and environmental stresses for its entire lifetime. The recommendations for performing the qualification will be fully described in the section 6.4, addressing also the current limitations.

In case the qualification is not passed, a revision of the design can be carried out with the same methodology described, addressing the issues that caused the qualification failure.

In general, deriving a model that is suitable to describe the propagation of voltage surges within the winding needs tuning the simulation parameters by trial and error. Determining parameters like stray capacitances, dielectric permittivity and skin effect, especially at high frequency, is challenging. In a more advance stage of the design, a dummy stator with accessible connections between the coils would enable the direct observation of the stresses appearing on the machine, allowing for revisions if necessary. It is worth noting that the tests to measure the voltage propagation should be performed using a signal generator having the same rise time of the inverter, not the same slew rate. Since the system is linear, changing the magnitude applying a waveform with the same rise time will simply scale the response of the system in an

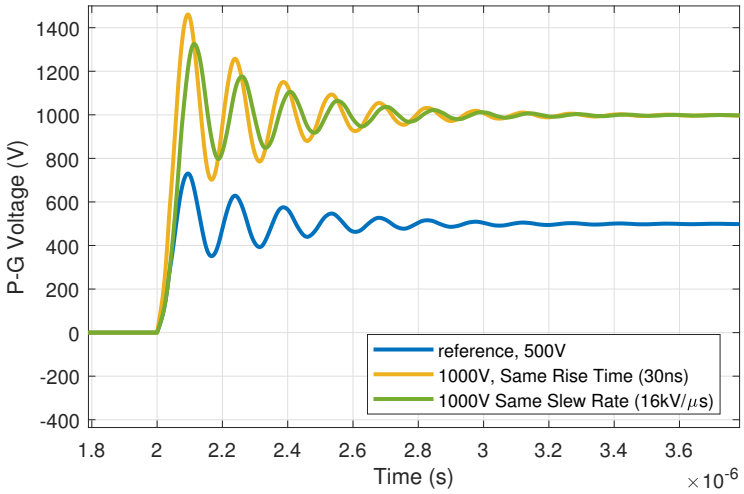

Figure 6.11: Simulated response of the drive system, when the voltage is doubled keeping constant either the rise time or the slew rate. Only keeping constant the rise time maintains the proportionality of the waveforms.

algebraic way. On the contrary, keeping the same slew rate will impact on the spectrum of the applied voltage, leading to incorrect values. Fig. 6.11 shows the difference between these two cases achieved using the propagation model of [62].

6.3.2 Machine-Level Solutions

To improve the T-T reliability on the machine side one option is to revise its winding design. As explained in Sec. 2.2.1, for randomly wound windings the first and last turn might be in contact, setting up the worst-case scenario. If instead the conductors are placed in an orderly way, the worst-case conditions can be avoided, immediately lowering the turn/turn stress. If this is achieved, the PDIV requirements could be relaxed, possibly avoiding the need of reinforcing the insulation. The solution is less effective for very fast rise times, where the inhomogeneity of voltage distribution is maximized. Achieving ordered structures for the winding is possible with:

- Use of sub-coils, where the line-side coil is realized putting three coils in series. The worst case is avoided at the cost of a more complex manufacturing procedure. The solution is an intermediate approach between random wound and form windings.
- Use of form-wound winding, with conductor of rectangular cross section (i.e. hairpin machines). The advantages come from (a) the deterministic control of the turn-turn voltage, which is selected by design and (b) the possibility of feature thicker insulation layers. In this regard, PDIV tests

were performed on flat wires with insulation thickness around 125 μm that provided a PDIV of 1814 V_{pk} at room temperature (1596 V_{pk} at 120°C). In comparison, the value of PDIV for a GR2 0.56 mm rounded wire (around 35 μm of insulation thickness) is around 830 V_{pk}. The use of form windings has been already widely adopted for high voltage machines, whereas the application to low voltage motors is limited to certain sectors, where a high level of automation in the manufacturing process is required, such as in the automotive industry, and electrical machines are supplied with a low fundamental frequency. In the aerospace sectors, the supply frequency of the electrical machines is in general higher than in automotive, since, for a given target power, a higher electrical speed implies a reduced torque and reduced volume and weight for the machine. Conventional hairpin windings do not perform well at high frequency, as electromagnetic effects, such as proximity and skin effects, contribute to increase the equivalent winding resistance (AC resistance) and thus power losses, preventing their use in such applications. However, innovative hairpin solutions, which minimize power losses at high frequency, have been proposed in [161][162], with promising result also for the aerospace sector. A further solution to look at with interest is the use of form-wound Litz wires windings, surely more costly and sophisticated but capable of combine the advantages of form windings stress control with optimal performances at high frequencies [163].

An alternative and simpler solution is based on increasing the thickness of the first turn only, without affecting the winding structure. The first turn is the only turn that is certainly exposed to a high potential difference with respect to the other turns during the commutations of the inverter and selectively increase its PDIV is a smart option. This could be achieved using sleeving tubes typically used to protect the wires from mechanical abrasion or heat shrink tubes. The solution has the drawback of increasing the manufacturing costs. Some preliminary tests have been performed on silicone sleeving pipes and demonstrated that PDIV increased satisfactorily under AC and WBG-convert waveforms, both at ambient and reduced pressures. Long-term performance of the sleeving need be proved. Sleeving pipes were very likely the origin of chemical incompatibility of Sec. 5.2.3. For such reason, the use of solventless pipes (UV cross-linked) is recommended.

Resins that both present good dielectric withstand properties and are able to fill the gaps should be preferred. These requirements should not jeopardize the other properties that remain critical. Vacuum pressure impregnation (VPI) should be preferred, to minimize the presence of voids in the inter-turn region. Low-viscosity epoxy resins suitable for double impregnation may be an option to not sacrifice the layer thickness in the end-winding. Alternatively, encapsulation may be a strategy, accepting the compromise of increased weight and reduced thermal conductivity in the end-winding. Industry has an experience in producing potting resins able to manage the large swings in

Phase/phase:	
Pk/pk fundamental frequency	$U_{pk/pk} = 2(U_{dc} + U_b) =$ $= 2(U_{dc} + (OF - 1) \times \frac{U_{dc}}{(n-1)})$
Phase/ground:	
Pk/pk fundamental frequency	$U_{pk/pk} = (U_{dc} + U_b) =$ $= (U_{dc} + (OF - 1) \times \frac{U_{dc}}{(n-1)})$
Jump voltage	$U_j = 0.7(U_{dc}/(n-1) + U_b) =$ $= 0.7 \times OF \times \frac{U_{dc}}{(n-1)}$

Table 6.2: Voltages appearing in the insulation subsystems, depending on the number of converter levels n, adapted from [39] for a split bus system $\pm U_{dc}/2$ (see Sec. 6.4).

temperature of the MEA sector (from -55°C to +155°C are common in the automotive sector, developed for the Russian market), therefore it would not be a technological problem. If the main issues are present at the end winding, a partial encapsulation of the end-winding only may be envisaged.

6.3.3 Converter-Level Solutions

Matching the converter design with the insulation requirement is an often overlooked solution, resulting from poor integration of the power electronics design to the one of the machine.

The first option that should always be considered to reduce the stresses is to select very short cables between the converter and the machine, so to reduce the overvoltages. Also, increasing the number of levels of the converter n is beneficial to the insulation subsystem, especially for the T-T as the stressing voltage is proportional to the jump voltage:

$$U_{T-T} \propto U_j \propto U_{dc}/(n-1) \tag{6.9}$$

With the sole use of a multilevel converter instead of a 2-level one, the stress on the T-T might be halved. The table 6.2 from [39] summarizes the voltage stresses appearing in each subsystem as function of the number of converter levels n, adapted for a split bus system $\pm U_{dc}/2$. OF is the overshoot factor and U_b the magnitude of the peak voltage in excess of the steady state impulse voltage. Whilst able to reduce overvoltages at the machine terminals, multilevel converter feature an higher number of devices in series, decreasing the converter reliability, shifting the bottleneck point from the winding insulation to the power electronics. Their employment has to be considered with a reliability analysis of the entire system.

Another option is to employ passive filters at the inverter output, probability the most common solution adopted nowadays. With the insertion of

RLC filters, a damping action is forced on the voltage overshoot ensuring a smooth variation. The rise time of the waveform is increased and the voltage distributes more uniformly in the windings. The drawbacks of this solution are multiple: an increased complexity of the system, increased volume and weight of the drive, increased component count and thus reduced reliability, and increased power losses [164][165].

More innovative approaches have been attempted, with novel inverter architectures and the so called active filtering. Innovative inverter architectures has been proposed to minimize the voltage overshoot at the motor terminal maintaining the advantage of fast devices' commutations [166][167]. This is in general counterbalanced by an increase complexity, and an increment in the number of components. Active dv/dt filtering, may involve the use of active gate drivers, which basically slow down commutation speed to maintain the voltage overshoot below a given threshold [168][169]. This comes at the price of increased switching losses and a reduced efficiency of the converter but has the advantage to tailor the converter dv/dt to the specific application layout.

In case the DC bus is subjected to transients, DC bus transients control systems might be employed to block the voltage under a certain threshold, fixing a defined expected maximum voltage at which the design of the machine can be carried out. That implementation is called crowbar circuit. Components as simple as Voltage-Suppression-Diodes might fulfill the scope [170], possibly on the DC-side [171].

6.4 Qualification

The qualification goal is to ensure that a given machine, comprehensive of its design, materials and manufacturing processes is able to operate within the requirements for its entire design lifetime. Qualification of the insulation is usually achieved performing accelerated ageing tests on relevant samples.

The recommended qualification path, in light of the recent knowledge gathered for WBG-driven transportation motors, is to follow IEC 60034-18-41 [39], realizing machines that have to be PD-free for their entire lifetime. Despite the fact that IEC 60034-18-41 is part of the set of standards written by the IEC TC 2 and is thus valid for industrial drives, the absence of universally recognized standards in the transportation sector led to their extensive application for both electric vehicles and the more electrical aircraft.

Currently the IEC 60034-18-41 assign an IVIC (impulse voltage insulation class) to each machine, that similarly to the thermal class determines the maximum voltage severity allowable for that machine (the IVIC is based on the magnitude of voltage overshoots and duration of the impulse rise). The compliance is guaranteed by qualification tests, performed on machine models and subsequent acceptance tests (type tests), performed on new complete windings. If qualification is carried out on complete winding or full stators,

acceptance is already reached and no additional type test is required. Qualification investigates the capability of the EIS to withstand various stresses and is performed with accelerated thermal aging tests coupled with mechanical and moisture conditioning. The EIS is deemed qualified if endures the same or more cycles than a reference system with proven service experience without PD occurring below the specified test values. Type tests demonstrate that the machine is indeed PD-free and assign the IVIC.

If the thermal class hasn't already been determined, the qualification according IEC 60034-18-41 can be performed integrating the necessary tests with the ones for thermal class qualification (in IEC 60034-18-21 [92]), that are performed with aging cycles for at least three different aging temperatures. Otherwise, if the thermal class has already been determined it is only necessary to perform aging and PD tests at one of the appropriate temperatures.

In the standard enhancement factors (EF) are used to represent phenomena not included in the testing conditions that may reduce the PDIV. Those factors are multiplied to the operating voltage to increase the peak/peak voltage of the testing voltage.

6.4.1 WBG-Converter and Transportation Drives in IEC 60034-18-41

The IEC 60034-18-41 was first published in 2006, 16 years ago. Since then IEC TC2 MT10 (Maintenance Team) recognized that the recent novelties in the power electronic changed the framework and is planning to publish its second edition, transferring the content related to testing into the recently-published IEC 60034-27-5 [172]. It became clear that the advent of wide-bandgap (SiC) semiconductors, with their slew rates easily reaching 60 kV/μs, had changed drastically the scenario, with previously established limits being probably not able to protect the machines fed by inverters with SiC MOSFETs. An example of such increase is reported in Fig. 2.6, from [62].

With the next-generation voltages, the stresses might become very difficult to deal with. A possibility that is currently discussed is the introduction of a multi-IVIC approach. The phase-phase, phase-ground and turn-turn insulation systems can each be assigned a separate impulse voltage insulation class, to avoid over-design of the other subsystems or meet the high voltage stress requirements only where needed, so to improve performance and efficiency. Even better would be the definition of the maximum tolerable stress for each insulation subsystem instead of dividing these stresses into classes.

The next standard revision should also embed various drive topologies typical of transportation electrification, today not excluded but neither made explicit, so that oftentimes the stress calculation is performed with the worst-case equation causing insulation over-designed, leading to a sub-optimal power density. It is obvious that the producing a complete list of possible topologies is not convenient and a compendium of all of them may be impractical. The

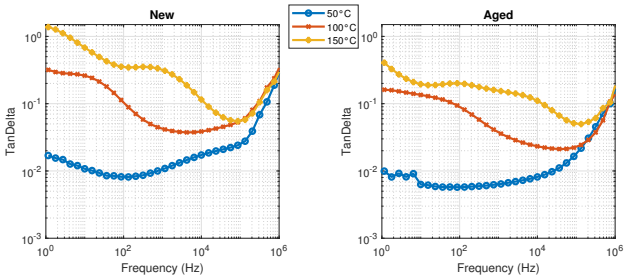

Figure 6.12: Dielectric losses recorded for a complete stator before and after a 1000 h aging cycle, for various temperatures.

standard should provide a way to differentiate them. For the most common ones, formulas for calculating stresses might be made explicit, for the less common ones it could simply provide a reference to the manufacturers on how to calculate them. For instance, TE drives are operated by batteries, differently than industrial drives that usually feature a rectifier to obtain the DC voltage. Many of the TE drives employ split bus configurations $\pm U_{dc}/2$ where the DC bus is solidly connected to the mass at its central point. This is common in the MEA sector [29][33] and less common for EVs that prefer instead a floating DC bus [173].

The standard does mentions that different earthing systems lead to different P-G stresses, but to improve the coordination these difference need be made clear. For drives in normal operation the two poles of the DC bus will be at $+U_{dc}/2$ and $-U_{dc}/2$, either from symmetry in an un-referenced system or from the reference at the central point in a split bus configuration. Thus, in the P-G a voltage equal in peak to $U_{P-G} = (U_{dc}/2+(OF-1)U_{dc}/(2(n-1))$ appears (in peak to peak, $U_{P-G} = (U_{dc} + (OF-1)U_{dc}/(n-1))$. In case the system is grounded at one of the two poles, the ground voltage is doubled. The standard currently considers 2/3 of such voltage as the one appearing at the P-G, confusing the P-G voltage with the phase to star point voltage and should be revised. In case of operation during a fault, different conditions apply. If an industrial drive system is distributed with insulated neutral, in the event of an earth fault on one of the phases of a system where the neutral star point is not grounded, the machine may be permitted to run until a suitable outage can be arranged for repairs. In this scenario the poles of the DC bus will swing from $+U_{dc}$ to $-U_{dc}$ and for such reason the P-G insulation have to be designed to withstand in peak the full DC bus voltage plus overshoots and not half of it. For TE drive configurations typical of the EV sector, the scenario is exactly the same and the same design rule applies, unless operation in fault condition is not enabled. For TE drive configurations typical of the MEA sector, where a split bus is used, such operation is not possible by design.

The practice of testing new machines with an overvoltage and declaring them good or bad depending on the inception of PD during the tests has been

established has a common praxis. However, there are some doubts that alone it can ensure the reliability of the insulation. Some of the concerns can be dealt with pre-qualification procedures. Pre-qualification tests might help to exclude:

- Chemical incompatibility, like the one shown in Sec. 5.2.3 for motorettes samples. Dielectric producers have rarely the complete insulation system including winding wires, liners, interphase separators, impregnating resin, bandaging, and sleeving. Very often, machine manufacturers purchase different parts of the insulation from different producers. This might lead to problems associated with the chemical compatibility of the different parts. Electrical (PDIV) and mechanical (Young modulus) tests can be carried on simple insulation model before and after thermal aging in a sealed environment, to demonstrate that no compatibility issues are present between the materials selected.

- Impregnating resin critical PDIV reduction in temperature, like the one reported in Sec. 5.1.3 where the PDIV at service temperature dropped below the one of un-impregnated samples. PDIV test should be performed at operating temperature to identify resins that cause a PDIV drop incompatible with operation.

- High dielectric losses under converter operation, like the one recorded in Sec. 5.1.5 for impregnated TP. High dielectric losses were recorded in other occasions, for example feeding a complete stator with the SiC-converter of Sec. 3.2.6. The dielectric losses coefficient is illustrated in Fig. 6.12. As it is shown, dielectric losses vary with temperature and also as the materials age. The pre-qualification should be performed at service temperature, with thermocouples placed inside the slot of a full stator or by means of thermal imaging. The test of aged samples might be evaluated.

Furthermore, the results of Sec. 5.1.5 demonstrated that with aging the PDIV drops faster under converter waveforms. This evidence is at odds with the current standard, since the testing frequency is considered not important for PDIV tests and the same enhancement factor is considered for qualification, independently of the test voltage waveforms. For the time being, it seems that the higher decline recorded under converter never falls below the absolute values recorded in AC. Hence, if the turn-turn tests are carried out in AC, which is the most conservative condition as discussed in Sec. 6.2.1, there is no need to change the enhancement factor relative to aging for converter operation. Generally, testing the PDIV using AC 50 Hz waveforms appears to be a conservative approach, provided that the relevant stressing voltage is generated in the insulation subsystem. For testing in AC the T-T a dummy unconnected wire might be inserted in the slot of motorette models or the

dummy stator. When testing the wire should be connected to the voltage source and the machine windings grounded.

Many manufacturers complain about the excessive amount of resources to perform qualification tests, which often have to be performed after modification of an already qualified insulating system that is already in production. A complete qualification procedure indeed is costly and time consuming. Under certain circumstance its superfluous to carry out a complete qualification, as minor changes or conservative changes in a machine with successful service experience are unlikely to decrease the reliability. Such changes may be:

1. Geometry conservative variations, when the geometry of the machine is changed but the maximum electric field in the different subsystems remains unvaried or is lowered.

2. Materials and/or processing changes for insulation system parts that are not responsible for withstanding high electrical fields (bandaging, lead sleeving, coil-nose tape, connection tape, cables, tie cord, bracing).

A discussion is ongoing to enable the possibility of performing only type tests for the changes of (1) and type tests coupled with a "quick-scan" procedure in case of (2). The "quick-scan" can be based on the comparison of electrical and mechanical properties for the new design and the reference one, with tests similar to the one discussed for the test of chemical incompatibility in pre-qualification.

Lastly, under the current version of the standards the proposed EIS is always qualified by comparing it to a reference one, with proven service experience. In some circumstances operational records are not available, because of an innovative design approach or because unique/unusual stresses are present (the latter is very likely for the MEA systems). Also, a new company could be established and not have any internal records. This qualitative approach could be substituted with a more quantitative one, where a target reliability is set to be met for the insulation system at any given age time, practically setting a reliability target at the desired lifetime. This approach is described in [174][148]. The end of life criterion of an insulation subsystem in this context is the inception of partial discharges, hence the life value is the time required for the PDIV to drop below the target PDIV under a given aging stress. The most important aging stress factor is the temperature, which is the only one employed in current qualification. Nonetheless, a multi-factor approach might be integrated if needed. Later in the chapter an electro-thermal qualification bench will be described. Considering the thermal stress only, the qualification procedure would require to obtain the life value of a series of samples for different aging temperature, through accelerated aging tests. A life statistical distribution is built for each aging temperature, with a population equal to the number of samples. Then regression lines can be traced from the points at any selected reliability percentile and the reliability of the subsystem at the

design lifetime can be estimated. The reliability of the entire motor can be derived from the ones of the subsystems, taking advantage of scaling factors if needed. The methodology enables the creation of hierarchies of insulation systems, producing a number (reliability at the target lifetime) that can be easily compared to other EIS, providing an universal metric to manufacturers. The limitation of the proposal is that if qualification is not carried out together with thermal class qualification, PD qualification tests must be re-performed for at least three aging temperatures rather than a single one. Moreover, the calculation might appear cumbersome to whom is not expert in the insulation reliability field.

Qualification for Aeronautic Conditions

Compared with industrial drives, actuators for the MEA have different ROC. In order to adapt the standard to fit the high altitude conditions, the pressure variation has to be accounted. The use of such parameter can be envisaged also for EV operating at very high altitudes. Pressure is the single parameter that mostly affects the PDIV, and such variation could be accounted with an enhancement factor. The enhancement factor for temperature could be modified to account also for the pressure, as both reductions are mostly caused by air density reduction. This is possible assuming that the eventual changes in the dielectric permittivity of the materials under aging and at elevated temperatures does not cause important extra PDIV decrements, hypothesis that is in general in agreement to the experimental results. The model of [86] can be used to estimate the PDIV value when pressure is p and temperature T, given the PDIV at standard atmospheric conditions, using the number density $n(p,T)$. The number density is proportional to the air density. Then, the enhancement factor takes the form:

$$E_{p,T} = \frac{PDIV_{n(p,T)}}{PDIV_{n(p_{std},T_{std}))}} \tag{6.10}$$

The possibility of testing at reduced pressures without the use of enhancement factors should be evaluated, following the idea that testing in realistic conditions is better than testing using artificially increased voltages. The main problem relies on the fact that discharge changes as the pressure reduces and the detection with electromagnetic methods becomes nearly impossible. Fig. 6.13 illustrates the emission spectra of PD activity at the inception and at voltages well above inception for low pressures. It can be observed that as pressure decreases the PD spectrum amplitude is reduced. This is an important issue for the development of monitoring systems, making the qualification even more important for achieving a good reliability of the machine.

For type tests, an extra aging enhancement factor is needed, as the machine is tested when new. The standard suggests that, for an insulation system operating always at its class temperature, $EF_{Aging} = 1.2$, implying a maximum

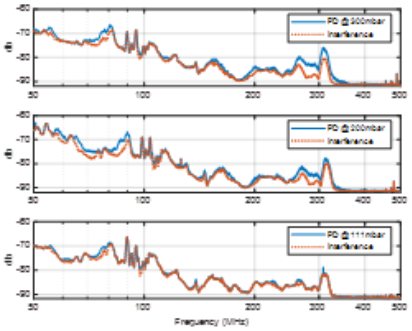

(a) Acquired spectrum for different pressures, at PDIV and in absence of PD.

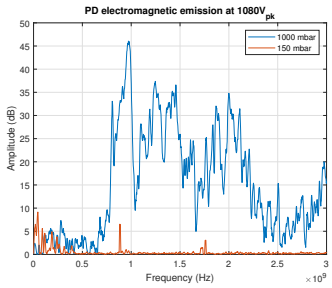

(b) PD spectra recorded at constant voltage (1080 V_{pk}), above the PDIV. At 150 mbar the voltage is more than double the PDIV.

Figure 6.13: Amplitude of PD emitted signal reduced as pressure decreases.

reduction of the PDIV over time of 1/1.2=83%. In case the service temperature T_s is lower than the class one T_c, the $EF_{Aging} = max(1.2(T_s/T_c), 1)$. As the role of solid dielectrics is de-emphasized at lower pressures, the enhancement factor for aging should be reduced, reducing the burden on the EIS. A 10% PDIV decrement is the value obtained in Sec. 5.1.5 for aged TP tested at 100 mbar, when the same samples at ground pressure reported a reduction of 20%. Considering that the driving mechanism of PDIV reduction is the insulation shrinking and permittivity increase, simulations using the tool of Sec. 3.4 with 20 μm thickness reduction and permittivity variation of around 1 point produce the exact same figure. The tests on motorettes of Sec. 5.2.3 reported similar drops.

Therefore, the aging enhancement factor can be reduced to:

$$EF_{Aging} = max(1, k * (T_s/T_c)) \tag{6.11}$$

where k is the drop expected at low pressure if the system is operated at its class temperature. At 100/150 mbar that value can be estimated around 1.1. As the machine has to withstand the same voltage at potentially different altitudes, until the aging factor is less relevant than the pressure one (condition always met for the range of variations observed under aging), the aging factor considered for the design could be the less restrictive one (hence the one of the highest altitude).

Ultimately, the standard considers a safety factor $EF_{PD} = 1.25$ that relates to the hysteresis effect by which PDEV is usually 25 % below the PDIV (figure derived from practical experience, also in line with the results for impregnated T-T samples of Sec. 5.1.3). Its usage is relevant if PD activity is initiated in a transient over-voltage exceeding the normal peak voltage, since the PDs must extinct once the voltage returns to normal operation levels. For MEA applications, in sight of the endurance results, PD activity is not acceptable

even in transient over-voltages and the coefficient can be dropped in favor of more restrictive PDIV requirements.

6.4.2 Working Case

A case study for the calculation of voltage stressing values for type tests according to the modified IEC 60034-18-41 and their comparison with measured PDIV is presented. Different drive types and two scenarios of cable length and rise time are considered. The four drive topologies considered are: two-level inverter with ground connection to the negative DC rail or in split bus configuration and three- and five-level inverter with the split bus configuration.

The drive analyzed is an high-performance electric drive intended for a EHA in the MEA, described in [62]. The basic structure of the system consists of an inverter connected to the motor via a three core cable having wires with a diameter of 8AWG, twisted triple, single shielded (Nickel-coated copper), single jacket. The electrical machine is an interior permanent magnet rotor rated for a continuous power of 5.7 kW, featuring an 8-poles, 36-slots stator, with a double-layer, integer-slot, three-phase winding comprising 3 coils-per-pole-per-phase, each consisting of 12 turns. The reference PDIV levels of the EIS were derived based on measurements performed on twisted pairs (810 V peak) for the T-T and motorettes (1160 V peak) for the P-G, in sections 5.1.5 and 5.2.3 respectively. One of the assumptions made to derive the analysis reported in the following is that the PDIV increment conferred by the impregnation process should not be considered in the design phase. The reason behind this choice is twofold: the measurements performed on impregnated twisted pairs show that a large dispersion and the PDIV increment in impregnated at operating temperature is significantly lower than what observed at room temperature. Furthermore, the results obtained for the T-T of motorettes are comparable to the results obtained in TP. The use of the un-impregnated sample T-T is conservative choice (unfortunately condition likely not far from the real case).

The total enhancement of the DC voltage to be used for type test qualification is:

$$EF_{tot} = (WF * OF) * EF_{PD} * EF_{p,T} * EF_{Aging} \tag{6.12}$$

where the enhancements are the one produced according to the recommendation of the previous section. In particular: $EF_{PD} = 1$ as no voltage transients are allowed, $EF_{p,T} = 1/0.55 = 1.8$ (combined impact of pressure and temperature reduction of 45%) and $EF_{Aging} = 1.1$ (operation at thermal class, with aging causing 10% PDIV drop at low pressure) coherent to the experimental results on the models.

The combination of OF and WF (dependent on cable length and rise time) was calculated for the specific design of the random-wound machine under investigation through simulation. The propagation model of [62] predicts the electrical stress levels acting on a stator in an accurate fashion in the T-T and

Drive type	Levels	Insulation	U_{DC}	$WF*OF$	EF_{PD}	$EF_{p,T}$	EF_{Aging}	Total	V_{stress}	PDIV	$V_{DC,lim}$
$0-V_{DC}$	2	T/T	540V	1.12	1	1.8	1.1	2.22	1198	810	365
	2	P/G		1.28				2.53	1369	1160	458
$\pm V_{DC}/2$	2	T/T		1.12				2.22	1198	810	365
	2	P/G		0.78				1.54	834	1160	751
$\pm V_{DC}/2$	3	T/T		0.56				1.11	599	810	731
	3	P/G		0.64				1.27	684	1160	915
$\pm V_{DC}/2$	5	T/T		0.28				0.55	299	810	1461
	5	P/G		0.32				0.63	342	1160	1831

Table 6.3: Estimation of type tests stressing voltage value and limit DC bus voltage level for a EHA. Cable length = 2 m. Rise time = 90 ns.

Drive type	Levels	Insulation	U_{DC}	$WF*OF$	EF_{PD}	$EF_{p,T}$	EF_{Aging}	Total	V_{stress}	PDIV	$V_{DC,lim}$
$0-V_{DC}$	2	T/T	540 V	1.37	1	1.8	1.1	2.71	1465	810	299
	2	P/G		1.7				3.37	1818	1160	345
$\pm V_{DC}/2$	2	T/T		1.37				2.71	1465	810	299
	2	P/G		1.2				2.38	1283	1160	488
$\pm V_{DC}/2$	3	T/T		0.685				1.36	732	810	597
	3	P/G		0.85				1.68	909	1160	689
$\pm V_{DC}/2$	5	T/T		0.342				0.68	366	810	1196
	5	P/G		0.425				0.84	454	1160	1378

Table 6.4: Estimation of type tests stressing voltage value and limit DC bus voltage level for a EHA. Cable length = 15 m. Rise time = 20 ns.

P-G systems, accounting for both the overvoltage at the machine terminals and the voltage distribution within windings. Those stress values exceed the maximum stressing value in the curve of the standard, due to the extremely short rise times.

From the PDIV values the maximum permissible DC bus voltage can be estimated as:

$$V_{DC,lim} = PDIV/EF_{tot} \tag{6.13}$$

The results of these calculations are reported in Tab. 6.3 for a 2 meter long cable and a 90 ns rise time and in Tab. 6.4 for a 15 meter long cable and a 20 ns rise time (more challenging scenario). The results show that for the materials selected under a DC bus voltage equal to 540 V can operate reliably only when using three- or five-level inverter with split DC bus if no additional stress mitigation solutions are employed. If higher DC bus voltage levels are sough (800 V) only five-level inverter topology can withstand the stress generated.

6.4.3 Combined Electro-Thermal Stress

Regarding the qualification on full stators, the application of testing voltages that are produced by testing generators introduce the need to model the voltage distribution and adjust the testing level to apply the proper stresses to

each of the subsystems. Also, they add the need to understand how the features of not only the real operating voltage impacts the PDIV, but also how the testing voltages specific to the generator impact the EIS.

If a testing system able to employ the converter that is used in the operation is realized, the problem of producing relevant qualification testing is completely removed. Also, an appropriate cable should be used to have the proper stresses at the machine terminals.

If the concept is pushed further, such system might be used to subject the materials with the real electrical stress as part of the aging cycle, either as sequential stress to the thermal aging, or even better in a simultaneous multi-factor stress, capable of capturing degradation synergies [175]. As mentioned earlier, the current standard do not envisage any tests in which thermal and electrical stress conditions are applied simultaneously; indeed, only thermal aging cycles alternated with electrical diagnostic tests are carried out, that are supposed to not provide any electrically aging to the system and only verifying its state. The introduction of multi-factor aging stress might be very important in light of the contribution of the electrical stress to aging.

The possibilities for thermo-electrical aging stress cycles are many, but can be carried out in two main methods, both of them at temperatures according to [92] to perform accelerated thermal aging tests:

- With voltage stressing levels equal to the service ones.
- With voltage levels higher than the service ones, making up additional accelerated electrical degradation. The stressing voltage should be anyhow lower than the PDIV of the pristine stator, to avoid the transition from intrinsic electrical aging to extrinsic one, that have completely different aging phenomenology and impact on the material degradation.

The first approach will be explored, as enables a very useful simplification in the qualification process. Since the machine is constantly fed with a voltage corresponding to the in-service one, if the insulation does not feature CR materials, the diagnostic sub-cycle can be avoided. Indeed, if PD activity is incepted the machine will fail in a time that is negligible to the test times. So, the lifetime under the accelerated life tests is recorded easily as the time elapsed between and the failure of the machine and no PD detection instrument is needed. The procedure would greatly ease the proposed qualification methodology employing the reliability target instead of the reference operating system described in Sec. 6.4.1 and provide better distributed life values (otherwise discretized to the aging cycles).

A full machine, comprehensive of the rotor might be used and left rotating in the no-load condition or connected to a test bench able to provide the braking torque desired. This approach makes the realization of the setup a quite complex problem, having a machine rotating at high speed inside a close environment where temperature is artificially increased. Typically an oven is

used. The system produces vibration that must be controlled, is noisy and requires extra safety measurements. In case the machine is operated in loaded condition, the energy consumption may be considerable if the bench doesn't feature an energy recovery system. Furthermore, the accelerated degradation should be applied only on the electrical subsystem of the machine. It is very likely that the mechanical parts like bearings and their lubricants cannot operate at the temperatures required for the insulation accelerated thermal test.

Alternatively, the machine can be fed in absence of the rotor, connecting the inverter to the stator alone and avoiding any moving part and the aforementioned problems. This way, without the counter-electromotive forces generated by the rotor rotation, the currents flowing through the windings are limited only by their impedance (too small to cause an important voltage drop). In the absence of the electro-mechanical power conversion of power both the heat dissipated in the stator windings from joule losses and the current magnitude withdrawn from the converter would be unacceptable. The solution to this issue is to limit the stator currents using resistors whose potential drop can be compared to that caused by the presence of the counter-electromotive force. They can be inserted in series to the windings, before the star point (an accessible star point is assumed, otherwise a custom dummy with connections suitable for this test or a dummy with at least three adjacent windings should be realized). The addition of this resistors alters the voltage profile that the winding experiences, an undesired effect that shall be limited. First, the steady state voltage will drop more on the resistor than the windings, increasing the steady state voltage on the intermediate coils of the P-G. Secondly, voltage reflections between the windings and the resistor may appear, changing the transient voltage profile, a more important issue. Another important drawback is that joule losses (and eventual dielectric losses), despite reduced, cannot be eliminated. Hence, the set temperature of the oven must be carefully chosen so that the hotspot temperature inside the slot reaches the aging value selected. For that the use of thermocouples in the machine slot is strongly advised. Due to those joule losses, in the slot the temperature gradually decreases outward, recreating a profile akin to the service temperature but less appropriate for the scopes of an accelerated thermal test. The temperature gradient is stronger for higher absorbed currents (lower resistors values). This approach requires much lower powers to operate, equal to the mentioned joule losses, enabling the use of much smaller and cheaper high voltage generators.

A setup was realized as demo of the system. The stator features concentrated windings in the tooth-coil winding type (Fig. 6.14), with 6 windings per phase connected together in parallel, for a total of 18 teeth making 12 magnetic poles. Litz wires are employed as conductors. The converter used, described in Sec. 3.2.6 presented specific criticalities. The control system is based on the field oriented control (FOC) which through current measure-

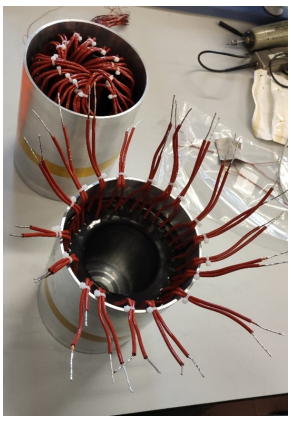

(a) Stator employed for the demo of the electro-thermal qualification system.

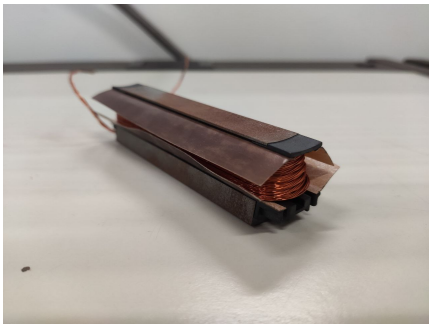

(b) Tooth, sub-component of the stator.

Figure 6.14: Open and short circuit impedance, obtained from s-parameter (S_{11}) acquisition though a VNA as function of frequency.

ment adjusts the voltage modulation (SVPWM-type modulation). In absence of the rotor the current sensor would read very high current values and would attempt to provide an almost null voltage reference. This makes the control to switch simultaneously to the ON state all phases (there will be very short delays that cause voltage spikes to occur anyway) so that the line-line voltage is set to zero, repeating the process each switching period in an attempt to obtain average zero currents. This abnormal operating regime of the inverter should be avoided because it is not representative of service conditions. Furthermore, the speed control is not possible, as the encoder or resolver assigned to measure angular speed clearly does not receive any signal. For this reason, the "measured" speed value will have to be fixed fictitiously in the control system, effectively bypassing the control loop.

Regarding the propagation of the voltage wave on the system, the target would be to alter the wave shape of the voltage across the first coil as little as possible by the insertion of the resistor. The resistor should be inserted after the windings and ideally they should share the same characteristic impedance so to not to generate reflections and cause voltage wave distortions (to be avoided particularly on the first coil). For this reason, the characteristic impedance of a wound tooth was calculated through reflectometry measurement with a VNA (described in Sec. 3.3.5) in the frequency range 50 Hz to 150 MHz. Knowing the characteristic impedance spectrum, the resistor impedance could be matched with that of the winding, mitigating reflections.

The machine can be considered as first instance a propagation line. This is an approximation, as the characteristic impedance of a rotating machine varies along the voltage wave path, meeting different stray parameters in different location, especially from inside the slot to the end-winding. To perform the

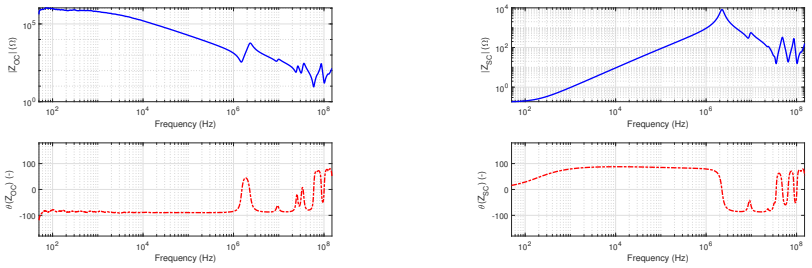

(a) The open-circuit impedance. (b) The short-circuit impedance.

Figure 6.15: Open and short circuit impedance of a stator tooth, obtained from s-parameter (S_{11}) acquisitions though a VNA as function of frequency.

calculation of the characteristic impedance, the theory of propagation has to be briefly reviewed. From the Telegrapher's equations, the input impedance Z_{IN} of a line of length d is:

$$Z_{IN}(d) = \frac{V(d)}{I(d)} = Z_0 \frac{Z_L + Z_0 tanh(\gamma d)}{Z_0 + Z_L tanh(\gamma d)} = Z_0 \frac{1 + \Gamma_L exp(-2\gamma d)}{1 - \Gamma_L exp(-2\gamma d)} \tag{6.14}$$

where γ is the propagation constant of the line, while Z_0 and Z_L are the characteristic impedance of the line and the load at the end of it, respectively. Considering the equation Eq. 6.14 for a load:

$$Z_L = 0 \rightarrow Z_{IN} = \frac{Z_0}{\tanh(\gamma d)} = Z_{OC} \tag{6.15}$$

$$Z_L = \infty \rightarrow Z_{IN} = Z_0 \tanh(\gamma d) = Z_{SC} \tag{6.16}$$

and then re-substitute them into Eq. 6.14 one obtains:

$$\gamma = \frac{1}{d} \tanh^{-1}\left(\sqrt{\frac{Z_{SC}}{Z_{OC}}}\right) \tag{6.17}$$

$$Z_0 = \sqrt{Z_{SC} Z_{OC}} \tag{6.18}$$

The short-circuit and open-circuit impedance can be calculated resorting to s-parameter theory, from the reflection coefficient:

$$S_{11} = \Gamma_{IN} = \Gamma_L \tag{6.19}$$

knowing that the measurement instrument has a characteristic impedance of 50 Ω, finally obtaining:

$$Z_{OC} = 50 * \frac{1 + S_{11,OC}}{1 - S_{11,OC}} \tag{6.20}$$

$$Z_{SC} = 50 * \frac{1 + S_{11,SC}}{1 - S_{11,SC}} \tag{6.21}$$

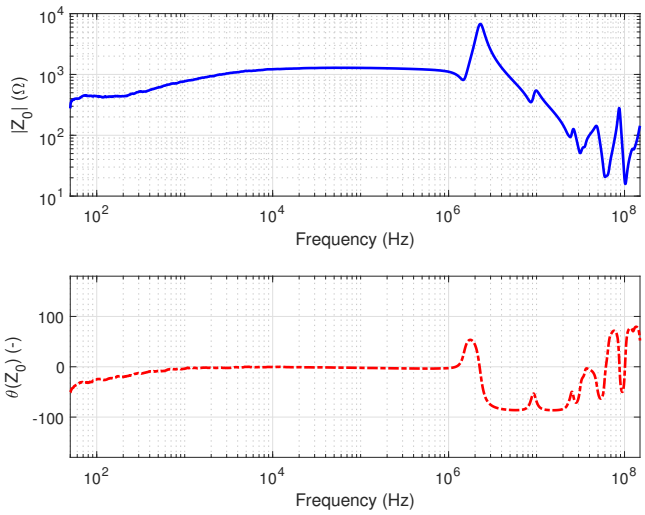

Figure 6.16: Characteristic impedance of a tooth, as function of frequency.

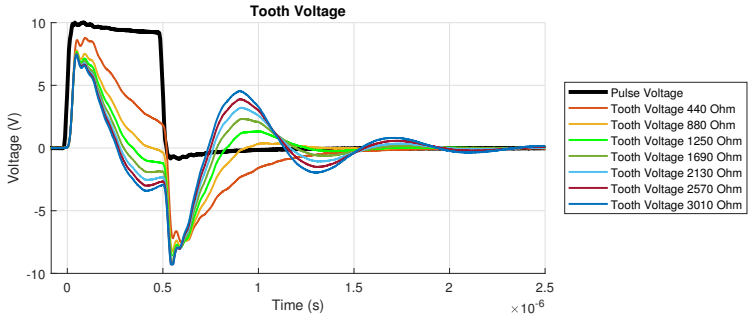

Figure 6.17: Values of the potential difference at the ends of the stator tooth for different values of resistance after it.

Before the measurement of the reflection coefficient, the instrument was calibrated and the fixture compensated. The results obtained were used to calculate through Eq. 6.21 the open circuit and short circuit impedance, that are in Fig. 6.15. From them, using Eq. 6.18 the characteristic impedance of the tooth Z_0 (Fig. 6.16) is calculated. The characteristic impedance exhibits a large region where the impedance is constant around 1000 Ω with a null phase.

The selection of the resistor value is a compromise between the needs of reducing the distortion (achievable only matching its value to the one of the windings, task impossible to meet accounting also the phase angle with a pure resistor) and increase the resistance so that the current is reduced to values that enable the employment of the converters. As the voltage wave goes through the entire phase winding before reaching the resistor, lower frequency components are likely more relevant than the high frequency one for the matching, as the latter gets reduced following stray capacitive paths. Fig.

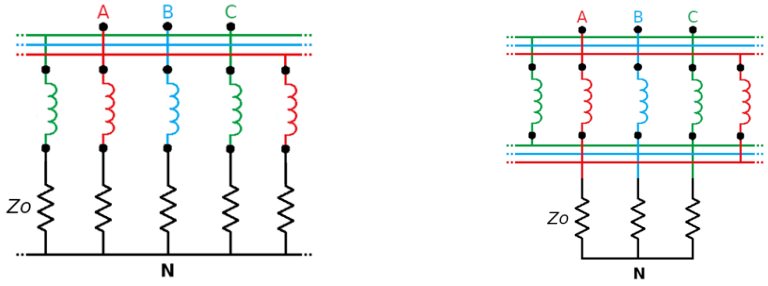

(a) The equivalent resistance in series for each tooth is Z_0.

(b) The equivalent resistance is series for each tooth is $6Z_0$.

Figure 6.18: Resistor connection configurations.

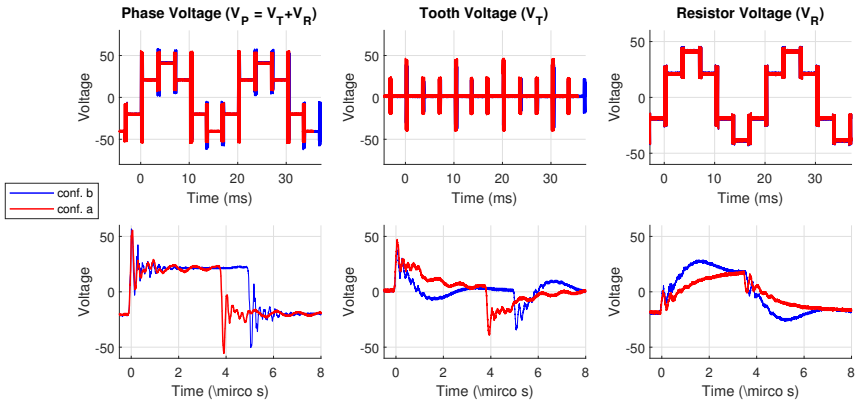

Figure 6.19: Comparison of the voltage appearing under the two configurations.

6.17 shows the voltage on the stator tooth as function of the resistor after it. A value around 880 Ω for the resistor is deemed to generate an acceptable voltage reflection (hence distortion) at the interconnection between the resistor and the tooth producing acceptable voltage ringing and at the same time reducing the current to values bearable by the converter in use.

To compare the voltage with a different resistance value, two configurations were used. They are shown in Fig. 6.18. Configuration "a" is using the value estimated from reflectometry measures for each tooth, configuration "b" connecting all the tooth in parallel before the connection to the same resistor, resulting in a resistance value six times higher than the estimated one for each tooth. Acquisition of the voltages appearing on the resistor and the tooth are in Fig. 6.19. The measurements were performed using 60V of DC bus and low-voltage low-inductance resistors. In configuration "b" it can be seen that the voltage on the tooth is subject to a voltage ripple that is not present on the phase voltage and that the peak is reduced compared to the "a" configuration, reducing the turn-turn stress that instead should be preserved. Nonetheless, the great difference in the resistor value affects the voltages in a modest way,

Figure 6.20: Electro-thermal qualification demo setup.

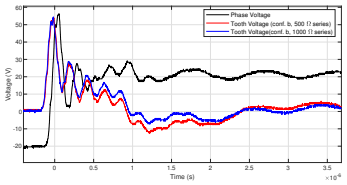

(a) Comparison of voltage appearing for different resistance values at 60 V.

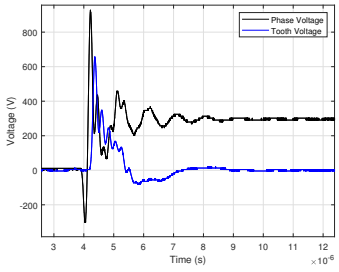

(b) Full 860 V operating voltage.

Figure 6.21: Voltage appearing on one stator tooth.

giving a good margin for the selection of the resistor.

Considering configuration "a", the current circulating can be estimated from the equivalent impedance for each phase. The impedance is:

$$Z_{eq} = \frac{n_s \left(Z_{tooth} + Z_0\right)}{n_p} \tag{6.22}$$

where n_s is the number of windings connected in parallel and n_s the number of the ones connected in series. Hence, an active power will be dissipated (mainly on the resistors, which will have to be capable to withstand both voltages, currents and temperature). Installing the resistors on a suitable heatsink with a cooling system to keep the temperature contained is probability the best approach. Heat recovery systems or direct installation in the oven permits to avoid the waste of the thermal energy and employ it as support of the oven. The latter requires very high operating temperatures for the resistors and is likely difficult to exploit.

In Fig. 6.20 is a picture of the setup realized. Due to strong limitation on the maximum current withdrawable from the available generator and the

limited range of available resistors an insertion identical to configuration "b" had to be employed. In Fig. 6.21a it is shown how varying the resistor value does not affect strongly the wave shape, as already observed. In Fig. 6.21b are the final waveshapes obtained for the demo setup. An important portion of the phase voltage is not present on the tooth, as consequence of the limitations faced. Yet, preliminary measurements for 300 hours of aging showed that the electro-thermal aging reduced the PDIV of 10% while comparative thermal-only aging caused no PDIV reduction in the same time frame. Reliability issue of the SiC-converter forced the interruption of the investigation. The lack of temperature monitoring inside the slot, estimated from modeling and measure on the stator frame raised some doubts on the real slot temperature and highlighted the need of installing temperature sensors for this kind of qualification. Anyhow, the promising results obtained push for a more complete investigation performed with the most appropriate equipment.

When proposing a qualification methodology, its simplicity and straightforwardness are key aspect to evaluate. The complexity (and cost) of the reflectometry measurements and the need for their verification is something that inhibits the realization of the proposed setup. However, in light of the results obtained a more detailed analysis should be carried out to understand if reflectometry measures are needed at all. In addition, the resistor might feature a set of characteristics not easy to find on the market. Beside the resistance value equal to the selected one, other properties are crucial: low parasitic parameters, sufficient maximum operating voltage and current, proper temperature range and power dissipation. Meeting these characteristics might not be feasible at reasonable costs, with the most critical aspect being the low parasitic, as they tend to increase proportionally to the resistance and dissipated power values.

Furthermore, the specific characteristic of a machine winding topology might increase the difficulty of this methodology. The machine analyzed has single wounded teeth, an optimal configuration for the analysis. Machines with many windings in parallel will feature lower Z_{eq}, requiring higher currents and consequently dissipating more heat (requiring more power from the generator). As already mentioned, for designs without the star point accessible, an ad-hoc stator for this qualification approach should be realized. The modification might be costly or difficult to perform, and important variation from the stator original structure can make the qualification less meaningful, nullifying the benefits that would be obtained.

Chapter 7

Conclusions

The pivotal changes in the transportation sector require careful scrutiny of insulation materials properties to provide the desired reliability. Aeronautic and automotive environments, in conjunction with unprecedented stresses generated by WBG-converters require for advancement in ensuing the reliability of modern systems, obtained by deriving prescription for insulation coordination and qualification.

Extensive experimental activity has been carried out to extend the body of knowledge on insulation materials, with focus on partial discharge phenomena. The danger of sustained PD activity in motors have been reaffirmed in light of new empirical results. Experimental results show that purely organic materials of enamels present in the T-T insulation system can not sustain PD activity in the current conditions of the automotive sector, enduring voltages comparable to the PDIV only for some minutes. Life under PD activity is even worse at low pressures (100—150 mbar), which are characteristic for cruise and qualification altitudes of unpressurized equipment in airliners. Even organic nano-filled corona resistant materials designed to withstand some PD activity are insufficient to design a reliable insulating system operating above PDIV. The major contributor to the increased degradation rate is the higher kinetic energy that discharge electrons are able to reach when the pressure is decreased. Indeed, results hint the presence of a threshold in the degradation mechanisms above a certain electron energy, depending on both voltage and pressure (roughly situated at 700 V peak at 150 mbar). It is likely that, above such threshold, the enhanced etching of the polymeric matrix, or the breaking of previously inaccessible chemical bonds are able to rapidly bring the insulation to failure (within tens of seconds). The effect is so dramatic that little difference is found comparing the performance of wires insulated with standard or CR materials. Additionally, an increase of degradation rates were observed when converter waveforms are used, in comparison with AC sinusoidal supplies with the same voltage and frequency. This phenomenon is also aggravated by moderate air moisture level. Thus, operation of any transport electrification drive in the presence of continuous PD activity is likely

not feasible when discharges are incepted in the T-T subsystem.

Estimation of lifetimes performed through simple models of cumulative damage opened the door (strictly at sea-level pressure levels) for operation in mixed PD regime, where PD are incepted only during transients or anomalous operating conditions for a percentage of service time lower than 1%. This is clearly more relevant for EV than for aircraft systems. However, since the possibility of having sustained converter generated PD activity in subsystems including nano-filled or completely inorganic liners is yet to be scrutinized, the most appropriate strategy for motors manufacturers would be to prefer a PD-free design for those applications. This goal is achievable by coordinating the inverter voltage stress with the PDIV level of the stator insulation. The selection of the insulation system must be carried out prioritizing the maximization of PDIV and dielectric performance, also at elevated temperature. Since the inception of PD proved to be a turning point in machine reliability, understanding which factors reduce an insulating system's PDIV, and to what extent, becomes critical.

A reassuring result is that features of converter waveforms appear to not reduce the PDIV to values below the one recorded for AC 50 Hz sources. Higher PDIV peak reported for fast oscillating waveforms in previous studies have been confirmed with experiments in presence of UV-irradiation sources on T-T samples. With no UV irradiation, higher PDIV (+7%) was obtained with pulses of shorter duration (lower than 2 μs), possibly due to the statistical delay of seed electron appearance. Introducing UV radiation (hence free electrons on the surface of the samples) uniformed PDIV values for short pulses to the ones obtained with pulses of longer duration. The increase of PDIV recorded for fast oscillating waveforms (with a time scale of tens of nanoseconds) remain to be fully explained, and the contribution of dielectric relaxation phenomena is hypothesized for this case. Regardless, it would be implausible to be able to exploit this effect to reach higher voltages in rotating machines.

Impregnating resin has a critical role in defining the PDIV level of a machine. This has been investigated on T-T impregnated samples. The results achieved through a combination of PDIV tests, dielectric spectroscopy and FEM-simulation appear to indicate that more efforts should be put on increasing coating effectiveness. The requirement might be at odds with the need for the resin to fill every void in the slot, as opposite viscosity values are required to effectively fulfill the two tasks. Operation of resins above their glass transition temperatures did not reveal critical PDIV drops, despite the important permittivity variation recorded. The effect of thermal aging on PDIV of impregnated samples was found to be increased when testing with converter waveforms, compared to AC sinusoidal voltages. On the other hand, non-impregnated specimens did not yield similar results. This phenomenon is mainly attributable to the different variation of the dielectric permittivity of the resins along the frequency spectrum, and the relative dielectric losses.

In aeronautic conditions (i.e., in low pressure environments), the role of the solid insulation was found to be de-emphasized, due to the elongation of discharge field lines. Using thicker insulation has a mild impact in improving the PDIV at reduced pressures, making stress mitigation techniques preferable than insulation over-design. The same phenomenon has a positive effect reducing the aging contribution to PDIV decrements, typically caused by insulation shrinking and permittivity increase, improving the scenario in comparison to sea-level conditions. The addition of aging sub-cycles including high-moisture exposition, aircraft-typical vibration profile, and thermal shock to the standard aging process did not reveal particular influence on results. Unfortunately, it is too early to rule out these factors as contributors to insulator degradation, as their continuous application as aging stresses may play a role in mechanical degradation. Importantly, during the same aging cycles an unexpected chemical incompatibility was discovered, raising concerns about the use of materials from different manufacturers without a prior compatibility analysis.

These results and their critical discussion are another important step towards gaining a comprehensive and cohesive understanding of the subject. Integrating the current body of knowledge with the mentioned experimental findings enabled the proposal of a PDIV coordination route to assist the insulation designer in making more secure decisions. Stress mitigation solutions were illustrated on both the machine and converter sides, to be used in conjunction with traditional insulation design techniques aided by PDIV prediction tools (of which novel advancements for systems of impregnated T-T samples and P-P/P-G were presented). At the present time, it is not possible to identify an optimal single solution for easily coordinating the insulation to the converter stresses, whereas a combination of them would most likely result in the best performance in terms of drive system reliability and efficiency. The use of ordered winding structures and multilevel converters is probably the most technologically mature path to achieve the reliability level desired by the transportation sector.

Finally, the discussion has been completed with recommendations for an updated qualification under WBG-converter stresses based on a modified IEC 60034-18-41, accounting for the requisites of transportation sector. The enhancement factors have been revised to account for aeronautical conditions. Simple pre-qualification tests are suggested to eliminate underperforming resins and reveal potential chemical incompatibilities. The ideas of using a "reference system with proven service experience" and a single IVIC coefficient have been challenged, with a reliability target method proposed for the former and a more flexible multi-IVIC alternative proposed for the latter. Finally, an electro-thermal aging bench was prototyped to simplify qualification and achieve a more representative solution.

Bibliography

[1] Intergovernmental Panel on Climate Change and Ottmar Edenhofer, eds. *Climate Change 2014: Mitigation of Climate Change: Working Group III Contribution to the Fifth Assessment Report of the Intergovernmental Panel on Climate Change*. New York, NY: Cambridge University Press, 2014. 1435 pp. ISBN: 978-1-107-05821-7 978-1-107-65481-5.

[2] IEA - International Energy Agency. "CO2 Emissions from Fuel Combustion 2019 - Highlights". In: (2019).

[3] European Environment Agency. *Greenhouse Gas Emissions from Transport in Europe*. URL: https://www.eea.europa.eu/ims/greenhouse-gas-emissions-from-transport (visited on 01/02/2023).

[4] David Adam. "How Far Will Global Population Rise? Researchers Can't Agree". In: *Nature* 597.7877 (Sept. 23, 2021), pp. 462–465. ISSN: 0028-0836, 1476-4687. DOI: 10.1038/d41586-021-02522-6.

[5] IEA - International Energy Agency. *World Air Passenger Traffic Evolution, 1980-2020 – Charts – Data & Statistics - IEA*. URL: https://www.iea.org/data-and-statistics/charts/world-air-passenger-traffic-evolution-1980-2020 (visited on 01/02/2023).

[6] Will Steffen et al. "Trajectories of the Earth System in the Anthropocene". In: *Proc. Natl. Acad. Sci. U.S.A.* 115.33 (Aug. 14, 2018), pp. 8252–8259. ISSN: 0027-8424, 1091-6490. DOI: 10.1073/pnas.1810141115.

[7] S. Pacala and R. Socolow. "Stabilization Wedges: Solving the Climate Problem for the Next 50 Years with Current Technologies". In: *Science* 305.5686 (Aug. 13, 2004), pp. 968–972. ISSN: 0036-8075, 1095-9203. DOI: 10.1126/science.1100103.

[8] James H. Williams et al. "The Technology Path to Deep Greenhouse Gas Emissions Cuts by 2050: The Pivotal Role of Electricity". In: *Science* 335.6064 (Jan. 6, 2012), pp. 53–59. ISSN: 0036-8075, 1095-9203. DOI: 10.1126/science.1208365.

[9] Berker Bilgin et al. "Making the Case for Electrified Transportation". In: *IEEE Trans. Transp. Electrific.* 1.1 (June 2015), pp. 4–17. ISSN: 2332-7782. DOI: 10.1109/TTE.2015.2437338.

[10] Alexandre Milovanoff, I. Daniel Posen, and Heather L. MacLean. "Electrification of Light-Duty Vehicle Fleet Alone Will Not Meet Mitigation Targets". In: *Nat. Clim. Chang.* 10.12 (Dec. 2020), pp. 1102–1107. ISSN: 1758-678X, 1758-6798. DOI: 10.1038/s41558-020-00921-7.

[11] Michael Kelly. "Electrifying the UK and the Want of Engineering". In: *Essay 11, The Global Warming Policy Foundation* ().

[12] Shrey Verma, Gaurav Dwivedi, and Puneet Verma. "Life Cycle Assessment of Electric Vehicles in Comparison to Combustion Engine Vehicles: A Review". In: *Materials Today: Proceedings* 49 (2022), pp. 217–222. ISSN: 22147853. DOI: 10.1016/j.matpr.2021.01.666.

[13] Troy R. Hawkins et al. "Comparative Environmental Life Cycle Assessment of Conventional and Electric Vehicles". In: *Journal of Industrial Ecology* 17.1 (Feb. 2013), pp. 53–64. ISSN: 1088-1980, 1530-9290. DOI: 10.1111/j.1530-9290.2012.00532.x.

[14] Giulio Mattioli. "Transport Needs in a Climate-Constrained World. A Novel Framework to Reconcile Social and Environmental Sustainability in Transport". In: *Energy Research & Social Science* 18 (Aug. 2016), pp. 118–128. ISSN: 22146296. DOI: 10.1016/j.erss.2016.03.025.

[15] International Civil Aviation and Organization. *Innovation for the Green Transition, 2022 Enviormental Report.*

[16] Jose Millan et al. "A Survey of Wide Bandgap Power Semiconductor Devices". In: *IEEE Trans. Power Electron.* 29.5 (May 2014), pp. 2155–2163. ISSN: 0885-8993, 1941-0107. DOI: 10.1109/TPEL.2013.2268900.

[17] Ajay Kumar Morya et al. "Wide Bandgap Devices in AC Electric Drives: Opportunities and Challenges". In: *IEEE Trans. Transp. Electrific.* 5.1 (Mar. 2019), pp. 3–20. ISSN: 2332-7782, 2372-2088. DOI: 10.1109/TTE.2019.2892807.

[18] Juergen Biela et al. "SiC versus Si—Evaluation of Potentials for Performance Improvement of Inverter and DC–DC Converter Systems by SiC Power Semiconductors". In: *IEEE Trans. Ind. Electron.* 58.7 (July 2011), pp. 2872–2882. ISSN: 0278-0046, 1557-9948. DOI: 10.1109/TIE.2010.2072896.

[19] Pourya Shamsi, Matthew McDonough, and Babak Fahimi. "Wide-Bandgap Semiconductor Technology: Its Impact on the Electrification of the Transportation Industry". In: *IEEE Electrific. Mag.* 1.2 (Dec. 2013), pp. 59–63. ISSN: 2325-5897, 2325-5889. DOI: 10.1109/MELE.2013.2293931.

[20] Woongkul Lee et al. "A Review of Integrated Motor Drive and Wide-Bandgap Power Electronics for High-Performance Electro-Hydrostatic Actuators". In: *IEEE Trans. Transp. Electrific.* 4.3 (Sept. 2018), pp. 684–693. ISSN: 2332-7782, 2372-2088. DOI: 10.1109/TTE.2018.2853994.

[21] Kaushik Rajashekara. “Parallel between More Electric Aircraft and Electric\/Hybrid Vehicle Power Conversion Technologies”. In: *IEEE Electrific. Mag.* 2.2 (June 2014), pp. 50–60. ISSN: 2325-5897, 2325-5889. DOI: 10.1109/MELE.2014.2312460.

[22] IATA. *Aircraft Technology Roadmap to 2050*. 2021.

[23] Jean Thomassin and Greg Winn. *The Pragmatic Future of Hybrid-Electric Flight A Technical Analysis of United Technologies Advanced Projects X-Plane.Pdf*. Mar. 2019.

[24] Bulent Sarlioglu and Casey T. Morris. “More Electric Aircraft: Review, Challenges, and Opportunities for Commercial Transport Aircraft”. In: *IEEE Trans. Transp. Electrific.* 1.1 (June 2015), pp. 54–64. ISSN: 2332-7782. DOI: 10.1109/TTE.2015.2426499.

[25] I. Moir and A. G. Seabridge. *Aircraft Systems: Mechanical, Electrical, and Avionics Subsystems Integration*. 3rd ed. Aerospace Series. Chichester, West Sussex, England ; Hoboken, NJ: Wiley, 2008. 504 pp. ISBN: 978-0-470-05996-8.

[26] P.C. Vratny and U. Kling. “Impact of Electric Taxiing on Hybrid-Electric Aircraft Sizing”. Version 1.0. In: (2019), 10 pages. DOI: 10.25967/480115.

[27] Vincenzo Madonna, Paolo Giangrande, and Michael Galea. “Electrical Power Generation in Aircraft: Review, Challenges, and Opportunities”. In: *IEEE Trans. Transp. Electrific.* 4.3 (Sept. 2018), pp. 646–659. ISSN: 2332-7782, 2372-2088. DOI: 10.1109/TTE.2018.2834142.

[28] Ian Cotton et al. “Design Considerations for Higher Electrical Power System Voltages in Aerospace Vehicles”. In: *2016 IEEE International Power Modulator and High Voltage Conference (IPMHVC)*. 2016 IEEE International Power Modulator and High Voltage Conference (IPMHVC). San Francisco, CA, USA: IEEE, July 2016, pp. 57–61. ISBN: 978-1-5090-2354-7. DOI: 10.1109/IPMHVC.2016.8012771.

[29] J. Brombach et al. “Optimized Cabin Power Supply with a +/- 270 V DC Grid on a Modern Aircraft”. In: *2011 7th International Conference-Workshop Compatibility and Power Electronics (CPE)*. 2011 7th International Conference-Workshop "Compatibility And Power Electronics" (CPE). Tallinn, Estonia: IEEE, June 2011, pp. 425–428. ISBN: 978-1-4244-8806-3. DOI: 10.1109/CPE.2011.5942274.

[30] Dominique Van Den. “The A380 Flight Control Electrohydrostatic Actuators, Achievements and Lessons Learnt.” In: *25th International Congress of the Aeronautical Sciences.* 2006.

[31] J.W. Bennett et al. “Safety-Critical Design of Electromechanical Actuation Systems in Commercial Aircraft”. In: *IET Electr. Power Appl.* 5.1 (2011), p. 37. ISSN: 17518660. DOI: 10.1049/iet-epa.2009.0304.

[32] Robert Abebe et al. “Integrated Motor Drives: State of the Art and Future Trends”. In: *IET Electric Power Applications* 10.8 (Sept. 2016), pp. 757–771. ISSN: 1751-8660, 1751-8679. DOI: 10.1049/iet-epa.2015.0506.

[33] Wenping Cao et al. “Overview of Electric Motor Technologies Used for More Electric Aircraft (MEA)”. In: *IEEE Trans. Ind. Electron.* 59.9 (Sept. 2012), pp. 3523–3531. ISSN: 0278-0046, 1557-9948. DOI: 10.1109/TIE.2011.2165453.

[34] Noureddine Bessous. “Reliability Surveys of Fault Distributions in Rotating Electrical Machines : – Case Study of Fault Detections in IMs –”. In: *020 1st International Conference on Communications, Control Systems and Signal Processing (CCSSP)*. 2020 1st International Conference on Communications, Control Systems and Signal Processing (CCSSP). EL OUED, Algeria: IEEE, May 2020, pp. 535–543. ISBN: 978-1-72815-835-8. DOI: 10.1109/CCSSP49278.2020.9151672.

[35] G.C. Stone, I. Culbert, and B.A. Lloyd. “Stator Insulation Problems Associated with Low Voltage and Medium Voltage PWM Drives”. In: *2007 IEEE Cement Industry Technical Conference Record*. 2007 IEEE Cement Industry Technical Conference Record. Charleston, SC, USA: IEEE, Apr. 2007, pp. 187–192. ISBN: 978-1-4244-1195-5 978-1-4244-1196-2. DOI: 10.1109/CITCON.2007.358997.

[36] M. Chapman, N. Frost, and R. Bruetsch. “Insulation Systems for Rotating Low-Voltage Machines”. In: *Conference Record of the 2008 IEEE International Symposium on Electrical Insulation*. 2008 IEEE International Symposium on Electrical Insulation. Vancouver, BC: IEEE, June 2008, pp. 257–260. ISBN: 978-1-4244-2091-9. DOI: 10.1109/ELINSL.2008.4570323.

[37] *IEC 60317-0- 1:2014 - Specifications for Particular Types of Winding Wires General Requirements. Enamelled Round Copper Wire*. Definitive. 2019. ISBN: 978-0-539-00308-6.

[38] *IEC 60317-0-2:2020 - Specifications for Particular Types of Winding Wires. Part 0-2, General Requirements. Enamelled Rectangular Copper Wire*. London: British Standards Institution, 2020.

[39] *IEC 60034-18-41:2014 - Rotating Electrical Machines Partial Discharge Free Electrical Insulation Systems (Type I) Used in Rotating Electrical Machines Fed from Voltage Converters. Qualification and Quality Control Tests*. Withdrawn. 2014. ISBN: 978-0-580-73798-5.

[40] Greg Stone. *Electrical Insulation for Rotating Machines*. ISBN: 978-1-118-05706-3.

[41] Ahmed Selema, Mohamed N. Ibrahim, and Peter Sergeant. “Electrical Machines Winding Technology: Latest Advancements for Transportation Electrification”. In: *Machines* 10.7 (July 12, 2022), p. 563. ISSN: 2075-1702. DOI: 10.3390/machines10070563.

[42] N. Frost, M. Chapman, and R. Bruetsch. “Considerations for Rotating Low-Voltage Machine Insulation Designs”. In: *Conference Record of the 2008 IEEE International Symposium on Electrical Insulation*. 2008 IEEE International Symposium on Electrical Insulation. Vancouver, BC: IEEE, June 2008, pp. 571–574. ISBN: 978-1-4244-2091-9. DOI: 10.1109/ELINSL.2008.4570397.

[43] G.C. Montanari and L. Simoni. “Aging Phenomenology and Modeling”. In: *IEEE Trans. Elect. Insul.* 28.5 (Oct./1993), pp. 755–776. ISSN: 00189367. DOI: 10.1109/14.237740.

[44] *IEC 60505:2011 - Evaluation and Qualification of Electrical Insulation Systems*. Definitive. 2017. ISBN: 978-0-580-98246-0.

[45] Raphael Färber and Christian M. Franck. “Streamer Inception Thresholds Derived from a Statistical Electron Transport Model”. In: *J. Phys. D: Appl. Phys.* 54.43 (Oct. 28, 2021), p. 435202. ISSN: 0022-3727, 1361-6463. DOI: 10.1088/1361-6463/ac1888.

[46] John M. Meek and J. D. Craggs, eds. *Electrical Breakdown of Gases*. Wiley Series in Plasma Physics. Chichester ; New York: Wiley, 1978. 878 pp. ISBN: 978-0-471-99553-1.

[47] Alexander A. Fridman. *Plasma Chemistry*. First paperback edition. Cambridge: Cambridge University Press, 2012. 978 pp. ISBN: 978-1-107-68493-5 978-0-521-84735-3.

[48] Andrea Cavallini, Davide Fabiani, and Gian Montanari. “Power Electronics and Electrical Insulation Systems - Part 1: Phenomenology Overview”. In: *IEEE Electr. Insul. Mag.* 26.3 (May 2010), pp. 7–15. ISSN: 0883-7554. DOI: 10.1109/MEI.2010.5482783.

[49] Andrea Cavallini, Dav Fabiani, and Gian Montanari. “Power Electronics and Electrical Insulation Systems - Part 2: Life Modeling for Insulation Design”. In: *IEEE Electr. Insul. Mag.* 26.4 (July 2010), pp. 33–39. ISSN: 0883-7554. DOI: 10.1109/MEI.2010.5511187.

[50] Andrea Cavallini, Davide Fabiani, and Gian Carlo Montanari. “Power Electronics and Electrical Insulation Systems - Part 3: Diagnostic Properties”. In: *IEEE Electr. Insul. Mag.* 26.5 (Sept. 2010), pp. 30–40. ISSN: 0883-7554. DOI: 10.1109/MEI.2010.5585006.

[51] D. Fabiani, G.C. Montanari, and A. Contin. “Aging Acceleration of Insulating Materials for Electrical Machine Windings Supplied by PWM in the Presence and in the Absence of Partial Discharges”. In: *ICSD'01. Proceedings of the 20001 IEEE 7th International Conference on Solid Dielectrics (Cat. No.01CH37117)*. ICSD'01. Proceedings of the 2001 IEEE 7th International Conference on Solid Dielectrics. Eindhoven, Netherlands: IEEE, 2001, pp. 283–286. ISBN: 978-0-7803-6352-6. DOI: 10.1109/ICSD.2001.955625.

[52] *IEC 60034-18-42:2017 - Rotating Electrical Machines Partial Discharge Resistant Electrical Insulation Systems (Type II) Used in Rotating Electrical Machines Fed from Voltage Converters - Qualification Tests*. Withdrawn. 2017. ISBN: 978-0-580-81910-0.

[53] E. Persson. “Transient Effects in Application of PWM Inverters to Induction Motors”. In: *IEEE Trans. on Ind. Applicat.* 28.5 (Sept.-Oct./1992), pp. 1095–1101. ISSN: 00939994. DOI: 10.1109/28.158834.

[54] M. Kaufhold et al. “Failure Mechanism of the Interturn Insulation of Low Voltage Electric Machines Fed by Pulse-Controlled Inverters”. In: *IEEE Electr. Insul. Mag.* 12.5 (Sept. 1996), pp. 9–16. ISSN: 0883-7554. DOI: 10.1109/57.537190.

[55] A. Mbaye et al. “Electrical Stresses Applied to Stator Insulation in Low-Voltage Induction Motors Fed by PWM Drives”. In: *IEE Proc., Electr. Power Appl.* 144.3 (1997), p. 191. ISSN: 13502352. DOI: 10.1049/ip-epa:19970940.

[56] Weijun Yin. “Failure Mechanism of Winding Insulations in Inverter-Fed Motors”. In: *IEEE Electrical Insulation Magazine* 13.6 (Nov. 1997), pp. 18–23. ISSN: 0883-7554, 1558-4402. DOI: 10.1109/57.637150.

[57] R.J. Kerkman et al. “PWM Inverters and Their Influence on Motor Overvoltage”. In: *Proceedings of APEC 97 - Applied Power Electronics Conference*. APEC 97 - Applied Power Electronics Conference. Vol. 1. Atlanta, GA, USA: IEEE, 1997, pp. 103–113. ISBN: 978-0-7803-3704-6. DOI: 10.1109/APEC.1997.581440.

[58] M. Kaufhold et al. “Electrical Stress and Failure Mechanism of the Winding Insulation in PWM-inverter-fed Low-Voltage Induction Motors”. In: *IEEE Trans. Ind. Electron.* 47.2 (Apr. 2000), pp. 396–402. ISSN: 02780046. DOI: 10.1109/41.836355.

[59] M.J. Melfi. “Low-Voltage PWM Inverter-Fed Motor Insulation Issues”. In: *IEEE Transactions on Industry Applications* 42.1 (Jan. 2006), pp. 128–133. ISSN: 0093-9994, 1939-9367. DOI: 10.1109/TIA.2005.861308.

[60] *IEC 61800-8:2010 - Adjustable Speed Electrical Power Drive Systems Specification of Voltage on the Power Interface*. Definitive. 2010. ISBN: 978-0-580-62645-6.

[61] Russel J Kerkman. “Interaction of Drive Modulation and Cable Parameters on AC Motor Transients”. In: *IEEE TRANSACTIONS ON INDUSTRY APPLICATIONS* 33.3 (1997).

[62] Marco Pastura et al. “Partial Discharges in Electrical Machines for the More Electric Aircraft—Part I: A Comprehensive Modeling Tool for the Characterization of Electric Drives Based on Fast Switching Semiconductors”. In: *IEEE Access* 9 (2021), pp. 27109–27121. ISSN: 2169-3536. DOI: 10.1109/ACCESS.2021.3058083.

[63] Gian Carlo Montanari et al. “Noise Rejection and Partial Discharge Identification in PDIV Tests of Insulated Wires under Repetitive Impulse Supply Voltage”. In: *2019 IEEE Electrical Insulation Conference (EIC)*. 2019 IEEE Electrical Insulation Conference (EIC). Calgary, AB, Canada: IEEE, June 2019, pp. 505–508. ISBN: 978-1-5386-7624-0. DOI: 10.1109/EIC43217.2019.9046587.

[64] Luca Lusuardi. “Towards a Partial Discharge Free Insulation System for the More Electrical Transportation .Pdf”. Università di Bologna, 2020.

[65] Peng Wang et al. “Effect of Rise Time on PD Pulse Features under Repetitive Square Wave Voltages”. In: *IEEE Trans. Dielect. Electr. Insul.* 20.1 (Feb. 2013), pp. 245–254. ISSN: 1070-9878. DOI: 10.1109/TDEI.2013.6451364.

[66] N Hayakawa et al. “Partial Discharge Inception Voltage for Magnet Wire of Inverter-Fed Motors under Surge Voltage Application”. In: *2010 Annual Report Conference on Electrical Insulation and Dielectic Phenomena*. 2010 IEEE Conference on Electrical Insulation and Dielectric Phenomena (CEIDP 2010). West Lafayette, IN: IEEE, Oct. 2010, pp. 1–4. ISBN: 978-1-4244-9468-2. DOI: 10.1109/CEIDP.2010.5723994.

[67] Satoshi Matsumoto et al. “Partial Discharge Characteristics of Twisted Magnet Wire under High Frequency AC Voltage”. In: *Proceedings of 2014 International Symposium on Electrical Insulating Materials*. 2014 International Symposium on Electrical Insulating Materials (ISEIM). Niigata: IEEE, June 2014, pp. 57–60. ISBN: 978-4-88686-086-6. DOI: 10.1109/ISEIM.2014.6870719.

[68] T. J. A. Hammarstrom. “Partial Discharge Characteristics at Ultra-Short Voltage Risetimes”. In: *IEEE Trans. Dielect. Electr. Insul.* 25.6 (Dec. 2018), pp. 2241–2249. ISSN: 1070-9878, 1558-4135. DOI: 10.1109/TDEI.2018.007445.

[69] Zhuo Wei et al. “Partial Discharge Behavior on Twisted Pair under Ultra-short Rise Time Square-wave Excitations”. In: *2019 IEEE Electrical Insulation Conference (EIC)*. 2019 IEEE Electrical Insulation Conference (EIC). Calgary, AB, Canada: IEEE, June 2019, pp. 493–496. ISBN: 978-1-5386-7624-0. DOI: 10.1109/EIC43217.2019.9046624.

[70] M. Fenger, S.R. Campbell, and G. Gao. “The Impact of Surge Voltage Rise-Time on PD Inception Voltage in Random Wound Motors of Different Designs”. In: *2001 Annual Report Conference on Electrical Insulation and Dielectric Phenomena (Cat. No.01CH37225)*. 2001 Annual Report Conference on Electrical Insulation and Dielectric Phenomena (Cat. No.01CH37225). Oct. 2001, pp. 352–355. DOI: 10.1109/CEIDP.2001.963555.

[71] Alberto Rumi, Andrea Cavallini, and Luca Lusuardi. “Impact of WBG Converter Voltage Rise-Time and Switching Frequency on the PDIV of Twisted Pairs”. In: *2020 IEEE 3rd International Conference on Dielectrics (ICD)*. 2020 IEEE 3rd International Conference on Dielectrics (ICD). Valencia, Spain: IEEE, July 5, 2020, pp. 902–905. ISBN: 978-1-72818-983-3. DOI: 10.1109/ICD46958.2020.9341897.

[72] Vanessa Neves Höpner and Volmir Eugênio Wilhelm. “Insulation Life Span of Low-Voltage Electric Motors—A Survey”. In: *Energies* 14.6 (Mar. 21, 2021), p. 1738. ISSN: 1996-1073. DOI: 10.3390/en14061738.

[73] J.C.G. Wheeler. “Effects of Converter Pulses on the Electrical Insulation in Low and Medium Voltage Motors”. In: *IEEE Electrical Insulation Magazine* 21.2 (Mar. 2005), pp. 22–29. ISSN: 0883-7554, 1558-4402. DOI: 10.1109/MEI.2005.1412216.

[74] Peng Wang, Andrea Cavallini, and Gian Carlo Montanari. “Characteristics of PD under Square Wave Voltages and Their Influence on Motor Insulation Endurance”. In: *IEEE Transactions on Dielectrics and Electrical Insulation* 22.6 (Dec. 2015), pp. 3079–3086. ISSN: 1070-9878, 1558-4135. DOI: 10.1109/TDEI.2015.005158.

[75] F. Guastavino and A. Dardano. “Life Tests on Twisted Pairs in Presence of Partial Discharges: Influence of the Voltage Waveform”. In: *IEEE Trans. Dielect. Electr. Insul.* 19.1 (Feb. 2012), pp. 45–52. ISSN: 1070-9878. DOI: 10.1109/TDEI.2012.6148501.

[76] H. Kikuchi and H. Hanawa. “Inverter Surge Resistant Enameled Wire with Nanocomposite Insulating Material”. In: *IEEE Trans. Dielect. Electr. Insul.* 19.1 (Feb. 2012), pp. 99–106. ISSN: 1070-9878. DOI: 10.1109/TDEI.2012.6148507.

[77] *IAGOS Database – In-service Aircraft for a Global Observing System*. URL: https://www.iagos.org/ (visited on 12/17/2022).

[78] Takefumi Kaji et al. “Combined Effect of Temperature and Humidity of Magnet-Wires on Partial Discharge Inception Voltage under Inverter-Surge Voltage”. In: *2018 IEEE Conference on Electrical Insulation and Dielectric Phenomena (CEIDP)*. 2018 IEEE Conference on Electrical Insulation and Dielectric Phenomena (CEIDP). Cancun: IEEE, Oct. 2018, pp. 554–557. ISBN: 978-1-5386-6192-5. DOI: 10.1109/CEIDP.2018.8544745.

[79] Yusuke Kikuchi et al. “Effects of Ambient Humidity and Temperature on Partial Discharge Characteristics of Conventional and Nanocomposite Enameled Magnet Wires”. In: *IEEE Trans. Dielect. Electr. Insul.* 15.6 (Dec. 2008), pp. 1617–1625. ISSN: 1070-9878. DOI: 10.1109/TDEI.2008.4712665.

[80] Waqar Hassan et al. “Effects of Environmental Factors on Partial Discharge Activity and Estimation of Insulation Lifetime in Electrical Machines”. In: *IEEE Access* 8 (2020), pp. 108491–108502. ISSN: 2169-3536. DOI: 10.1109/ACCESS.2020.2998373.

[81] Alberto Rumi, Andrea Cavallini, and Luca Lusuardi. “Combined Effects of Temperature and Humidity on the PDIV of Twisted Pairs”. In: *2020 IEEE 3rd International Conference on Dielectrics (ICD)*. 2020 IEEE 3rd International Conference on Dielectrics (ICD). Valencia, Spain: IEEE, July 5, 2020, pp. 906–909. ISBN: 978-1-72818-983-3. DOI: 10.1109/ICD46958.2020.9342030.

[82] L. Lusuardi et al. “Insulation Design of Low Voltage Electrical Motors Fed by PWM Inverters”. In: *IEEE Electr. Insul. Mag.* 35.3 (May 2019), pp. 7–15. ISSN: 0883-7554, 1558-4402. DOI: 10.1109/MEI.2019.8689431.

[83] Vincenzo Madonna et al. “Electrical Machines for the More Electric Aircraft: Partial Discharges Investigation”. In: *IEEE Trans. on Ind. Applicat.* 57.2 (Mar. 2021), pp. 1389–1398. ISSN: 0093-9994, 1939-9367. DOI: 10.1109/TIA.2020.3046434.

[84] Stephane Duchesne et al. “Prediction of PDIV in Motor Coils Using Finite Element Method”. In: *2016 IEEE International Conference on Dielectrics (ICD)*. 2016 IEEE International Conference on Dielectrics (ICD). Montpellier, France: IEEE, July 2016, pp. 638–641. ISBN: 978-1-5090-2804-7. DOI: 10.1109/ICD.2016.7547696.

[85] C. Van de Steen, C. Abadie, and G. Belijar. “Partial Discharge Detection, Experimental-Simulation Comparison and Actual Limits”. In: *2020 IEEE Electrical Insulation Conference (EIC)*. 2020 IEEE Electrical Insulation Conference (EIC). Knoxville, TN, USA: IEEE, June 2020, pp. 537–541. ISBN: 978-1-72815-485-5. DOI: 10.1109/EIC47619.2020.9158654.

[86] Luca Lusuardi et al. “Partial Discharge Phenomena in Electrical Machines for the More Electrical Aircraft. Part II: Impact of Reduced Pressures and Wide Bandgap Devices”. In: *IEEE Access* 9 (2021), pp. 27485–27495. ISSN: 2169-3536. DOI: 10.1109/ACCESS.2021.3058089.

[87] F. Koliatene et al. “Impact of the Aeronautic Environment on the Partial Discharges Ignition: A Basic Study”. In: *Conference Record of the 2008 IEEE International Symposium on Electrical Insulation*. 2008 IEEE International Symposium on Electrical Insulation. Vancouver, BC: IEEE, June 2008, pp. 603–606. ISBN: 978-1-4244-2091-9. DOI: 10.1109/ELINSL.2008.4570404.

[88] Rui Rui and Ian Cotton. “Impact of Low Pressure Aerospace Environment on Machine Winding Insulation”. In: *2010 IEEE International Symposium on Electrical Insulation*. 2010 IEEE International Symposium on Electrical Insulation (ISEI). San Diego, CA, USA: IEEE, June 2010, pp. 1–5. ISBN: 978-1-4244-6298-8. DOI: 10.1109/ELINSL.2010.5549718.

[89] Luca Lusuardi et al. “Assessing the Severity of Partial Discharges in Aerospace Applications”. In: *2019 IEEE Conference on Electrical Insulation and Dielectric Phenomena (CEIDP)*. 2019 IEEE Conference on Electrical Insulation and Dielectric Phenomena (CEIDP). Richland, WA, USA: IEEE, Oct. 2019, pp. 267–270. ISBN: 978-1-72813-121-4. DOI: 10.1109/CEIDP47102.2019.9009970.

[90] Cedric Abadie, Thibaut Billard, and Thierry Lebey. “Influence of Pressure on Partial Discharge Spectra”. In: *2016 IEEE Electrical Insulation Conference (EIC)*. 2016 IEEE Electrical Insulation Conference (EIC). Montreal, QC, Canada: IEEE, June 2016, pp. 507–510. ISBN: 978-1-4673-8706-4. DOI: 10.1109/EIC.2016.7548648.

[91] *IEC 60851-5:2008 - Winding Wires. Test Methods Electrical Properties*. Definitive. 2019. ISBN: 978-0-539-02627-6.

[92] *IEC 60034-18-21:2013 - Rotating Electrical Machines Functional Evaluation of Insulation Systems. Test Procedures for Wire-Wound Windings. Thermal Evaluation and Classification*. Definitive. 2013. ISBN: 978-0-580-61688-4.

[93] *IEC 61934:2011 - Electrical Insulating Materials and Systems. Electrical Measurement of Partial Discharges (PD) under Short Rise Time and Repetitive Voltage Impulses*. Definitive. 2011. ISBN: 978-0-580-71782-6.

[94] Andrea Caprara et al. “The Definition of RPDIV in Impulsive Testing and the Effect of the Electrical Conditioning on the Variability of the Results”. In: *2020 IEEE Electrical Insulation Conference (EIC)*. 2020 IEEE Electrical Insulation Conference (EIC). Knoxville, TN, USA: IEEE, June 2020, pp. 234–237. ISBN: 978-1-72815-485-5. DOI: 10.1109/EIC47619.2020.9158761.

[95] Jeffrey Voas, Nir Kshetri, and Joanna F. DeFranco. "Scarcity and Global Insecurity: The Semiconductor Shortage". In: *IT Prof.* 23.5 (Sept. 1, 2021), pp. 78–82. ISSN: 1520-9202, 1941-045X. DOI: 10.1109/MITP.2021.3105248.

[96] *IEC 60270:2001 - High-voltage Test Techniques. Partial Discharge Measurements*. Under Review. 2016. ISBN: 978-0-580-71746-8.

[97] Shinichi Okada et al. "Comparison of Electromagnetic Wave, Light Intensity and Electric Charge of PD on Crossed Magnet Wires under Repetitive Impulses". In: *2008 Annual Report Conference on Electrical Insulation and Dielectric Phenomena*. 2008 Annual Report Conference on Electrical Insulation and Dielectric Phenomena (CEIDP). Quebec City, QC, Canada: IEEE, Oct. 2008, pp. 391–394. ISBN: 978-1-4244-2548-8. DOI: 10.1109/CEIDP.2008.4772812.

[98] A. Contin et al. "Digital Detection and Fuzzy Classification of Partial Discharge Signals". In: *IEEE Transactions on Dielectrics and Electrical Insulation* 9.3 (June 2002), pp. 335–348. ISSN: 1558-4135. DOI: 10.1109/TDEI.2002.1007695.

[99] F.H. Kreuger, E. Gulski, and A. Krivda. "Classification of Partial Discharges". In: *IEEE Trans. Elect. Insul.* 28.6 (Dec./1993), pp. 917–931. ISSN: 00189367. DOI: 10.1109/14.249365.

[100] T. Billard, T. Lebey, and F. Fresnet. "Partial Discharge in Electric Motor Fed by a PWM Inverter: Off-Line and on-Line Detection". In: *IEEE Trans. Dielect. Electr. Insul.* 21.3 (June 2014), pp. 1235–1242. ISSN: 1070-9878. DOI: 10.1109/TDEI.2014.6832270.

[101] L. Niemeyer. "A Generalized Approach to Partial Discharge Modeling". In: *IEEE Transactions on Dielectrics and Electrical Insulation* 2.4 (Aug. 1995), pp. 510–528. ISSN: 1070-9878, 1558-4135. DOI: 10.1109/94.407017.

[102] A Pedersen. "On the Electrical Breakdown of Gaseous Dielectrics". In: *Transactions on Electrical Insulation* (1959), p. 19.

[103] A. Pedersen et al. "Formulation of the Streamer Breakdown Criterion and Its Application to Strongly Electronegative Gases and Gas Mixtures". In: *Archiv f. Elektrotechnik* 67.6 (Nov. 1984), pp. 395–402. ISSN: 0003-9039, 1432-0487. DOI: 10.1007/BF01614884.

[104] David B. Go and Daniel A. Pohlman. "A Mathematical Model of the Modified Paschen's Curve for Breakdown in Microscale Gaps". In: *Journal of Applied Physics* 107.10 (May 15, 2010), p. 103303. ISSN: 0021-8979, 1089-7550. DOI: 10.1063/1.3380855.

[105] Gerjan Hagelaar. *BOLSIG+ - Electron Boltzmann Equation Solver*. URL: http://www.bolsig.laplace.univ-tlse.fr/ (visited on 12/09/2022).

[106] Laboratoire des Plasmas et Conversion d'Energie LAPLACE. *LXCat Database*. URL: https://fr.lxcat.net/home/ (visited on 12/09/2022).

[107] G J M Hagelaar and L C Pitchford. "Solving the Boltzmann Equation to Obtain Electron Transport Coefficients and Rate Coefficients for Fluid Models". In: *Plasma Sources Sci. Technol.* 14.4 (Nov. 1, 2005), pp. 722–733. ISSN: 0963-0252, 1361-6595. DOI: 10.1088/0963-0252/14/4/011.

[108] *Finite Element Method Magnetics*. URL: https://www.femm.info/wiki/HomePage (visited on 12/09/2022).

[109] *RTCA DO-160G - Environmental Conditions and Test Procedures for Airborne Equipment*.

[110] F.J. Campbell et al. "Hydrolytic Deterioration of Polyimide Insulation on Naval Aircraft Wiring". In: *1988. Annual Report., Conference on Electrical Insulation and Dielectric Phenomena*. 1988. Annual Report., Conference on Electrical Insulation and Dielectric Phenomena. Ottawa, Ont., Canada: IEEE, 1988, pp. 180–188. DOI: 10.1109/CEIDP.1988.26329.

[111] Peng Wang, Andrea Cavallini, and Gian Carlo Montanari. "The Effect of Impulsive Voltage Rise Time on Insulation Endurance of Inverter-Fed Motors". In: *2015 IEEE 11th International Conference on the Properties and Applications of Dielectric Materials (ICPADM)*. 2015 IEEE 11th International Conference on the Properties and Applications of Dielectric Materials (ICPADM). Sydney, Australia: IEEE, July 2015, pp. 84–87. ISBN: 978-1-4799-8903-4. DOI: 10.1109/ICPADM.2015.7295214.

[112] J. C. Devins. "The 1984 J. B. Whitehead Memorial Lecture the Physics of Partial Discharges in Solid Dielectrics". In: *IEEE Trans. Elect. Insul.* EI-19.5 (Oct. 1984), pp. 475–495. ISSN: 0018-9367. DOI: 10.1109/TEI.1984.298770.

[113] K. Kimura et al. "Discharge Condition and Surface Charge Distribution under Repetitive Bipolar Impulses". In: *Proceedings of the 7th International Conference on Properties and Applications of Dielectric Materials (Cat. No.03CH37417)*. Proceedings of the 7th International Conference on Properties and Applications of Dielectric Materials (Cat. No.03CH37417). Vol. 3. June 2003, 1061–1064 vol.3. DOI: 10.1109/ICPADM.2003.1218606.

[114] Luca Lusuardi et al. "The Impact of Test Voltage Waveform in Determining the Repetitive Partial Discharge Inception Voltage of Type I Turn/Turn Insulation Used in Inverter-Fed Induction Motors". In: *2018 IEEE Electrical Insulation Conference (EIC)*. 2018 IEEE Electrical Insulation Conference (EIC). San Antonio, TX: IEEE, June 2018,

pp. 478–481. ISBN: 978-1-5386-4178-1. DOI: 10.1109/EIC.2018.8481018.

[115] Ken Kimura et al. “PDIV Characteristics of Twisted-Pair of Magnet Wires with Repetitive Impulse Voltage”. In: *IEEE Transactions on Dielectrics and Electrical Insulation* 14.3 (June 2007), pp. 744–750. ISSN: 1558-4135. DOI: 10.1109/TDEI.2007.369539.

[116] K. R. Allen and K. Phillips. “Correlation of the Formative Time Lags with the Light Emitted from Spark Discharges”. In: *Proc. R. Soc. Lond. A* 278.1373 (Mar. 24, 1964), pp. 188–213. ISSN: 0080-4630, 2053-9169. DOI: 10.1098/rspa.1964.0054.

[117] Robert R. Wilson. “Very Short Time Lag of Sparking”. In: *Phys. Rev.* 50.11 (Dec. 1, 1936), pp. 1082–1088. ISSN: 0031-899X. DOI: 10.1103/PhysRev.50.1082.

[118] Sedat Adili. “Pulsed X-ray Induced Partial Discharge Measurements”. ETH Zurich, 2013, 1 Band. DOI: 10.3929/ETHZ-A-010099044.

[119] Sedat Adili and Christian Franck. “Application of Pulsed X-Ray Induced Partial Discharge Measurements”. In: *IEEE Trans. Dielect. Electr. Insul.* 19.5 (Oct. 2012), pp. 1833–1839. ISSN: 1070-9878. DOI: 10.1109/TDEI.2012.6311534.

[120] Yuji Murata and Isao Hiyoshi. “Characteristics of Photoemission of High Polymers”. In: *Jpn. J. Appl. Phys.* 36 (Part 1, No. 8 Aug. 15, 1997), pp. 5329–5334. ISSN: 0021-4922, 1347-4065. DOI: 10.1143/JJAP.36.5329.

[121] S. Savin, S. Ait-Amar, and D. Roger. “Turn-to-Turn Capacitance Variations Correlated to PDIV for AC Motors Monitoring”. In: *IEEE Trans. Dielect. Electr. Insul.* 20.1 (Feb. 2013), pp. 34–41. ISSN: 1070-9878. DOI: 10.1109/TDEI.2013.6451339.

[122] Davoud Esmaeil Moghadam, Christoph Herold, and Rolf Zbinden. “Effects of Resins on Partial Discharge Activity and Lifetime of Insulation Systems Used in eDrive Motors and Automotive Industries”. In: *2020 IEEE Electrical Insulation Conference (EIC)*. 2020 IEEE Electrical Insulation Conference (EIC). June 2020, pp. 221–224. DOI: 10.1109/EIC47619.2020.9158737.

[123] J H Christie, S H Krenek, and I M Woodhead. “The Electrical Properties of Hygroscopic Solids”. In: *biosystems engineering* (2009), p. 10.

[124] Jean-Luc Gardette, Bénédicte Mailhot, and Jacques Lemaire. “Photooxidation Mechanisms of Styrenic Polymers”. In: *Polymer Degradation and Stability* 48.3 (Jan. 1995), pp. 457–470. ISSN: 01413910. DOI: 10.1016/0141-3910(95)00113-Z.

[125] Emmanuel Richaud and Jacques Verdu. “Aging Behavior and Modeling Studies of Unsaturated Polyester Resin and Unsaturated Polyester Resin-Based Blends”. In: *Unsaturated Polyester Resins*. Elsevier, 2019, pp. 199–231. ISBN: 978-0-12-816129-6. DOI: 10.1016/B978-0-12-816129-6.00009-0.

[126] *UL Standard | UL 1446*.

[127] *IEC 60664-1:2020 - Insulation Coordination for Equipment within Low-Voltage Supply Systems Principles, Requirements and Tests*. Definitive. 2020. ISBN: 978-0-539-15877-9.

[128] *IEC 60664-3:2016 - Insulation Coordination for Equipment within Low-Voltage Systems Use of Coating, Potting or Moulding for Protection against Pollution*. Under Review. 2017. ISBN: 978-0-580-93185-7.

[129] Howard W Penrose. “Evaluating Reliability of Insulation Systems for Electric Machines”. In: *2014 IEEE Electrical Insulation Conference (EIC)*. 2014 IEEE Electrical Insulation Conference (EIC). Philadelphia, PA, USA: IEEE, June 2014, pp. 421–424. ISBN: 978-1-4799-2789-0 978-1-4799-2787-6 978-1-4799-2786-9. DOI: 10.1109/EIC.2014.6869422.

[130] M. Pecht and A. Dasgupta. “Physics-of-Failure: An Approach to Reliable Product Development”. In: *IEEE 1995 International Integrated Reliability Workshop. Final Report*. IEEE 1995 International Integrated Reliability Workshop. Final Report. Lake Tahoe, CA, USA: IEEE, 1995, pp. 1–4. ISBN: 978-0-7803-2705-4. DOI: 10.1109/IRWS.1995.493566.

[131] Huai Wang et al. “Transitioning to Physics-of-Failure as a Reliability Driver in Power Electronics”. In: *IEEE J. Emerg. Sel. Topics Power Electron.* 2.1 (Mar. 2014), pp. 97–114. ISSN: 2168-6777, 2168-6785. DOI: 10.1109/JESTPE.2013.2290282.

[132] Davide Fabiani. “Accelerated Degradation of Ac-Motor Winding Insultation Due to Voltage Waveforms Generated by Adjustable Speed Drives: Ph.D. Thesis”. Bologna: Gedit, 2003.

[133] S. Serra, G. C. Montanari, and G. Mazzanti. “Theory of Inception Mechanism and Growth of Defect-Induced Damage in Polyethylene Cable Insulation”. In: *Journal of Applied Physics* 98.3 (Aug. 2005), p. 034102. ISSN: 0021-8979, 1089-7550. DOI: 10.1063/1.1978986.

[134] B Crowley et al. “Measurement of the Electron Energy Distribution Function by a Langmuir Probe in an ITER-like Hydrogen Negative Ion Source”. In: *Nucl. Fusion* 46.6 (June 2006), S307–S312. ISSN: 0029-5515, 1741-4326. DOI: 10.1088/0029-5515/46/6/S11.

[135] M. J. Druyvesteyn and F. M. Penning. “The Mechanism of Electrical Discharges in Gases of Low Pressure”. In: *Rev. Mod. Phys.* 12.2 (Apr. 1, 1940), pp. 87–174. ISSN: 0034-6861. DOI: 10.1103/RevModPhys.12.87.

[136] J P Bellomo, S Dinculescu, and T Lebey. “Lifetime of Conventional and Corona Resistant Enamels”. In: (), p. 4.

[137] Masayuki Hikita et al. “Partial Discharge Endurence Test on Several Kinds of Nano-Filled Enameled Wires under High-Frequency AC Voltage Simulating Inverter Surge Voltage”. In: *2009 IEEE Conference on Electrical Insulation and Dielectric Phenomena*. 2009 IEEE Conference on Electrical Insulation and Dielectric Phenomena (CEIDP). Virginia Beach, VA, USA: IEEE, Aug. 2009, pp. 719–722. ISBN: 978-1-4244-4557-8. DOI: 10.1109/CEIDP.2009.5377729.

[138] M. Q. Nguyen et al. “Investigations on Dielectric Properties of Enameled Wires with Nanofilled Varnish for Rotating Machines Fed by Inverters”. In: *2009 IEEE Electrical Insulation Conference*. 2009 IEEE Electrical Insulation Conference (EIC) (Formerly EIC/EME). Montreal, QC, Canada: IEEE, May 2009, pp. 377–381. ISBN: 978-1-4244-3915-7. DOI: 10.1109/EIC.2009.5166374.

[139] Hitoshi Okubo et al. “Lifetime Characteristics of Nanocomposite Enameled Wire under Surge Voltage Application”. In: *2007 Annual Report - Conference on Electrical Insulation and Dielectric Phenomena*. 2007 Annual Report - Conference on Electrical Insulation and Dielectric Phenomena. Vancouver, BC, Canada: IEEE, 2007, pp. 13–16. ISBN: 978-1-4244-1481-9. DOI: 10.1109/CEIDP.2007.4451535.

[140] J.M. Meek. “The Influence of Irradiation on the Measurement of Impulse Voltages with Sphere-Gaps”. In: *Journal of the Institution of Electrical Engineers - Part I: General* 93.67 (July 1946), pp. 318–319. ISSN: 2054-0582. DOI: 10.1049/ji-1.1946.0093.

[141] Edwin G. Schneider. “An Estimate of the Absorption of Air in the Extreme Ultraviolet”. In: *J. Opt. Soc. Am.* 30.3 (Mar. 1, 1940), p. 128. ISSN: 0030-3941. DOI: 10.1364/JOSA.30.000128.

[142] D R Hardy and H Wroe. “The Electrical Breakdown of Pre-Stressed Air at Atmospheric Pressure”. In: *Br. J. Appl. Phys.* 5.9 (Sept. 1954), pp. 335–339. ISSN: 0508-3443. DOI: 10.1088/0508-3443/5/9/307.

[143] D. R. Hardy and J. D. Craggs. “The Irradiation of Spark Gaps for Voltage Measurement”. In: *Trans. Am. Inst. Electr. Eng.* 69.1 (Jan. 1950), pp. 584–590. ISSN: 0096-3860. DOI: 10.1109/T-AIEE.1950.5060190.

[144] N. Hayakawa, F. Shimizu, and H. Okubo. "Estimation of Partial Discharge Inception Voltage of Magnet Wires under Inverter Surge Voltage by Volume-Time Theory". In: *IEEE Trans. Dielect. Electr. Insul.* 19.2 (Apr. 2012), pp. 550–557. ISSN: 1070-9878. DOI: 10.1109/TDEI.2012.6180249.

[145] L. A. Dissado and J. C. Fothergill. *Electrical Degradation and Breakdown in Polymers*. IEE Materials and Devices Series 9. London: P. Peregrinus, 1992. 601 pp. ISBN: 978-0-86341-196-0.

[146] R. Bartnikas and J.P. Novak. "On the Character of Different Forms of Partial Discharge and Their Related Terminologies". In: *IEEE Trans. Elect. Insul.* 28.6 (Dec./1993), pp. 956–968. ISSN: 00189367. DOI: 10.1109/14.249369.

[147] D. Fabiani et al. "Relation between Space Charge Accumulation and Partial Discharge Activity in Enameled Wires under PWM-like Voltage Waveforms". In: *IEEE Transactions on Dielectrics and Electrical Insulation* 11.3 (June 2004), pp. 393–405. ISSN: 1070-9878, 1558-4135. DOI: 10.1109/TDEI.2004.1306718.

[148] Andrea Cavallini. "Reliability of Low Voltage Inverter-Fed Motors: What Have We Learned, Perspectives, Open Points". In: *2017 International Symposium on Electrical Insulating Materials (ISEIM)*. 2017 International Symposium on Electrical Insulating Materials (ISEIM). Toyohashi: IEEE, Sept. 2017, pp. 13–22. ISBN: 978-4-88686-099-6. DOI: 10.23919/ISEIM.2017.8088680.

[149] Louiza Fetouhi, Juan Martinez-Vega, and Benoit Petitgas. "Electric Conductivity, Aging and Chemical Degradation of Polyesterimide Resins Used in the Impregnation of Rotating Machines". In: *IEEE Trans. Dielect. Electr. Insul.* 25.1 (Feb. 2018), pp. 294–305. ISSN: 1070-9878. DOI: 10.1109/TDEI.2018.006823.

[150] Jun Jiang et al. "Partial Discharge Investigation under Low Air Pressure and Variable Frequency for More-electric-aircraft". In: *IEEE Trans. Dielect. Electr. Insul.* 28.5 (Oct. 2021), pp. 1793–1801. ISSN: 1070-9878, 1558-4135. DOI: 10.1109/TDEI.2021.009639.

[151] E. A. Burke. "Secondary Emission from Polymers". In: *IEEE Transactions on Nuclear Science* 27.6 (Dec. 1980), pp. 1759–1764. ISSN: 1558-1578. DOI: 10.1109/TNS.1980.4331102.

[152] A Shih et al. "Secondary Electron Emission Studies". In: *Applied Surface Science* (1997).

[153] Y. Kemari et al. “A Townsend’s Secondary Ionization Coefficient Estimation Method for Partial Discharge Inception Voltage Prediction for Insulating Polymers”. In: *2022 IEEE 4th International Conference on Dielectrics (ICD)*. 2022 IEEE 4th International Conference on Dielectrics (ICD). Palermo, Italy: IEEE, July 3, 2022, pp. 226–229. ISBN: 978-1-66541-833-1. DOI: 10.1109/ICD53806.2022.9863604.

[154] Zhongwei Meng, Zhentao Liu, and Jinlong Liu. “Investigation of In-Cylinder Combustion Deterioration of Diesel Engines in Plateau Regions”. In: *Fuel* 324 (Sept. 2022), p. 124824. ISSN: 00162361. DOI: 10.1016/j.fuel.2022.124824.

[155] L. Arnedo and K. Venkatesan. “Pspice Simulation for Conducted EMI and Overvoltage Investigations in a PWM Induction Motor Drive System”. In: *2002 IEEE Workshop on Computers in Power Electronics, 2002. Proceedings.* COMPEL 2002. IEEE Workshop on Computers in Power Electronics. Mayaguez, Puerto Rico: IEEE, 2002, pp. 132–137. ISBN: 978-0-7803-7554-3. DOI: 10.1109/CIPE.2002.1196728.

[156] Andreas Krings et al. “Experimental Investigation of the Voltage Distribution in Form Wound Windings of Large AC Machines Due to Fast Transients”. In: *2016 XXII International Conference on Electrical Machines (ICEM)*. 2016 XXII International Conference on Electrical Machines (ICEM). Lausanne, Switzerland: IEEE, Sept. 2016, pp. 1700–1706. ISBN: 978-1-5090-2538-1. DOI: 10.1109/ICELMACH.2016.7732753.

[157] C. Petrarca et al. “Analysis of the Voltage Distribution in a Motor Stator Winding Subjected to Steep-Fronted Surge Voltages by Means of a Multiconductor Lossy Transmission Line Model”. In: *IEEE Trans. On Energy Conversion* 19.1 (Mar. 2004), pp. 7–17. ISSN: 0885-8969. DOI: 10.1109/TEC.2003.821834.

[158] Ioan Tilea and Calin Munteanu. “Motor Cable Electric Parameter Effects on the Overvoltage Phenomenon in Inverter Driven Motors”. In: *2013 8TH INTERNATIONAL SYMPOSIUM ON ADVANCED TOPICS IN ELECTRICAL ENGINEERING (ATEE)*. 2013 8th International Symposium on Advanced Topics in Electrical Engineering (ATEE). Bucharest, Romania: IEEE, May 2013, pp. 1–6. ISBN: 978-1-4673-5980-1 978-1-4673-5979-5 978-1-4673-5978-8. DOI: 10.1109/ATEE.2013.6563441.

[159] H.A. Toliyat, G. Suresh, and A. Abur. “Estimation of Voltage Distribution on the Inverter Fed Random Wound Induction Motor Windings Supplied through Feeder Cable”. In: *IEEE Trans. On energy Conversion* 14.4 (Dec./1999), pp. 976–981. ISSN: 08858969. DOI: 10.1109/60.815016.

[160] Yanyan Xie et al. “Voltage Stress Modeling and Measurement for Random-Wound Windings Driven by Inverters”. In: *2019 IEEE International Electric Machines & Drives Conference (IEMDC)*. 2019 IEEE International Electric Machines & Drives Conference (IEMDC). San Diego, CA, USA: IEEE, May 2019, pp. 1917–1924. ISBN: 978-1-5386-9350-6. DOI: 10.1109/IEMDC.2019.8785133.

[161] Md Sariful Islam et al. “Asymmetric Bar Winding for High-Speed Traction Electric Machines”. In: *IEEE Trans. Transp. Electrific.* 6.1 (Mar. 2020), pp. 3–15. ISSN: 2332-7782, 2372-2088. DOI: 10.1109/TTE.2019.2962329.

[162] A. Arzillo et al. “Challenges and Future Opportunities of Hairpin Technologies”. In: *2020 IEEE 29th International Symposium on Industrial Electronics (ISIE)*. 2020 IEEE 29th International Symposium on Industrial Electronics (ISIE). Delft, Netherlands: IEEE, June 2020, pp. 277–282. ISBN: 978-1-72815-635-4. DOI: 10.1109/ISIE45063.2020.9152417.

[163] Yalin Wang et al. “Partial Discharge Investigation of Form-Wound Electric Machine Winding for Electric Aircraft Propulsion”. In: *IEEE Trans. Transp. Electrific.* 7.1 (Mar. 2021), pp. 78–90. ISSN: 2332-7782, 2372-2088. DOI: 10.1109/TTE.2020.2992052.

[164] Marco Pastura et al. “Dv/Dt Filtering Techniques for Electric Drives: Review and Challenges”. In: *IECON 2019 - 45th Annual Conference of the IEEE Industrial Electronics Society*. IECON 2019 - 45th Annual Conference of the IEEE Industrial Electronics Society. Lisbon, Portugal: IEEE, Oct. 2019, pp. 7088–7093. ISBN: 978-1-72814-878-6. DOI: 10.1109/IECON.2019.8926663.

[165] C. Choochuan. “A Survey of Output Filter Topologies to Minimize the Impact of PWM Inverter Waveforms on Three-Phase AC Induction Motors”. In: *2005 International Power Engineering Conference*. 2005 International Power Engineering Conference. Singapore: IEEE, 2005, pp. 1–544. ISBN: 978-981-05-5702-7. DOI: 10.1109/IPEC.2005.206967.

[166] T Fuchslueger et al. “Reducing Dv/Dt of Motor Inverters by Staggered-Edge Switching of Multiple Parallel SiC Half-Bridge Cells”. In: (2017).

[167] Sangcheol Lee and Kwanghee Nam. “An Overvoltage Suppression Scheme for AC Motor Drives Using a Half DC-link Voltage Level at Each PWM Transition”. In: *IEEE Trans. Ind. Electron.* 49.3 (June 2002), pp. 549–557. ISSN: 0278-0046. DOI: 10.1109/TIE.2002.1005379.

[168] “A New Active Gate Driver for MOSFET to Suppress Turn-off Spike and Oscillation”. In: *Chin. J. Electr. Eng.* 4.2 (June 2018), pp. 43–49. ISSN: 2096-1529. DOI: 10.23919/CJEE.2018.8409349.

[169] Parthasarathy Nayak and Kamalesh Hatua. "Active Gate Driving Technique for a 1200 V SiC MOSFET to Minimize Detrimental Effects of Parasitic Inductance in the Converter Layout". In: *2016 IEEE Energy Conversion Congress and Exposition (ECCE)*. 2016 IEEE Energy Conversion Congress and Exposition (ECCE). Milwaukee, WI, USA: IEEE, Sept. 2016, pp. 1–8. ISBN: 978-1-5090-0737-0. DOI: 10.1109/ECCE.2016.7854819.

[170] M. Beninger-Bina et al. "A High-Voltage Transients Suppressor Diode". In: *2020 32nd International Symposium on Power Semiconductor Devices and ICs (ISPSD)*. 2020 32nd International Symposium on Power Semiconductor Devices and ICs (ISPSD). Vienna, Austria: IEEE, Sept. 2020, pp. 58–61. ISBN: 978-1-72814-836-6. DOI: 10.1109/ISPSD46842.2020.9170169.

[171] Nick Rigogiannis et al. "Voltage Transients Mitigation in the DC Distribution Network of More/All Electric Aircrafts". In: *Energies* 13.16 (Aug. 10, 2020), p. 4123. ISSN: 1996-1073. DOI: 10.3390/en13164123.

[172] *IEC 60034-27-5:2021 - Rotating Electrical Machines. Off-line Measurement of Partial Discharge Inception Voltage on Winding Insulation under Repetitive Impulse Voltage*. London: British Standards Institution, 2021.

[173] Khairy Sayed et al. "A Review of DC-AC Converters for Electric Vehicle Applications". In: *Energies* 15.3 (Feb. 8, 2022), p. 1241. ISSN: 1996-1073. DOI: 10.3390/en15031241.

[174] Paolo Mancinelli, Simone Stagnitta, and Andrea Cavallini. "Qualification of Hairpin Motors Insulation for Automotive Applications". In: *IEEE Trans. on Ind. Applicat.* 53.3 (May 2017), pp. 3110–3118. ISSN: 0093-9994, 1939-9367. DOI: 10.1109/TIA.2016.2619670.

[175] *IEEE Guide for Multifactor Stress Functional Testing of Electrical Insulation Systems*. IEEE. DOI: 10.1109/IEEESTD.1991.101027.